UNIVERSITY OF CALGARY

DEVELOPMENT AND ANALYSIS OF THE PRECISION MICRO MILLING SYSTEM

by

Jaehee Chae

A THESIS

SUBMITTED TO THE FACULTY OF GRAEDUATE STUDIES

IN PARTIAL FULFULMENT OF THE REQUIRE MENTS FOR THE

DEGREE OF MASTER OF SCIENCE

DEPARTMENT OF MECHANCIAL AND MANUFACTURING ENGINEERING

CALGARY, ALBERTA

July, 2006

Your file Votre référence
ISBN: 978-0-494-19225-2
Our file Notre référence
ISBN: 978-0-494-19225-2

ABSTRACT

The miniaturization of machine components plays a very important role in the future technological development of a broad spectrum of products owing to various advantages low material cost, portability, implant, lower power consumption and higher heat transfer since their surface-to-volume ratio is very high. In particular, one of the manufacturing processes for small parts is micro-mechanical machining. Similar to macro machining processes, the micro machining process can create three dimensional parts on a micro scale with various engineering materials (i.e. metallic alloys, ceramics, plastics) using miniature tools. The micro machining processes have several unique elements such as small size tools, high spindle speed, and miniaturized machine tools.

This thesis focuses on several aspects of micro machining operations in order to improve the performance of micro machining process. The survey of the current efforts in micro-mechanical machining investigated various aspects such as current research directions, limitations, similarities and differences between macro and micro in order to understand the fundamental knowledge of micro mechanical machining.

The prediction of the joint dynamics is vital to evaluate the micro machine tool performances through its dynamics because the joint plays significant roles in the micro system's behavior because the size of joint is relatively close to the assembled system. The fastener joint dynamics are identified with the classic receptance coupling technique. The proposed method is enhanced by identifying the joint dynamics between substructures through experimental and finite element analyses. This novel identification method increase the accuracy of the dynamic prediction of machine tool, by minimizing numerical errors and the problems associated with convergence. Various experimental dynamics and micro cutting tests are performed to verify the proposed methods.

The fragility of micro tools would require the operation to be monitored to avoid excessive forces and vibrations that will significantly affect the overall part and tool quality. In addition, the high rotational speeds represent high bandwidth requirements to measure micro cutting forces. In this thesis, a miniaturized milling system, and the accurate high bandwidth measurement of micro cutting forces using a 3-axis miniature force sensor and accelerometers are also developed in order to monitor the micro cutting forces accurately.

The developed miniaturized milling system can fabricate micro parts with various engineering materials and micro tools within an 8 μm resolution movement and an 80,000 rpm spindle speed. Since the inherent dynamics of the workpiece and overall machine tool affects the frequency bandwidth of sensors, the expanded Kalman filter is employed to compensate for unwanted dynamics by fusing the force sensor and accelerometer signals to increase the frequency bandwidth of the micro cutting forces measurement system.

ACKNOWLEDGEMENTS

I believe that last two years were a very valuable time in my life. What I learned is not only an advanced academic knowledge in mechanical engineering but also many lessons for my life.

I would like to thank my supervisor, who is Dr. Simon S. Park, for his support and guidance. Most of all, his endless encouragement was the most powerful source that makes my graduate school life succeed.

I want to acknowledge all members (Kevin, Brock, Damien, and ByungHee) of the Micro Engineering, Dynamics, and Automation Laboratory (MEDAL) and PanGi. I would like to share the result of my research with them. I wish to thank Dr. Theo Freiheit, who gave me invaluable inputs and feedbacks in my research.

Lastly, I would like to thank my family and friends for their support especially my wife Evvi.

TABLE OF CONTENTS

LIST OF TABLES

LIST OF FIGURES

NOMENCLATURE

ς	=	Damping ratio
ω_n	=	Natural frequency
G	=	Receptance (X/F)
A, B, C	=	Substructure
m, k, c	=	Mass, stiffness, damping constants
X	=	Displacement vector
F	=	Force vector
H	=	Receptance (x/f)
H^J	=	Dynamics characteristic of the joint
x	=	Translational displacement
θ	=	Rotational displacement
f	=	Lateral force
M	=	Moment
h_{ff}	=	x/f
h_{fM}	=	x/M
h_{Mf}	=	$\dot{\theta}/f$
h_{MM}	=	θ/M
h	=	Uncut chip thickness / depth of cut

Re	=	Edge radius of cutter
h_m	=	Minimum chip thickness
F_{ri}	=	Radial cutting forces
F_{ti}	=	Tangential cutting forces
F_a	=	Actual cutting forces
F_{air}	=	Air cutting forces
F_m	=	Measured cutting forces
T	=	Similarity transformation matrix
K	=	Kalman filter gain
P	=	Error covariance matrix
Q	=	System covariance
R	=	Measurement covariance
G_F	=	Kalman filter FRF of force sensor
G_A	=	Kalman filter FRF of accelerometer
Acc	=	Measured acceleration
Fc	=	Cutting forces

ACRONYMS

A/D	=	Analog to digital
BUE	=	Built-up edge
CAD	=	Computer aided design
CNC	=	Computer numerically controlled
DAQ	=	Data acqustion system
EMA	=	Experimental modal analysis
FEM	=	Finite element method
FFT	=	Fast fourier transform
FRF	=	Frequency response function
KF	=	Kalman filter
MEDAL	=	Micro engineering dyanmic automation laboratory
RC	=	Receptance coupling
RDOF	=	Rotational degree of freedom
SEM	=	Scanning electron microscopy
D/A	=	Digital to analog

CHAPTER 1. INTRODUCTION

Highly accurate miniaturized components are increasingly in demand for various industries such as aerospace, biomedical, electronics, environmental, communications, and automotive (See Figure 1-1). This miniaturization will provide micro-systems that promise to enhance health care, quality of life and economic growth in such applications as micro-channels for lab-on-chips, shape memory alloy "stents", fluidic graphite channels for fuel cell applications, subminiature actuators and sensors, and medical devices [Corbett 2000][Madou 1997][Weck 1997][Lang 1999]. In fact, the possibilities of the miniaturization are expanding into more complex systems owing to shifting from 2D components to 3D microstructures and from silicon to other materials, such as glass, polymers and metallic alloys. There are several benefits of miniaturization such as a good heat transfer rate due to high surface area to volume ratios , the possibility for non-invasive medical applications (i.e. hearing aid), increasing throughput and sensitivity for micro fluidic channels, reduction in space, material, and energy requirements and portability enable point of care testing [Okazaki 2004] [Geschke 2004]. The micro products can be fabricated with more expensive materials with better properties since they require a small amount of materials. They are also easy to transport and store due to the small size of the products.

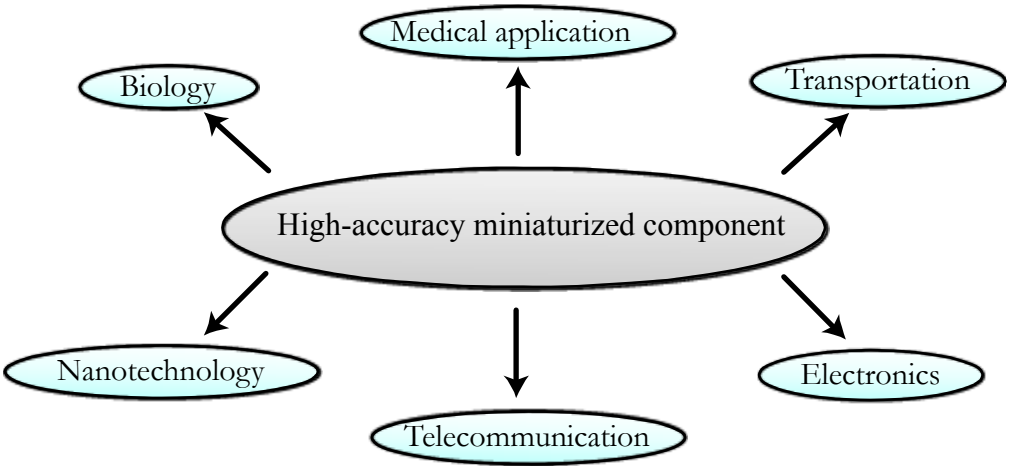

Figure 1-1 Functionality and Applications for the Miniaturized Component

Micro-component fabrication requires reliable and repeatable methods, with accurate analysis tools. Many common methods of manufacturing miniature components

have been based on semi-conductor processing techniques, where silicon materials are photo-etched through chemical or dry processes, usually in large batch production. Numerous researchers have investigated the feasibility of using other fabrication processes, such as LIGA (a photo-lithography method using a synchrotron), laser, ultrasonic, ion beam, and micro-electro discharge machining method, to manufacture commercially viable micro-components [Madou 1997][Alting 2003][Masuzawa 2000]. However, the majority of these methods are slow, and limited to a few silicon-based materials and essentially planar geometries. The broad commercialization of micro-systems is inhibited by low productivity and by the inability to manufacture in small batch sizes cost effectively.

Micro-mechanical machining is another fabrication method for creating miniature devices and components with features that range from tens of micrometers to a few millimeters in size (Figure 1-2). Recently, there has been strong interest in fabricating micro-meso-scale components through mechanical cutting processes [Liu 2004, A] [Liu 2004, B]. Even though the mechanical micro-machining process may not be capable of obtaining the smallest feature sizes as with lithographic processes, mechanical cutting processes are very important in bridging the macro domain and the nano- and micro-domains for making functional components. This is especially true for complex microstructures requiring a variety of materials, interfaces and functional shapes to form micro-systems that function with the macro-domain.

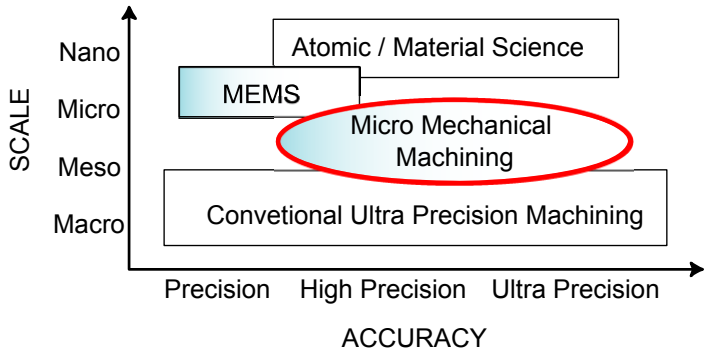

Figure 1-2 Dimensional Size for the Micro-Mechanical Machining

In most cases, the micro-products or micro-mechanical machines consist of several sub-products because it is impractical to produce a single product with multiple functions. This distinct feature can accommodate the diverse demands economically. Therefore, joining of micro-parts is an essential part of micro-assemblies. Common joining methods

include glue, snap fit, key lock, and miniature nut and bolt fasteners [Van Brussel 2000]. An accurate prediction of the overall structure dynamics of the micro machine tool system is critical to improve the micro machining performance. However, there is a lack of understanding in testing and modeling of 2D and 3D micro-components. Currently, the testing and modeling are heavily based on Finite Element (FE) simulation. The identification of joint dynamics has been of great interest since joint dynamic properties provide invaluable information, especially when predicting the dynamic properties of assembled structures using FE methods. The determination of joint dynamics, or of contact stiffness and damping, has been quite difficult due to the complex nature of the problem [Rivin 2000].

1.1 Motivation

The knowledge of the macro-mechanical machining has been well researched and established during last several decades. For micro-mechanical machining, there is a lack of knowledge developed. The translation of the wealth of knowledge developed for macro-machining operations to micro-processes is critical, both for the efficient development of practical micro-processes and for the understanding of the limitations of its application. Mechanically removing material using carbide tools can produce countless desired feature shapes and sizes. The micro-cutting process is challenging; however, the experiences learned from macro-processes provide a valuable resource for future micro-machining research. Therefore, it is necessary to research both macro and micro knowledge in machining processes.

Micro-mechanical-machining techniques bring many advantages to the fabrication of micro-sized features. One of the advantages of micro-mechanical machining is flexibility [Weck 1997]. In contrast to conventional machining, micro-mechanical machining can be easily modified to fulfill the production and operation requirements (i.e. Reconfigurable Manufacturing Systems). Further, they do not require very expensive setups of lithographic methods. They can produce micro-components cost effectively because there is no need for expensive masks. The process is suitable for accommodating individual components rather than large batch sizes, and has the ability to monitor the in-process quality of components

so that problems can be corrected during fabrication. It is capable of fabricating 3D free-form surfaces, which is especially important for the production of micro-injection molds. Moreover, it can process a variety of metallic alloys, composites, polymers and ceramic materials to form functional devices. Therefore, it is necessary to investigate the micro-mechanical machining in depth.

Micro-mechanical machining process has the ability to machine micro molds for mass micro-production. The quality of the final products depends on the quality of the surface of the micro molds. This requires an understanding of the system dynamics. Therefore, determining the dynamic performances of micro-mechanical machine is becoming increasingly important. Numerous approaches, such as analytical, numerical (i.e. finite element method) and experimental analyses, are used to predict the dynamic characteristics of micro-mechanical systems. However, analytical methods are often too complicated to predict dynamics, and numerical methods without joint dynamic characteristics have difficulties in providing reliable results for the dynamic characteristics of assemblies that have certain types of mechanical joints between substructures. Therefore, the joint dynamics identification technique is important to investigate prior to analysis of the dynamics of the micro system.

1.2 Challenges of Associated Precision Micro Milling Operation

There are several challenges associated with micro-fabrication that require a paradigm shift from macro-processes. These issues mainly come from the miniaturization of the components, tools and processes. The performance of miniaturized end mills is greatly influenced by small vibrations and excessive forces, which can be detrimental to the longevity of tools and the control of component tolerances. It is difficult to detect damage to cutting edges and even broken tool shafts. The majority of researchers who have investigated micro-machining processes have used cutting force for monitoring or improving the quality of sculptured products [Liu 2004] [Tansel 2000] [Bao 2000, A]. The accurate measurement of very small cutting forces is challenging because even a small amount of noise can give a false cutting-force signal since micro cutting forces are often less than 1 *N*. The frequency bandwidth of commercial force sensors is inadequate for the

majority of micro-machining cutting-force frequency regimes due to the very high rotational speeds used for micro-milling processes.

Furthermore, testing of micro-components and systems requires a succinct understanding of system dynamics behaviors. In general, a system consists of different substructures with distinctive joints (or interfaces). The role of mechanical joints is the transmission of forces and moments, alignment, and bonding between structures. Therefore, the response of the global system establishes the dynamic characteristics of each substructure. The joints, such as welds, bolts, rivets and bearings, between coupled substructures also play significant roles in the response of the global system, due to the differences in material properties, geometry, contact area and contact methods. However, the joints connecting the modular substructures in micro mechanical machining also face challenges because joint dynamics are very difficult to predict by analytical or numerical means.

1.3 Objectives

The objectives of this research are to translate some knowledge of the macro domain into micro machining processes for the efficient fabrication of miniaturized products. There are a number of issues that influence micro-mechanical machining processes; cutting forces, dynamics and stability, chip formation, and machine tools. Several subjects (literature review of the state-of-art micro milling operations, joint identification methods, development of the micro CNC machine, and a high bandwidth cutting force measurement system) are focused in this thesis in order to accelerate the micro-mechanical machining technology in both quality and productivity at the Micro Engineering, Dynamics, and Automation Laboratory (MEDAL), University of Calgary.

Review of The State Of The Art In Micro-Mechanical Machining

Understanding the fundamentals of micro-mechanical machining is essential to fabricate miniaturized products efficiently. It is very important to know the current limitations and research directions of the micro-mechanical machining operations. The

focus will be on micro-milling because this machining process is the most flexible for creating 3D surfaces from a variety of engineering materials. Traditionally, ultra-precision machining uses diamond tool-cutting operations, but because of the high demand for machining ferrous materials, a micro-milling operation using carbide tools is considered better suited to achieve these ends. In addition, the state of the art of the micro-milling operation will be examined for its transfer of knowledge from the macro-cutting domain to the micro-domain. Similarities and differences between macro-milling and micro-milling will be examined in this research.

Joint Identification Method Using Receptance Coupling Technique

One of advantages of the micro system is its versatility. Using various joints, the configuration of the micro system can be changed in order to increase the functionality of the system. Understanding the dynamics of the micro system is vital to increase the performance of the system. However, the dynamics of the joint are often ignored due to the difficulty of acquiring its dynamics. This thesis investigates the development of a joint identification method using the receptance coupling method to obtain and evaluate the dynamic responses of various linear joints in the macro domain.

Receptance is known as the dynamic relationship between the displacement and force in the frequency domain. In this work, the receptance coupling method, which couples two substructure receptance to evaluate overall assembled dynamics, utilizes both experiment modal analysis (EMA) and finite element analysis to identify joint dynamics. The accuracy and effectiveness of the proposed method have been verified through experimental tests using a fastener joint in the macro domain. However, this novel method can be utilized to predict the dynamics of any micro system without any modification.

Development of the Micro CNC Machine

The accuracy and quality of fabricated miniature components heavily depend on the machine tool structure. A precision micro computer-numerically-controlled (CNC) machine is designed and developed with various mechanical and electric systems. The developed

micro CNC machine is a 3-axis column knee type micro-milling machine. For this particular machine, various design aspects and control mechanisms were investigated in order to perform the same functions as the conventional CNC machine. However, the cost of the micro CNC machine is extremely low compared to the conventional CNC machine. The performance of the micro CNC machine has been verified through cutting tests using various sizes of micro end milling tools from 2 mm to 100 μm. The sensors (i.e. miniaturized force sensor, accelerometer, and laser sensor) are utilized and precisely calibrated in order to monitor the micro cutting processes. The result of this project, which is the micro CNC machine from the conceptual design, is used to gain a basic understanding of the micro machining operation.

Accurate Measurement Of High Bandwidth Micro Cutting Forces

Since tool diameters for micro milling operations are very small, the rotational speeds of the spindle need to be very high to achieve reasonable productivity. This poses a challenge to measure accurate cutting forces because it requires high frequency bandwidth force sensors. However, commercially available sensors do not meet this requirement and a compensation scheme is required to increase the bandwidth. To overcome the limitations, we utilize multiple sensors to fuse signals and compensate for unwanted dynamics in order to increase the frequency bandwidth. The fusion of signals increases the accuracy of the measurement and compensates for the incomplete data of each sensor. The sensor fusion techniques have been used in many applications. In this research, the bandwidth of the force measurement mechanism is increased by compensating for the force sensor dynamics. The compensation method, based on the expanded Kalman filter developed by Park et al. [Park 2004], is enhanced by using the force sensor and accelerometer signals to reconstruct high frequency bandwidth micro cutting forces from the distorted cutting force measurements. The experimental cutting tests are performed to measure high frequency bandwidth micro cutting forces using the developed micro CNC machine.

1.4 Organization

The thesis is organized as follows: Chapter 2 surveys precision and miniature machine tools for micro-machining operations, and cutting processes related to minimum chip thickness and micro-cutting force prediction. In addition, a variety of research related to joint identification is examined. Chapter 3 presents a novel methodology for predicting the joint dynamics of the assembled system, with some necessary assumptions based on the receptance coupling techniques. The difficulty of obtaining frequency response function (FRF) in rotational degree of freedom (RDOF) is overcome through the combination of analytical and experimental methods. Chapter 4 presents the development of the micro machining centre platform, where the characteristics and specifications of the machining centre are introduced with various controls and calibrations of sensors. In Chapter 5, the enhanced expanded Kalman filter methodology is examined to fuse the two different signals and compensate for unwanted dynamics. Then, the experimental cutting tests are performed to verify the feasibility of the method. Chapter 6 provides conclusions of this research and suggestions for future research directions.

CHAPTER 2. LITERATURE SURVEY

This chapter surveys various aspects in the micro-mechanical machining processes. Micro-mechanical machining is a manufacturing process where the feature size is on the micro scale. Its technology needs to incorporate the well established knowledge of macro machining such as a cutting condition monitoring system and dynamic identification of machine tools for chatter suppression technique. Joints also play an important role in micro assembly in order to increase its versatility. However, there are several unique features in micro-mechanical machining compared to macro machining; miniaturized tool, materials, cutting force measurement and prediction, spindle speed, and dynamics. A comparison between conventional macro machining and micro machining operations is presented in Table 2-1. Understanding similarities and differences between macro and micro machining is prior to studying micro-mechanical machining. Therefore, the primary subjects made in this chapter include: micro-mechanical machining, monitoring micro cutting process, and joint identification.

	Macro	Micro	Challenges Associated with Micro Machining
Machine Tool Accuracy	1 μm	0.1 μm	Requirement of highly accurate stages and control
Rotational Spindle Speeds	0 to 10,000 rpm (high torque)	20,000 to 500,000 rpm (low torque)	Changing dynamics due to centrifugal, gyroscopic, and thermal effects
Tool Material	Large grain carbide or HSS (typically more than 2 fluted cutters)	Small grain carbide (usually 2 fluted cutters)	May require special coatings (2.1.1.1)
Diameter of Tools	Above 2 mm	25 μm to 2 mm	Require precision ground flutes (2.1.1.1)
Rigidity of Machine	Rigid	Not very rigid	Natural frequency of micro machines are higher than macro machines (2.1.1.3)
Cutting Force Prediction	Sharp edge theorem	Shearing, Plowing, and Elastic recovery models	See Section 2.1.2.2
Cutting Force Measurement	Table dynamometer	Sensor fusion and compensation	Requires very high signal bandwidth for

		(accelerometers, non-contact displacement sensors, and force sensors)	measurement due to high spindle speeds (2.1.2.2)
Tool Deflection	Minor	Major	Requires a compensation scheme
Portability of Machine Tools	Stationary	Portable	Potential for desktop machining (2.1.1.3)
Joint dynamics	Important	Important	Verification with EMA (2.3)

Table 2-1 Comparison and Challenges Associated with Macro Machining vs. Micro Machining Operations

2.1 Micro-Mechanical Machining Survey

The micro-cutting of steel has recently received strong research interest with the advent of miniaturized systems using a variety of materials, especially for biomedical applications [El-Fantatry 2003]. Several research laboratories and universities have active research programs in micro-machining [Howe 2003] [Tanaka 2001] [Bang 2004] [Okazaki 2004] [Kussul 2002] [Kussul 1996]. According to Sandia, the need to fill the gap between nano/micro- and macro-domains is becoming an increasingly important research topic [Benavides 2001].

Several survey papers on micro-machining have addressed the importance of micro-fabrication techniques. Hesselbach [Hesselbach 2004] examined the international state of the art in micro-production technology from the perspective of how German industry fits within its limitations and economic potential. While outlining different fabrication processes, they draw the conclusion that in the micro-cutting area there is the need to fabricate steel micro-molds for injection molding or embossing processes. The research also briefly summarizes micro-assembly and metrology.

Masuzawa [Masuzawa 2000] examined non-photo etching technologies for micro-machining, and classified the basic machining phenomena of the processes required to fabricate micro-structures as: force, vaporization, ablation, dissolution, deformation, solidification, lamination, and re-composition. He examined their advantages and disadvantages, and listed publications that address the production of different feature types. He concluded that the size of micro-features currently being requested is 100 μm, with

micro-machining technology in the research stage being able to create 5 μm features. In the near future, requested feature sizes are expected to be reduced to 50 μm, with a research capability of 2 μm features.

Alting [Alting 2003] broadly examined the field of micro-engineering, from the design and development stages to modeling and fabrication, with a focus on how micro-products and their production systems can be designed. In their discussion of micro-mechanical cutting processes, the authors found major challenges to be that high cutting forces limit the accuracy and size due to the deflection of tools and workpieces, and that tool wear on the edge radius also influences cutting forces. The research also described micro-fabrication systems such as the micro-factory [Tanaka 2001], and concluded that "many benefits will come from applying a systematic approach to micro-engineering", with the achievement of complete process integration a fundamental issue.

Liu [Liu 2004, A] presented a survey of the mechanics of micro-machining processes, focused on chip formation as influenced by minimum chip thickness, elastic-plastic deformation, and the non-homogeneity in micro-workpieces. This thesis suggested that research is necessary in the modeling of the micro-machining process that will address thermal effects, dynamics, improved methods for estimating minimum chip thickness, and the nano-micro-meso continuum.

The consensus that can be derived from these survey researches are that micro-cutting technology is important to the fabrication of 3D structures (i.e. high aspect ratio and geometric complexities) using a variety of materials, especially steel. Very little has been studied on micro-machining with tungsten carbide tools, nor have the macro-phenomena such as chatter, tool wear, monitoring, and workpiece handling and testing been sufficiently investigated on a micro-scale. In the following section, the details of micro-cutting tools and machine tools, micro-cutting, and auxiliary processes are examined. The micro-fabrication research papers surveyed are summarized in Appendix A, and are categorized by their research areas.

2.1.1 Cutting Tools and Machine Tools

The majority of micro-machine tools are based on conventional ultra-precision

machines with high rigidity that is operated under a temperature-controlled environment. There has been strong interest by various research groups to build small-scale machine tools to fabricate micro-size components. The motivation for building miniature machine tools is derived from minimizing cost and size while increasing flexibility. However, the accuracy of these micro-machine tools is not yet on a par with conventional ultra-precision machine tools due to their lack of rigidity, base vibration, and accuracy [Okazaki 2004]. Tungsten carbide cutting tools are generally used for the micro-mechanical cutting process due to their hardness over a broad range of temperatures. This section examines the equipment necessary to fabricate accurate and repeatable micro-components.

2.1.1.1 Tungsten Carbide Micro-Tools

The size of precision micro-cutting tools (henceforth referred to as 'micro-tools') determines the limit of the size and accuracy of micro-structure features. Smaller tools have decreased thermal expansion relative to their size, increased static stiffness from their short structure, increased dynamic stability from their higher natural frequency, and potential for decreased cost due to smaller quantities of material [Cox 2004].

Diamond tools are often used for ultra-precision machining, but have a limited ability to machine ferrous materials. The high chemical affinity between diamond and ferrous materials causes severe wear [Kalpakjian 2002] [Shabouk 2003], limiting its use to nonferrous micro-mechanical machining operations. Therefore, micro-tools such as micro-end mills and drills are generally made from tungsten carbide (WC), which has high hardness and strength (Figure 2-1) at high temperatures.

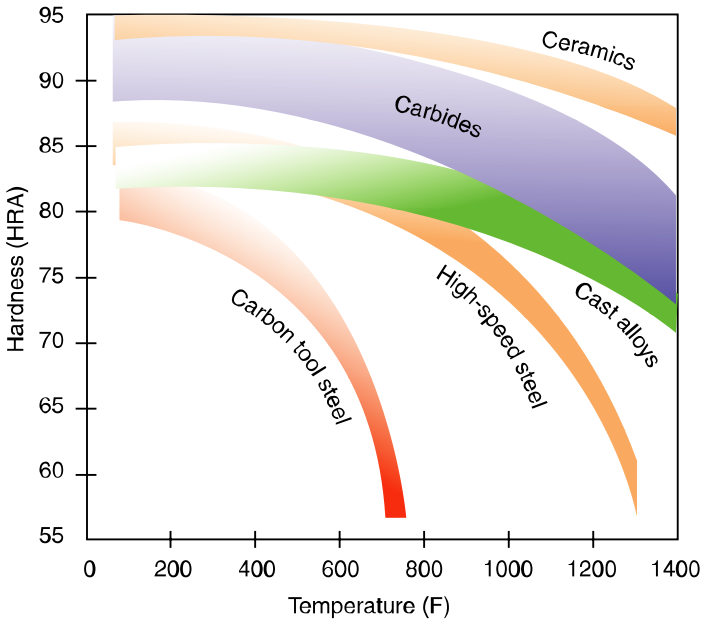

Figure 2-1 Hardness of Cutting Tool Materials as a Function of Temperature [Kalpakjian 2002]

To improve the wear resistance characteristics of micro-tools, very small grain size tungsten carbide (i.e. < 600 nm) is fused together to form the tool. Cobalt is typically used as a binder and its content influences tool hardness. Smaller cobalt content makes the carbide harder, but at the expense of higher brittleness. Commercially available micro-end mills can be as small as 50 micrometers in diameter, with their helix angle fabricated by grinding. Figure 2-2 depicts a typical two-fluted micro-end mill made of tungsten carbide.

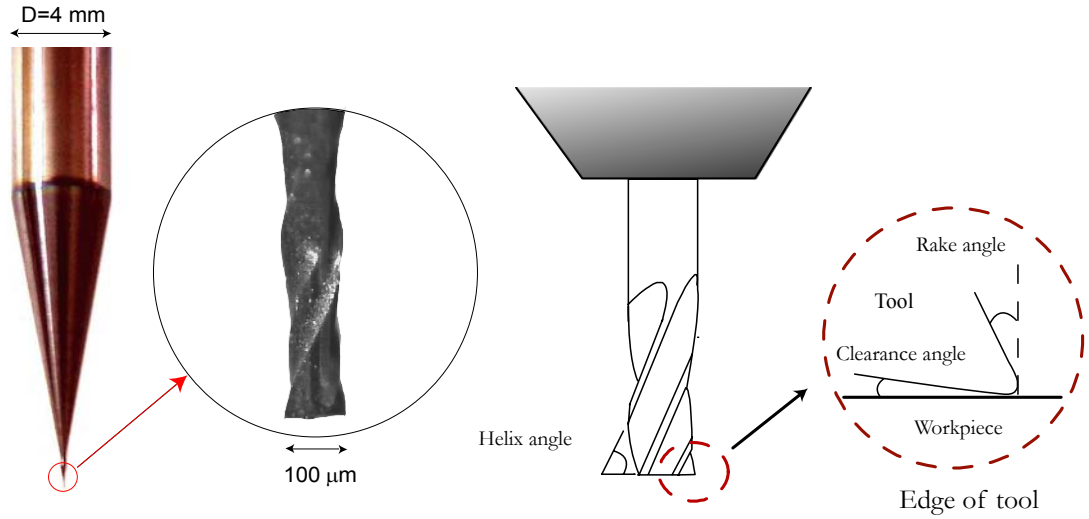

Figure 2-2 Tungsten Carbide Micro End Mill with Two Flutes

Micro-tools of less than 50 micrometers need a zero helix angle to improve their rigidity [Benavides 2001] [Schaller 1999] and to mitigate the limitations of fabrication techniques. Onikura [Onikura 2000] used ultrasonic vibration grinding to reduce the grinding forces and produced an 11 μm diameter micro-carbide tool. Sandia Labs has developed a 25 μm diameter carbide end mill tool with five cutting edges using focused ion beam machining, as shown in Figure 2-3. This end mill tool was used to fabricate micro-channels with a 25 μm depth and width [Adams 2001]. Schaller [Schaller 1999] fabricated micro tungsten carbide tools using diamond-grinding disks. These tools are shaped into the single-edge end mills and their diameters range from 35 μm to 120 μm. Fang [Fang 2003] investigated various micro-carbide tool geometries (i.e. triangular and semi-circular bases) using finite element method and experimentally verified their predictions. They found that the semi-circular-based mills are better than triangular or the conventional two fluted end-mills. They also concluded that when there is no helix angle on the micro-tools, poor chip evacuation may result in a poor surface finish.

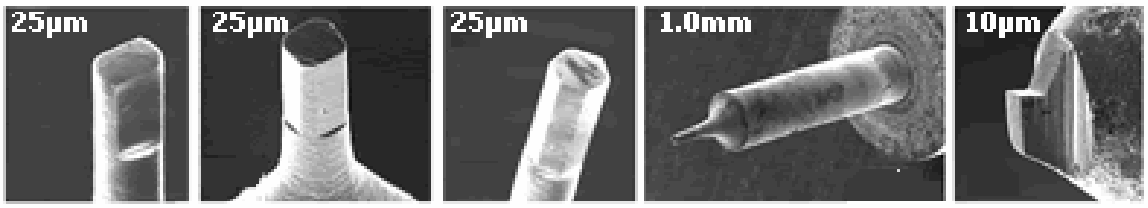

Figure 2-3 Scanning Electron Micrograph (SEM) of Micro-Cutting Tools [MMS online].

The material and geometry of micro-tools are important factors in micro-mechanical machining operations. The feature size is limited by the size of the micro-tools, and tungsten carbide tools are generally suitable for machining a variety of engineering materials. Several researchers [Schaller 1999] [Azizur Rahman 2004] have investigated the fabrication of micro-tools under 50 μm in diameters, making the cutting edges by intersecting two planes without a helix angle.

2.1.1.2 Precision Macro Machine Tools

In micro-machining applications, the rotational speed of the spindle should be very

high to maintain acceptable productivity, since the small tool diameter decreases the chip removal rate. When the torque requirements are high, electric motors with hybrid-angular contact bearings are used. This limits the maximum speed to approximately 60,000 rev/min, since friction in the contact bearing results in the thermal expansion of the spindle. When a higher spindle speed is required, air bearing spindles with air turbines are typically used, but they produce very low torque. Air bearing spindles that exceed 200,000 rev/min are commercially available. Often to achieve higher speeds, ultra-precision machine tools are retrofitted with high-speed spindles that fit in the conventional tool holder interfaces.

Ultra-precision macro-machine tools have several advantages including high rigidity, damping and the ability to actuate precisely based on precision sensors and actuators [Takeuchi 2000]. However, the large scale and precisely controlled machining environment may add very high costs for the fabrication of miniature components. Examples of commercially available precision micro-machining centers are depicted in Figure 2-4.

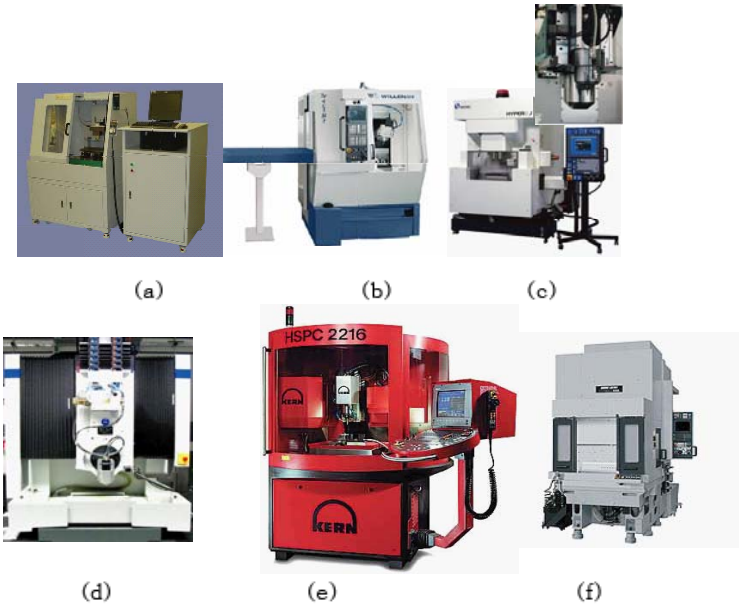

Figure 2-4 Commercial Ultra Precision Machine Tools: (a) DT-110 [Mikrotool Pte LTD]; (b) W-408MT [Willemin-Macodel SA]; (c) Hyper2j [Makino]; (d) Kugler [Kugler of America]; (f) HSPC 2216 [Kern]; (f) ULTIMILL V3000 [Mori Seiki]

2.1.1.3 Miniature Machines/Micro-Factories

Since micro-structures are very small, several researchers and companies are trying to scale down the machine tools necessary to produce micro-components [Tanaka

2001][Bang 2004][Kussul 1996][Kussul 2002]. Micro-machine tools do not necessarily have to be large to achieve the required precision [Okazaki 2004]; and, several benefits from this miniaturization include reduction in energy, space, materials and cost.

Micro-machine tools are cost-effective when compared with ultra-precision machine tools and require smaller amounts of materials when fabricated. Therefore, machining centers can be constructed with more expensive materials that exhibit better engineering properties. Micro-machine tools have higher natural frequencies compared with conventional macro-machines due to substantially smaller mass. This translates into a wide range of spindle speeds to fabricate components without regenerative chatter instability. In addition, smaller machine tools have lower vibration amplitudes relative to the conventional machining loads [Okazaki 2004]. Figure 2-5 illustrates miniature micro-machine tools.

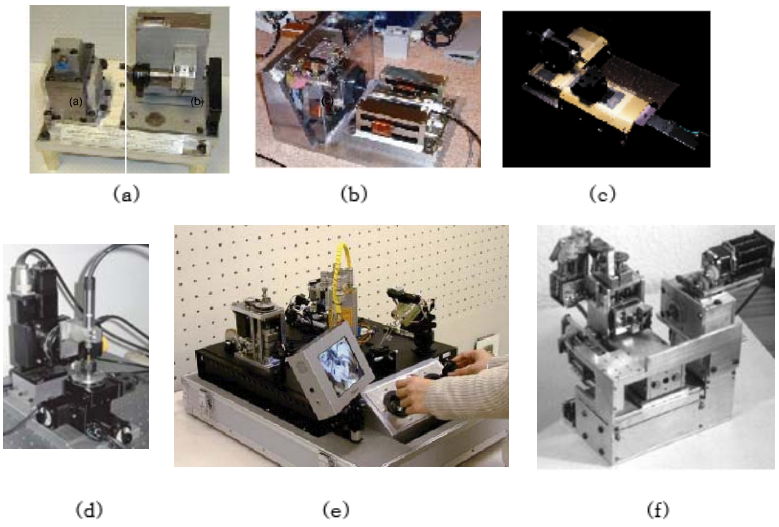

Figure 2-5 Micro-Machines (a) Micro-Factory [Vogler 2002]; (b) 2nd generation miniature machine [Vogler 2002]; (c) commercial miniature machine [Nanowave]; (d) Miniature machine [Bang 2004]; (e) Micro-factory [Okazaki 2004]; (f) Micro-machine tool [Kussul 1996]

The portability of such systems is beneficial. Miniature machines introduced the new concept of small footprint factories known as micro-factories [Tanaka 2001]. For example, the small size of the machines allows for their deployment to any building or site. Micro-factories may be suitable for the production of micro-components during military or space exploration applications, since the accessibility of large machine tools is very difficult. Miniature factories can also have significant energy savings since the energy requirements

are low.

Micro-factory actuators are either piezoelectric (i.e. flexure designs) or voice coil actuators, in order to achieve sub-micrometer accuracies. They use high-speed air bearing spindles, as used in the majority of ultra-precision machines. Further, micro-factories can have different cells with different functionalities such as micro-lathe, micro-milling, and micro-press. In MITI's micro-factory, micro-components are handled by a two-fingered tweezer-robot and miniature CCD cameras [Okazaki 2004].

There are challenges associated with the development of micro-machine tools. They require accurate sensors and actuators, which must be small enough to implant within the machines. The structural rigidity of micro-machine tools is less than those of precision machines. In addition, the micro-machine tools can be excited by external disturbances; therefore, micro-factories require vibration isolation to achieve desired tolerances.

The accuracy and small features of micro-components are dependent on the machine tools that produce them. Tungsten carbide micro-tools provide the flexibility to fabricate both ferrous and nonferrous components. Conventional ultra-precision machine tools can produce the desired tolerances; however, in order to produce micro-components cost effectively, the reduced cost potential of micro-factories holds a promising future for research. Further studies are needed to improve the rigidity of micro-factories. Also, integrated processing is still a significant challenge [Alting 2003].

2.1.2 Micro-Cutting

The principals of micro-machining are similar to those of conventional cutting operations. The surface of the workpiece is mechanically removed using micro-tools. Unlike conventional macro-machining processes, micro-machining displays different characteristics due to its significant size reduction. Most chip formation investigations are derived from macro-ultra-precision diamond and hardened steel cutting operations, with numerous publications on the effect of round edges and minimum chip thickness [Vogler 2002][Shaw 1995][Furukakwa 1988][Lucca 1991]. Often, the edge radius of the tools is relatively larger than the chip thickness to prevent plastic deformations or breakage of the micro-tools. In contrast to the conventional sharp-edge cutting model, chip shear in micro-

machining occurs along the rounded edge [Kim 1995]. As a result, cutting has a large negative rake angle, which affects the magnitude of the ploughing and shearing forces. Therefore, a relatively large volume of material has to become fully plastic for a relatively small amount of material to be removed, resulting in a significant increase in specific energy [Shaw 1995]. Further, when the chip thickness is below a critical chip thickness, chips may not be generated during the cutting process; instead, the workpiece material elastically deforms. For annealed steels, this results in a saw-toothed chip formation caused by high-frequency force fluctuation (over 10 kHz) [Matsubara 2000]. The increase in cutting forces leads to accelerated tool wear, large tool deflection, and a built-up edge [Weule 2001] [vogler 2003]. The build-up edge (BUE) on micro tool was taken at MEDAL using the vision system (Keyence; CV2600, Navitar; Zoom 6000) (Figure 2-6). It is also well known that non-homogenous materials have a profound influence on the surface roughness and the cutting force i

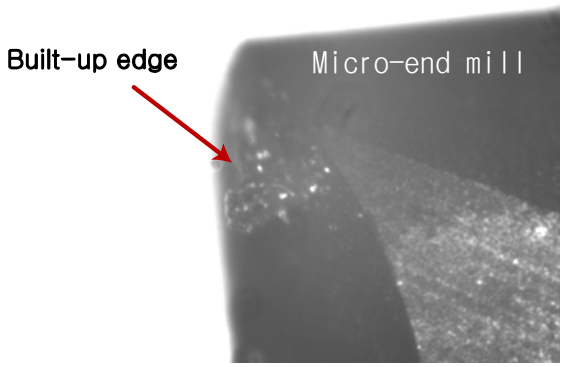

Figure 2-6 Built-up edge on Micro-end Mill (Dia. 500 μm)

2.1.2.1 Chip Formation and Minimum Chip Thickness

Chip formation is a dynamic process that is often non-linear in nature. Understanding micro-chip formation is important in an accurate prediction of cutting forces. Since a chip may not form when the depth of cut is less than a minimum chip thickness, finding the minimum chip thickness has received much attention [Weule 2001] [Vogler 2003] [Kim 2004]. In macro-milling operations, the feed per tooth (i.e. depth of cut) is generally deeper than the cutting tool edge radius. Therefore, macro-chip formation models are based on the assumption that the cutting tools completely remove the surface of the workpiece and generate the chips. According to Davies [Davies 1995, A] [Davies 1995, B], the material

flow pattern at low cutting speed is highly inhomogeneous, which affects segmented chip formation. This strain localization is due to the instability in the thermoplastic behaviour of materials with changing temperatures. In contrast, Konig [Konig 1993] found that periodic fracture caused chip formation. The chip thickness variation in milling operations, $h(\phi)$ can be approximated as $h(\phi) = c\sin(\phi)$, where ϕ is the angle of immersion (angle of the tool) and c is the feed rate (mm/ rev-tooth) as shown in Figure 2-7 [Altintas 2000]. However, simple scaling of the chip thickness variation model cannot be used for micro-machining. The small depth of cut due to the small feed rate and edge radius of the tool cause a large negative rake angle. This phenomenon causes ploughing, a rough surface and elastic recovery of the workpiece. Liu [Liu 2004, A] [Liu 2004, B] and Kim [Kim 2004] demonstrated that there is elastic-deformation of the workpiece during the micro-machining process.

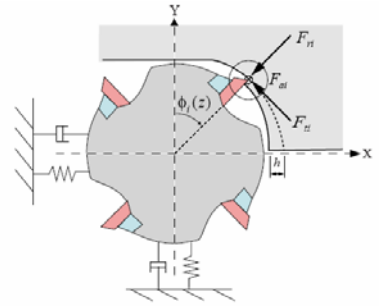

Figure 2-7 Milling Operation (Top View) [Altintas 2000]

The concept of minimum chip thickness is that the depth of cut or feed must be over a certain critical chip thickness before a chip will form. Figure 2-8 depicts the chip formation with respect to chip thickness. When the uncut chip thickness, *h*, is less than a critical minimum chip thickness, as shown in Figure 2-8(a), elastic deformation occurs and the cutter does not remove any workpiece material. As the uncut chip thickness approaches the minimum chip thickness, chips are formed by shearing of the workpiece, with some elastic deformation still occurring, as illustrated in Figure 2-8(b). As a result, the removed depth of the workpiece is less than the desired depth. However, when the uncut chip thickness increases beyond the minimum chip thickness, the elastic deformation phenomena decreases significantly and the entire depth of cut is removed as a chip, see Figure 2-8(c) [Liu 2004, A][Liu 2004, B] [Kim 2004].

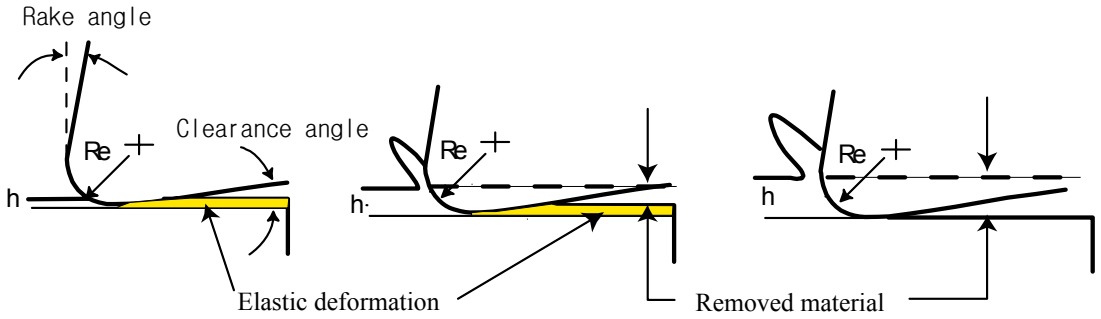

(a) h<hm (b) h≅hm (c) h>hm

Figure 2-8 the Effects of the Minimum Chip Thickness (R_e: radius of cutting tool, h = undeformed chip thickness, h_m = minimum chip thickness)

The relationship between the tool radius and minimum chip thickness depends on the cutting edge radius and the material of the workpiece. It is very difficult to directly measure the minimum chip thickness during the process, in spite of knowing the tool edge radius. Researchers have estimated the minimum chip thickness either through finite element (FE) or experimental predictions [Vogler 2004]. Moriwaki [Moriwaki 1993] used the FE method to analyze orthogonal micro-machining with the effect of the tool edge radius. Their FE analysis showed good agreement with experimental cutting of copper with a sharp diamond tool. Vogler [Vogler 2004] determined the minimum chip thickness of steel by using an FE simulation tool. They reported the critical chip thickness is 0.2 and 0.3 times the edge radius for pearlite and ferrite, respectively. Liu [K. Liu 2003] experimentally examined chip formation and micro-cutting forces. They concluded that a sudden change in thrust forces can be used to determine the minimum chip thickness. This sudden change in thrust forces was explained by a shifting from plowing/sliding dominant forces to shearing dominant forces as shown in Figure 2-9.

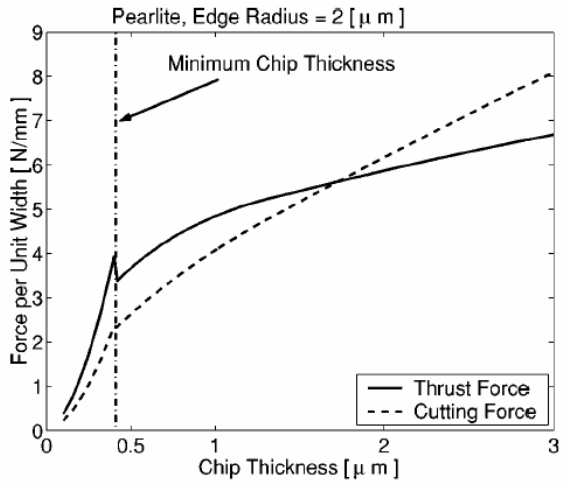

Figure 2-9 Chip Load and Force Relationship for Pearlite [Liu 2004, A].

Since the minimum chip thickness is dependent on material properties, Son [Son 2005] determined the minimum chip thickness based on the tool edge radius and the friction coefficient between the workpiece and tool. They analytically formulated that the minimum chip thickness can be approximated as $h_m = R_e(1-\cos(\frac{\pi}{4}-\frac{\beta}{2}))$, where β is a friction angle (i.e. *Frictional Force/Normal Force = Fu/Fv*) between tool and uncut-chip workpiece, and R_e is the cutting tool edge radius. They also observed that a continuous chip is generated at the minimum chip thickness, producing the best surface finishes.

In micro-mechanical machining, it is important to identify the minimum chip thickness prior to the cutting process, because the chip formation depends on the minimum chip thickness. The minimum chip thickness is influenced by the edge radius of cutting tools and by the workpiece materials.

2.1.2.2 Cutting Forces in Micro-Machining

The cutting force is directly related to chip formation. The cutting force also determines the tool deflection and bending stress that limits the feed rate [Budak 2003] [Dow 2004]. Well developed analytical cutting force models help operators to choose the right cutting conditions for their system. There are two components to cutting forces namely, shearing and plowing forces. Since the chip thickness in micro-machining

applications can be comparable in size to the edge radius of the tool, the conventional sharp-edged theorem cannot be applied in micro-machining operations due to their large negative rake angle. In addition, the elastic-plastic deformation of the workpiece also changes the cutting forces in micro-machining operations.

Micro-cutting forces are quite different from macro-forces, especially the static (dc component) of force. In a preliminary experiment of slot machining aluminum 7075 T-6, micro-cutting forces were compared to their predicted results using the conventional sharp-edge cutting force model [Altintas 2000], with compensation for the run-out forces, and the assumption that the machined materials were uniform (Figure 2-10). The dynamic component, which is mainly due to shearing forces, is similar to conventional cutting force simulations when the depth of cut is greater than the minimum depth of cut. However, the offset static component between the experiment and the predictions clearly indicated that plowing forces in micro-machining processes cannot be fully expressed in the macro-cutting model.

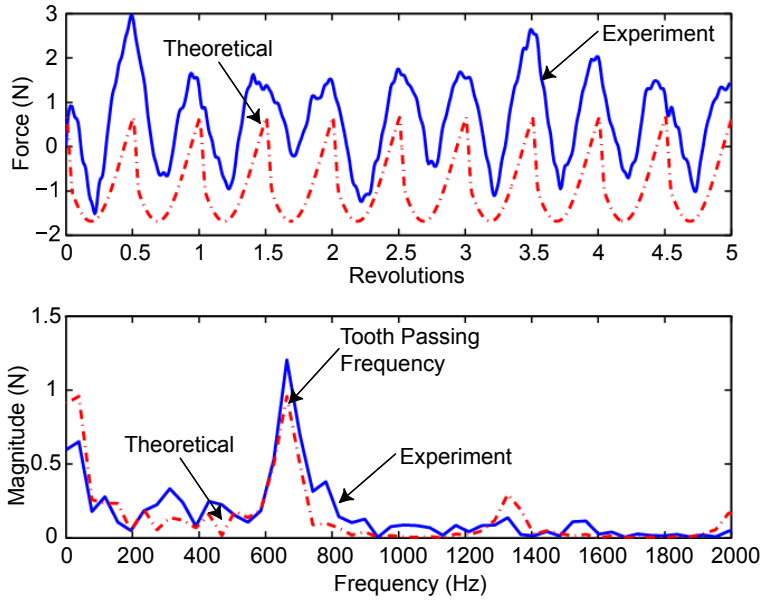

Figure 2-10 Micro-Cutting Forces in Feed Direction (20,000 rpm, 0.002 mm/tooth, 200 μm diameter, two fluted end mill).

Making a small depth of cut in micro-machining is impeded by the requirement to maintain cutting forces below the plastic deformation limit of the micro-tool; therefore, reducing the cutting forces in micro-operations significantly improves material removal

productivity. However, driving cutting forces up is the requirement for a minimum chip thickness necessary for chip formation. Moriwaki [Moriwaki 1995] presented the possibility of significantly reducing cutting forces in macro-turning and milling by providing an ultrasonic elliptical vibration that is synchronized with the chip flow direction to reduce cutting forces. However, their tool rotational speed was limited by the elliptical vibration speed. This could be addressed by utilizing a high-frequency piezoelectric actuator stage with higher bandwidth than the rotational speed in the micro-machining domain.

Bao [Bao 2000] developed an analytical micro-machining cutting force model for the calculation of chip thickness by considering the trajectory of the tool tip, but did not consider the negative rake angle effect, elastic-plastic workpiece, or the deflection of tool (they used relatively large diameter tools). According to the authors, it is not desirable to apply conventional macro-models [Tlusty 1983] [Tlusty 1975] to the micro-machining process when the ratio between the feed per tooth to tool edge radius is greater than 0.1.

Friction between the tool and workpiece has not been thoroughly investigated in micro-machining. Several researchers investigated the effects of flank tool wear by monitoring the plowing forces [Yao 1990] [Kountanya 2004] in macro-machining. In the macro-process, increased flank wear is caused by high friction and its consequent thermal load between the tool tip and workpiece material. This results in tensile residual stresses and creates a “white layer” with an extremely fine microstructure [Byrne 2003]. With an increase in the chip thickness in micro-machining, the plowing forces decrease as the chip forms [Liu 2004, A]. In addition, the elastic deformation of the workpiece affects changes in the plowing (or rubbing) forces.

Kountanya [Kountanya 2004] examined the flank wear of edge-radiused macro-cutting tools in orthogonal machining conditions. The authors report that the cutting force decreases when the chip thickness is less than the edge radius of the tool until the edge radius is worn away, then the cutting force increases. The reason for this phenomenon may be due to the sharpening effect on the blunt edge as flank wear increases as illustrated in Figure 2-11. Whether this macro-machining phenomenon occurs in the micro-cutting process is not yet known.

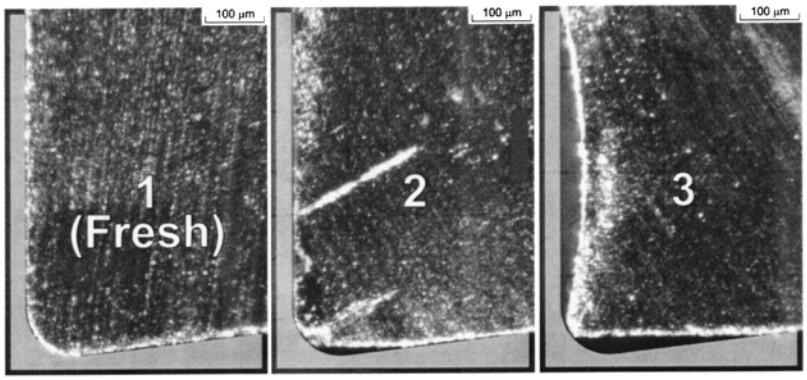

Figure 2-11 Flank Wear of Edge Radiused Tool (70 micrometers edge radius) [Kountanya 2004]

Kim [Kim 1995] showed analytically the differences in cutting forces between macro-machining and micro-machining processes. In the macro-model, shear takes place along a shear plane; whereas in micro-machining, the shear stress rises continuously around the cutting edge. Their orthogonal micro-cutting force analytical model considered the elastic recovery of the workpiece along the clearance face of the tool and the plowing effect by the tool edge radius. They estimated the elastic effects by simulating the cutting forces based on four separate regions. They found it matched closely with the experimental work of Moriwaki [Moriwaki 1991] and Lucca [Lucca 1991] and concluded that the cutting forces are different from the sharp-edge model.

In micro-mechanical machining, the depth of cut is often less than the critical minimum chip thickness to avoid tool breakage and to maintain desired tolerances. This causes a large negative rake angle between the tool and workpiece. Conventional sharp-edge macro-cutting models cannot be used to predict cutting forces in micro-machining applications.

2.1.2.3 Instability in Micro-Machining

Chaotic dynamic cutting processes, such as chatter, pose a significant problem in micro-machining because they result in excessive vibration that can lead to catastrophic failure. Chatter is an unstable self-excited vibration that occurs as a result of an interaction between the dynamics of the machine tool and the workpiece [Budak 2000] [Tlusty 1983]

[Tobias 1958] [Tobias 1965]. In traditional regenerative chatter stability, the occurrence of chatter is dependent on three factors: cutting conditions, workpiece material properties and the dynamics of the machine tool spindle system. Conventional macro-chatter stability assumes that the feed rate does not significantly affect stability. However in micro-machining, chatter stability needs to consider both the elasticity of the workpiece due to low feed rates, as well as the conventional macro-regenerative waves that result in a dynamic change in chip thickness, as shown in Figure 2-12 (c).

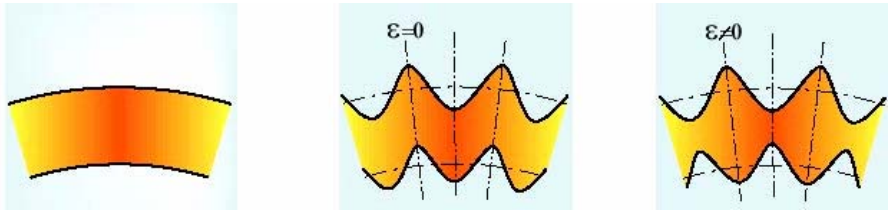

Figure 2-12 Chip Generations due to (a) No Vibration; (b) Forced Vibration; (c) Regenerative Chatter [Chae 2006 A]

Liu [Liu 2004, A] [Liu 2004, B] found that the forced vibration of the tool and the elastic recovery of the workpiece contribute to the magnitude of the cutting force at low feed rates. They proposed the micro-end milling process as having three types of mechanisms: only elastic deformation (the uncut chip thickness is smaller than the minimum chip thickness); elastic and shearing deformation; and, shearing deformation (the uncut chip thickness is greater than the minimum chip thickness). They have used the elastic recovery rate, p_e, based on the results from Jardret's work [Jardret 1998], in order to quantify different types of deformations. In addition, Liu [Liu 2004, A] [Liu 2004, B] also investigated the effect of low feed rate. They performed cutting at various feed rates and found that very low feed rates resulted in instability due to the elastic deflection of the workpiece. This, in turn, creates variation in chip thickness, which results in chatter. Figure 2-13 depicts the instability at different feed rates where the second and third row graphs show the instability.

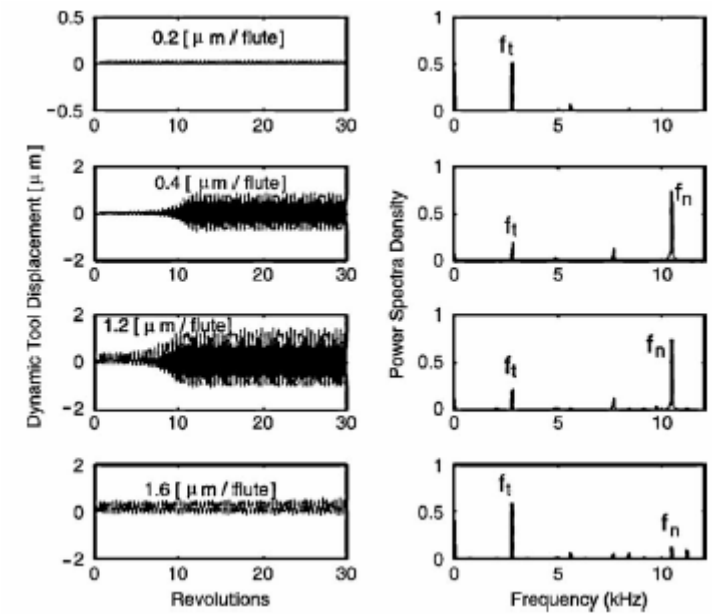

Figure 2-13 Tool Vibration and Frequency Spectra for Machining Pearlite [Liu 2004, A].

Kim and Ni [Kim 2004] investigated the effect of static tool deflection by assuming the tool as a simple cantilever beam. Their model corrected the actual depth of cut by subtracting the deflection of the cutting tool from the commanded depth of the cut. Dow [Dow 2004] compensated for the deflection errors in micro-tools by predicting the cutting and thrust forces. Since at micro-scales, cutting force influences tool deflection and tool deflection influences the cutting force, cutting force models should include this coupling.

High-speed machines also present new challenges for micro-machining. At higher speeds, the dynamics of machine tools change, with an unbalanced spindle producing centrifugal and gyroscopic effects [Jorgensen 1996]. Modeling and analysis of high-speed spindle dynamics with various bearing configurations is important. The majority of spindle research has dealt with static stiffness optimization rather than dynamic performance. The few papers addressing high-speed spindle dynamics were far below the operation range of micro-machining [Howe 2003] [Jorgensen 1996].

Finally, in the micro-scale, material property homogeneity cannot be assumed; thus, the cutting coefficients used in chatter control models will vary from macro-machining processes due to anisotropy of materials. Instability in micro-machining is a very challenging problem due to various non-linear effects and time-variant dynamics. In

particular, the feed rates of micro-milling operations can significantly affect the stability due to elastic deformation [Kim 2004]. In addition, the workpiece material's elastic-plastic effects and the static deflection of the tool cannot be discounted in micro-cutting force analysis.

2.1.2.4 Effect of Workpiece Material

In micro-machining, the nature of the workpiece must be considered in order to fabricate accurate micro-parts, as the depth of cut is sometimes less than the grain size in the workpiece material. The assumption of homogeneity in workpiece material properties is no longer valid. Because micro-grain-structure size is often of the same order of magnitude as the cutter radius of curvature, the grain structures will affect the overall cutting properties [Grum 2003]. And surface quality of the workpiece. Figure 2-14 shows the cross section of the machined workpiece (SAE 1045).

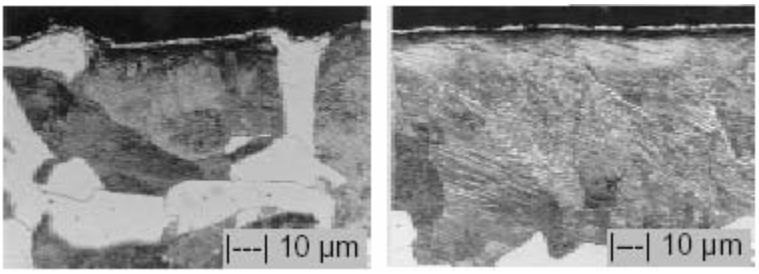

Figure 2-14 Influence of the Workpiece Material Property [Weule 2001]

This is a distinct difference between micro- and macro-mechanical machining. The assumption in macro-mechanical machining is always that the materials are isotropic and homogenous. The changing crystallography during the cutting process also causes variation in the micro-cutting force and generates vibration. This vibration is difficult to eliminate by changing the machine tool design or process conditions, because it is originates from the workpiece. Therefore, an averaged constant cutting coefficient cannot be used for micro-machining applications due to tool geometry, small grain size, and non-uniformity of the workpiece material.

Lee [Lee 1999] [Lee 2002] examined vibration caused by non-homogeneous

materials (i.e. aluminum single crystal with (110) and (111) plane) in precision machining operations. They found that changing crystallography and grain orientation affects shear angle and strength. Grum [Grum 2003] analyzed the cutting force in turning related to workpiece material and hardness. Using different aluminum and silicon alloys, they observed different microstructures significantly influence the magnitude of the cutting force, both in their static and dynamic components. When the cutting tool engages from one metallurgical phase to another, the cutting conditions change, causing machining errors, vibration or accelerated tool wear.

Vogler [Vogler 2003] used a three-step monitoring process for determining the cutting force of different metallurgical materials, especially steel. In steel, the toughness of ferrite and pearlite grains differs, affecting the machined surface roughness. Their first step was the generation of a micro-structural mapping using FE simulation. Step two was the determination of the location of the cutting edge. The cutting coefficients change depending on which material phase is engaged with the cutting edge. The final step was the estimation of the cutting coefficients by using an average chip thickness. With a defined cutting coefficient, an instantaneous chip thickness can be used to predict the cutting force.

To overcome non-homogeneity in workpiece material, Weule [Weule 2001] suggested micro-machining with uniform material. They quenched and tempered SAE 1045 steel with different temperatures ranging from 180^{o} to 600^{o}C in order to obtain a homogenized workpiece (Figure 2-15). They also showed that an increase in the feed rate would improve the surface finish. This conclusion is in agreement with the instability due to low feed rate observed by Liu [Liu 2004, A] [Liu 2004, B].

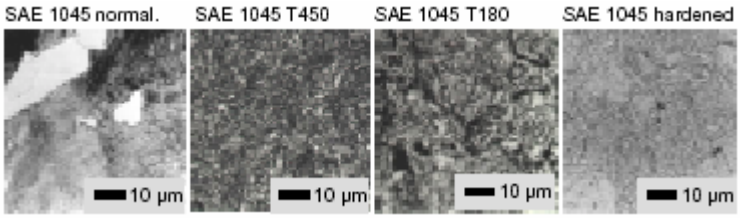

Figure 2-15 Cross sections of SAE 1045 tempered at Different Temperatures [Weule 2001]

The workpiece in micro-machining should be regarded as a non-homogenous

material since the grain size is comparable to chip size. If possible, treatment of the workpiece should be considered to provide uniform micro-structural properties, allowing for better cutting force prediction.

2.1.2.5 Tool Wear and Burrs

The small depth of cut in micro-machining significantly increases friction between the tool and the workpiece, resulting in thermal growth and wear. As a result, the increased radius of the tool decreases the quality of the produced part and increases the rate at which tools fail [Xiao 2003] [Liu 1996]. In addition, the suppression of burr development in micro-machining is very important because unlike in macro-machining, post-processing cannot always be applied to remove burrs on miniature fabricated parts.

Figure 2-16 shows the images of the new and the used micro-end mills using the vision system at MEDAL. It is clearly visible that the used micro end mill has larger edge radius of the tool. Also, the flank wear is more developed that rake face.

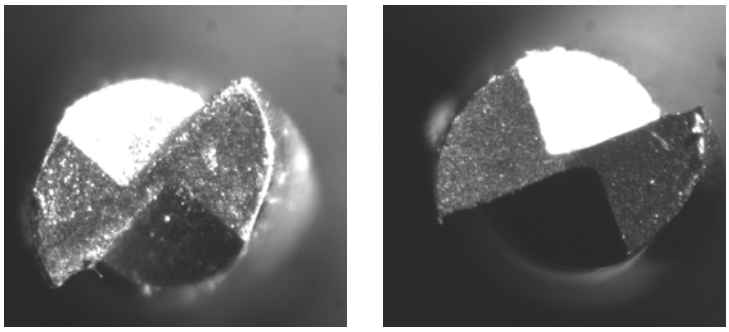

(a) Used micro tool (b) New micro tool

Figure 2-16 Images of the Micro End Mill (Dia. 500 μm)

While tool wear monitoring has been extensively studied on the macro-scale, very limited work has been conducted at the micro-scale. Tansel [Tansel 2000, A] [Tansel 2000, B] developed neural networks to predict tool wear using cutting force and wear lands of the tools. The neural networks estimated tool condition in the micro-machining of aluminum and steel, with slower tool wear rates for aluminum than in steel. This phenomenon is in agreement with tool wear in the soft/hard workpiece cutting observed by Weule [Weule

2001]. However, the neural network approach requires extensive experimental data and is often inconsistent for different material and cutting conditions. Rahman [Rahman 2001] investigated the micro-milling of copper. They concluded the wear of a 1 mm diameter tool depended on the tool helix angle and the depth of cut. Their experiments found a small depth of cut (0.15 mm) has a higher tool wear rate than a larger depth of cut (0.25 mm). They interpreted this phenomenon as resulting from a continuous chip being removed up the helix of the micro-tool, increasing the force on its rake face.

Prakash [Prakash 2001] and Dow [Dow 2004] empirically predicted tool life. With coated micro-end mills, Parkash [Prakash 2001] found that the flank wear at the end of the cutting edge is highest, and that the feed rate and cutting speed have a more significant influence over the micro-cutting tool than the axial depth of cut. Dow [Dow 2004] observed that as cutting tools wear, the edge of the cutting tool becomes flat. This flat area can be monitored with a scanning electron micro-scope (SEM) image of the tool edge. However, the applicability of this method is limited by the long and difficult setup of the SEM. The influence of the tool size on tool wear was investigated by Weinert [Weinert 2004], who also used an SEM to measure the tool wear. Mitsubishi [Mitsubishi Co.] investigated the relationship between the coolant pressure and tool wear in micro-machining. Their experimental results showed there is no relationship between the amount of wear and the coolant pressure.

In milling, the kinematics of the tool as it exits from the workpiece significantly affects burr formation due to plastic deformation (i.e. bending) of chips rather than shearing [Byrne 2003]. Weule [Weule 2001] reported that burrs frequently occur when micro-machining hard materials because of increased tool wear. Schaller [Schaller 1999] examined ways to remove burrs from brass and stainless steel micro-parts. To minimize burring, they coated brass with a cyanacylate polymeric material. The polymeric material filled voids around the edges of the workpiece where burrs form, allowing the cutting tool always to be engaged with the workpiece or the cyanacylate layer. After machining, the cyanacylate is removed with acetone in an ultrasonic bath. For stainless steel, they used electro-chemical polishing techniques to remove burrs. This post-processing to minimize micro-burrs can be expensive but necessary. Figure 2-17 shows the micro slots and micro burrs of the workpiece (AL-7075) from MEDAL.

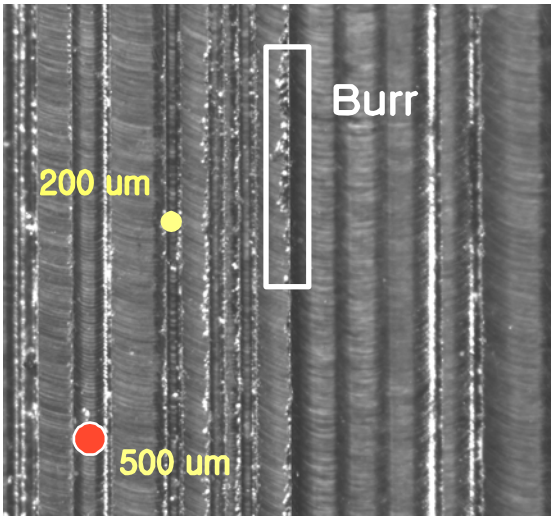

Figure 2-17 Micro-machined Workpiece (Al-7075) with various size of Micro End-mills (Top View)

The motivation for high-speed micro-machining is the reduction of production time in creating complex 3D shapes by maximizing material removal rates. It is important to understand the relationship between the micro-cutting tool and the workpiece in order to produce the desired micro-component. Cutting force prediction and measurement need meticulous care during their analysis so that the effect of built-up edge, run-out, tool deflection, and instability are included. Most of the papers surveyed have individually investigated these effects on tools with diameters greater than 200 μm, but a more comprehensive approach is required to addresses their interactions, including addressing non-linearity in micro-machining, and using tools with the smaller diameters. Improved productivity in micro-milling operations requires a chip thickness greater than the minimum chip thickness, while keeping below the plastic deformation limit of the workpiece or tool. If this cannot be achieved, the tool design should be improved to increase its strength and stiffness to permit cutting conditions where chips will always form.

2.2 Monitoring Micro Cutting Process

One of the biggest challenges in micro machining operations is maintaining cutting forces below a critical limit to prevent excessive tool wear and breakage while improving

productivity. In order to do that, accurate cutting force monitoring system is critical. However, the sensing and monitoring of micro-machining processes has limitations. It is anticipated that there will be more challenges associated with the micro-machining than macro-machining, and new paradigms may be required to overcome obstacles.

2.2.1 Sensing Methods

Significant research has been conducted on the monitoring of macro-machining processes using various sensors such as: a spindle motor current and power [Matsushima 1982] [Constantinides 1987]; a feed drive measurement [Altintas 1992] [Kim 1996] used to emulate force signals; vibration signatures [El-Wardany1996]; acoustic emission [Moriwaki 1980] [Sampath 1987] [Choi 1999]; and, cutting forces [Altintas 2000] [Tlusty 1983] [Moriwaki 1980] [Altintas 1989] [Tarn 1989] [Lister 1993] [Dimla 1999]. These sensing methods have very narrow frequency bandwidth requirements and are prone to small disturbances, or not applicable for milling operations due to the highly intermittent nature of the chip removal process [Yan 1995]. Tlusty [Tlusty 1983], Byrne [Byrne 1995], and Dimla [Dimla 2000] reviewed various sensors and their limitations for machine monitoring processes using dimensional, cutting force, feed force, spindle motor and acoustic emission (AE) sensors.

Cutting force measurement is the most effective method for monitoring tool conditions since it provides higher signal-to-noise ratios, and best represents the state of machine tools and machining operations [Tlusty 1983]. Despite years of research in this area, reliable, versatile and practical sensors are not yet available for the monitoring and controlling of high-speed machining processes [Dimla 2000]. The most common direct method to measure cutting force in machining operations is through table dynamometers or piezoelectric load cells. Park and Altintas [Park 2002] presented a Kalman filter (KF) algorithm, which reconstructs cutting forces from the distorted cutting force measurements obtained from a spindle integrated sensor system. Similar filtering techniques are needed to acquire high-frequency bandwidth cutting forces for micro-machining. The bandwidth of sensors needed for micro-cutting operations should be a few times higher than the tooth passing frequencies to reconstruct the cutting forces. This requires the development of new

sensors and the fusing of various sensor signals.

2.2.2 Process Optimization and Monitoring

Most micro-machining processes use conservative feed rates due to the fragility of micro-tools [El-Fatatry 2003]. To increase overall manufacturing output, micro-cutting requires higher feed rates and spindle speeds for higher volumetric material removal, while minimizing tool deflection and chatter. Adaptive control has been used in macro-machining processes [Park 2002] [Ulsoy 1989] [Koren 1983]. However, it has not been tried in the micro-scale, where it is even more important since tool deflection is considerable.

It is very difficult to detect damage to cutting edges and broken shafts in micro-end mills, making it nearly impossible to stop machining or change the cutting conditions before tool failure. Because feature sizes and cutting tools are small, it is nearly impossible to restart an interrupted machining process by aligning the tool to the workpiece. Also, damage to a workpiece by a broken tool may not be observable without special instruments. Tansel [Tansel 1998] have used Smart Workpiece Holders to prevent workpiece damage through the use of a piezoelectric actuator. Using a detected cutting force signal, the actuator can quickly move in the opposite direction in very small increments, thereby creating sufficient time to reduce the motor speed and decrease the cutting forces.

Process monitoring and control in high-speed micro-machining applications are very challenging with existing equipment and techniques. Therefore, the fusion and filtering of various process monitoring signals is essential for micro-control to enhance robustness and reconcile the limited frequency bandwidth of currently available sensors and actuators.

2.3 Literature Review for Joint Identification

The importance of the dynamics of the micro machine tool was already mentioned in Section 2.1.2.3: Chatter stability. This section examines the feasibility of translating macro-knowledge into the micro-realm by identifying the similar problems faced in the macro- and micro-domains. An accurate prediction of the overall structural dynamics of the machine tool system is critical to preventing chatter. However, experimental measurement

of the dynamics of the machine tool structure at the tool tip is not feasible for micro-tools. Due to micro-tool size and fragility, impact hammer force tests cannot be applied to measure tool tip vibration. Often, micro-tools are modeled as cantilever beams. However, this may not correctly represent the dynamics at the tool tip. To overcome this, receptance coupling and joint dynamics identification developed by Park [Park 2003] can be utilized to analytically couple tool and spindle dynamics. To acquire the overall dynamics, the dynamics of the micro-end mill tool is predicted through FE analysis and the dynamics of the spindle-tool holder assembly are measured through the experimental hammer test. The joint dynamics are then indirectly acquired based on two translational measurements using a blank tool. Many researchers have been studying the joint dynamics identification method.

2.3.1 Difficulties for Joint Identification

To evaluate dynamic characteristics of system, the FE method requires information such as stiffness, damping ratio, and material properties. Damping in mechanical systems usually occurs due to the loss of energy in the material of the component and the contact areas between fitting parts – micro asperities on the contacting surfaces.

For the joints or connections, it is not easy to obtain those parameters from the theoretical simulations. In such cases, an experimental test is necessary to identify the parameters. However, joints in the system cannot be tested easily due to access limitation. Even if the joints can be separated, another structure or joints are required to support the test specimen. In that case, the identified parameters of the joint in certain test environments cannot apply to other environments because the dynamic characteristic of joints depends on many different conditions such as the contacting surface and loading conditions.

A number of researchers have tried, and they have presented several methods for various kinds of joint identification from different perspectives [Liu 2000] [Ren 1990]. The main aim of joint identification is to obtain the dynamic characteristics of the joint (inertia, stiffness, and damping ratio) that can contribute to the minimization of the difference between the measured assembly frequency response function (FRF) and the predicted assembly FRF, analytically or numerically [Rivin 2000].

Kim [Kim 2001] and Yuan [Yuan 1985] identified joint stiffness and damping properties with mode shapes of the structure. They verified the proposed methods through simulation studies. These methods require the mode shapes at the joints and accurate modal parameters, which are difficult to extract from experiments. Some researchers investigated the determination of joint properties based on FRF, in order to overcome the difficulties of acquiring accurate modal parameters. Liu [Liu 2000] used the substructure synthesis method for the identification of the dynamic properties of elastic media (i.e. joints) between coupled substructures using measured FRFs (Figure 2-18).

They pointed out the least square solution, which is a general method to identify the joint dynamics, has a matrix rank deficiency problem. A numerical simulation was only used to verify their results. The elastic media, which is assumed to be a joint, is basically another substructure. The connected surface between media and structure is assumed to be rigid. The identified joint dynamics were obtained by a numerical solution with only the translational degree-of-freedom (TDOF) system.

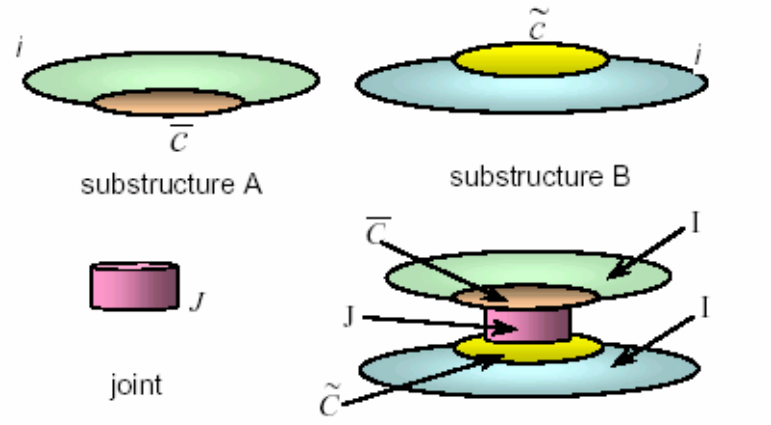

Figure 2-18 Elastic Joint with Substructure [Liu 2000]

Ren and Beards [Ren 1995] focused on the error effects on the joint identification. They also presented a mathematical formula used for elastic joint identification algorithm as well as measurement errors, which can decrease the accuracy of the identification results (Figure 2-19).

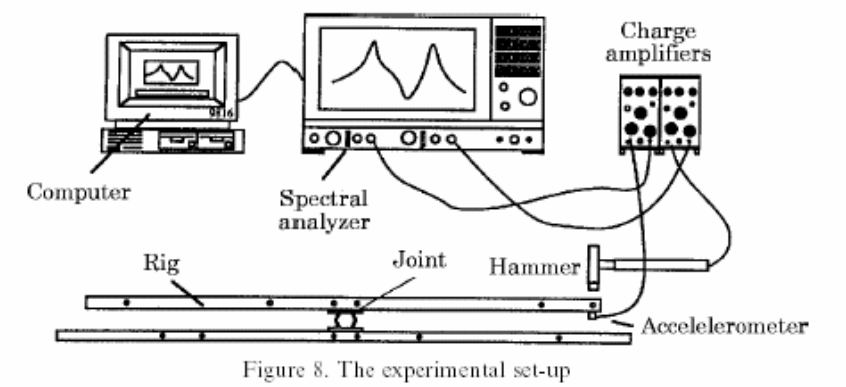

Figure 2-19 Experiment set-up for elastic joint by Ren and Beards [Ren 1995]

Wang and Chuang [Wang 2004] presented a mathematical model in order to minimize measurement errors in the FRFs for the joint identification. They showed that the inverse matrix of FRFs plays a significant role in prediction accuracy of the joint and minimized the errors numerically by selecting the best data set, which is evaluated by the error function.

The above methods considered only translational degree-of-freedom. The lack of rotational degree-of-freedom information can cause significant errors between predicted and measured FRFs on an assembled structure, especially if bending is involved [Park 2003].

Gialamas [Gialams 1996] also investigated the significance of the rotational degree of freedom (RDOF) system in substructuring by means of FRFs. They added the RDOF to the FRF substructuring synthesis, in order to correspond the predicted FRFs to measured FRFs on the assembled structure. Wang [Wang 2004] constructed a simple free-free system, consisting of two mass blocks joined by an elastic element, and identified the physical characteristics (i.e. stiffness and damping) of joints experimentally by including RDOF dynamics.

The dynamics of the joint play an important role of predicting the dynamics of the assembly. And it is difficult to evaluate the dynamics of the joint due to access limitation. Various researchers have tried to identify the joint dynamics through either analytical or experientially including RDOF. However, most cases are utilizing elastic materials as the joint in order to distinguish joint dynamics from the dynamics of the assembly.

2.3.2 Bolted and Welded Joint Dynamics

The most popular joints in mechanical systems are welding and fasteners such as a bolt. Ma [Ma 2001] modeled the bolted joint as a spring element and evaluated its dynamics based on the comparison of the overall dynamics of the bolted system to the unbolted system. They also investigated the non-linearity of the joint. Two simple cantilever beams are assembled with bolts. They varied the contacting areas on the joint by changing tightening forces. Wong and coworkers [Wong 1995] assumed the bolted connections to be semi-rigid joints in their work. It has been noted that the connection is a primary factor of hysteresis due to material damping and that its rigidity and hysteresis effect the overall dynamic response of the assembled system. However, the identified connection is modeled by a linear spring, which has a rotational and shear properties, with dynamic modal frequencies and mode shapes data and with static displacement data. Shen and Astaneh-Asl [Shen 2000] also modeled the bolt connection as a semi-rigid joint and performed cyclic tests on the connections in order to observe its hysteresis behaviors. The stiffness of the joints is obtained from the deformation and force graph. Song [Song 2004] adapted the multi-layer feed-forward (MLFF) neural network for the joint, which is a bolted connection in beam structures, parameter identification algorithm in order to overcome the inverse problem. However, the neural network needs the learning process to update the weighting in the hidden layers. It requires a lot of time and data sets by experiment or FE method to do so. Hanss and coworkers [Hanss 2002] discussed the modeling and identification of a bolted joint with normal load on the contact interface of two connected rods. In their work, the various natural frequencies and damping ratio due to non-linear property are averaged and only mean values are considered for the identification calculation. They tried to overcome the difficulty of modeling the damping of the joint by applying fuzzy algorithm.

Contrast to bolted type joints, the welded joint provides high static strength, improved fatigue strength, and better sealing performance [Darwish 2003]. However, the welded joint also does not act as a rigid connection either. Mottershead [Mottershead 1996] updated the finite element model consisting of two steel beams with a welded flange. The connection is assumed as non-rigid joints are modeled by uncertain parameters, which is

updated by minimizing the cost function. They focused on the effect of the weld joint to the global system rather than the identification of joint properties. Darwish [Darwish 2003] performed dynamic tests to obtain the natural frequencies of a system with welded joints. By comparing the amplitude of the FRFs, he showed that the weld-bonded joint has higher damping behavior than the spot-welded joints. Santos [Santos 2004] observed the overall quality and mechanical strength of the weld bonding of stainless steel with the numerical simulation by FEM and the tension shear testing.

2.3.3 Machine Tool Application of Joint Dynamics

Machining engineers have studied dynamics of a joint between a tool holder and a machine tool. Often the configuration of the machine tool is exchanged according to the machining process. For example, different size cutting tools are inserted into the tool holder. Due to the contact conditions, the dynamic properties of the tool holder assembly are changing. Schmitz [Schmitz 2000] used receptance coupling but considered only translational degree of freedom at the spindle portion of the substructure. The joint parameters were identified using iteration of the joint values until the measurement of a sample tool and model fitted. Park [Park 2003] presented the method for predicting the dynamics of the assembly between tool holder and tool, which include the translational and rotational degree of freedom, with receptance coupling by using the measured FRFs experimentally and analytically. The joints represent the discontinuity of the structure and influence the global dynamics of the system [Ibrahim 2005].

From the above literature, some efforts applied the receptance coupling techniques to the joint identification. The receptance coupling techniques have been developed by many researchers. They show the dynamic behavior of an assembled structure accurately based on a developed mathematical model [Maia 1997]. The tool and spindle are assembled by means of the receptance coupling techniques with TDOF and RDOF [Schmitz 2002] [Harris 1997].

2.4 Summary

The development of successful micro-mechanical cutting technologies will provide a catalyst for the broader development of micro-engineered systems. The investigation of micro-cutting processes is relatively new and further research is required to answer its many challenging questions. This chapter surveyed the current efforts in micro-mechanical machining research, monitoring micro cutting process, and joint identification.

Micro-mechanical machining is a promising fabrication method for creating high-accuracy miniaturized components, which are increasingly in demand for various industries. Micro-mechanical cutting is an enabling technology that can bridge the gap between the macro-and nano/micro-domain. The flexibility and efficiency of micro-end milling processes using carbide tools allow the fabrication of small batches compared with other processes. In some cases, the removal of material shows similar trends between the macro-and micro-machining processes, such as monitoring strategies and regenerative chatter. However, interfacing to the macro-domain has been a big challenge. In many instances, the direct scaling of macro-knowledge to the micro-domain was not successful.

Monitoring cutting condition is vital to maximize the efficiency of machining processes in both the micro and macro domain. Several different sensors are currently utilized to monitoring cutting condition; force sensor, spindle motor and acoustic emission (AE) sensors. Cutting force measurement is the most effective method for monitoring the state of machine tools and machining operations. However, due to the high spindle speed, the conventional force dynamometer does not satisfy the requirement of micro cutting forces measurement; high bandwidth of the sensor. In addition, detecting the micro tool wear and breakage is very challenge with existing equipment and techniques.

Understanding of the dynamic response of the micro system is prior to suppress chatter vibration. In order to evaluate the dynamics of either macro or micro machine tool system, the dynamic response of the joint must be identified. The majority of the joint identification methods relied on numerical simulations for static analysis to obtain the stiffness constants of the joints. Moreover, joints in the system cannot be easily tested experimentally, due to limited access; therefore, most joint identification procedures consider the identified parameters as deterministic values. If the joints can be separated, changes in boundary conditions alter the dynamics of joint parameters; and, the identified parameters of a joint in certain test environments cannot apply to other environments

Therefore, micro-mechanical machining requires extensive research in chip removal processes, cutting force predictions, material properties, sensing methods, and dynamic prediction in order to provide accuracy and productivity in micro-scales.

CHAPTER 3. JOINT IDENTIFICATION USING RECEPTANCE COUPLING

A micro-mechanical machining process is not designed for mass production. However, it has the ability to machine parts of complex geometry such as micro molds, which are key parts for mass micro-production. The key to good surface quality in micro milling operations is the minimization of tool chatter. This requires an understanding of the system dynamics; the system including both the micro milling tool and the micro milling structures.

The experimental modal analysis using impact hammer test is typically utilized in order to acquire the dynamics of the conventional machine tool. However, due to the miniature nature of micro end mills whose diameters are as small as 100 μm, the impact hammer testing cannot be applied directly to predict the dynamics at the tool tip. In addition, the micro machine tool can be modified easily by interchanging the structure having different functionalities. Whenever the configuration of the system is changed, the dynamics of the system is also changed. The experimental modal analysis [Altintas 2000] is a time consuming process to identify the dynamics of the newly assembled system each time.

However, if we are able to access the dynamics of the joints between machine tool and the tip of micro tool, or between the assembled system and the sub-systems, the dynamics of the micro machine tool can be identified through the combination of the joint dynamics and the dynamics of subsystem. For instant, depending on the workpiece geometry, various micro tools and machines are used. With dynamics of the joint between tools and machine tool, the dynamics of each configuration can be identified through several mathematical processes. Using the identified joint dynamics and receptance coupling techniques, engineers can predict dynamics of any machine tool and micro tool assembly with the database of the dynamics of each system and various joint. Once the database is set-up, engineers don't need to re-perform the experimental modal analysis in order to acquire the dynamics of the micro machining tool system. As a result, the receptance coupling technique with the identified joint dynamics allows increasing the productivity of the micro machining process due to minimize the chatter problem as well as

reduce the operating cost and time. Therefore, the reliable joint dynamics identification method must be investigated prior to considering the dynamics of the micro machine tool system.

The objective of this investigation is the development of a joint identification method using receptance coupling methods to obtain and evaluate the dynamic responses of various linear joints. In general, a system consists of different substructures with distinctive joints (or interfaces). The objective of mechanical joints is the transmission of forces and moments, alignment, and bonding between structures. Therefore, the response of the global system establishes the dynamic characteristics of each substructure. The joints, such as welds, bolts, rivets and bearings, between coupled substructures also play significant roles in the response of the global system, due to the differences in material properties, geometry, contact area and contact methods. Using Experimental modal analysis (EMA) and FE method, the dynamics of a fastener joint in several configurations are identified in order to verify the accuracy and effectiveness of the proposed method.

One of the concerns in this experimental analysis is that the measured data may be contaminated with surrounding noise, especially during assessment of the impact forces [Ibrahim 2005][Wang 2004]. The identified fastener joint dynamics from one structure are utilized to predict the dynamic characteristic of the other structure, which has the same joint but different substructures. By doing this, the method overcomes apparent discrepancies due to the deterministic dynamics of the identified joint. The technique enables designers to predict overall assembly dynamics. It also allows designers to optimize the design to enhance the dynamic performances of systems.

This chapter is organized in the following manner. First, this chapter presents a novel methodology for predicting the frequency response function FRF of the assembled system, with some necessary assumptions based on the receptance coupling techniques. Second, the difficulty of obtaining FRF in rotational degree of freedom (RDOF) is overcome through the combination of analytical and experimental methods. Third, the dynamic characteristics of a joint in both the translational degree of freedom (TDOF) and RDOF are obtained by the enhanced receptance coupling techniques. Fourth, the methodology's applications with experiments identifying the dynamic characteristics of the joint are demonstrated. At the end, this chapter concludes with possible applications and contributions of this approach.

3.1 Methodology

The frequency response functions (FRFs) of the structure play important roles in predicting the system behaviours and instability [Altintas 2000]. The essence of the proposed approach is the verification of the effects of joints by the comparison of FRFs between the dynamics of a rigid structure and a joined structure of identical dimensions. In this study, a classical receptance coupling technique [Park 2003][Ren 1995][Schmitz 2000][Schmitz 2002][Harris 1997] is enhanced by proposing a method to identify joint dynamics. Using receptance coupling, the dynamics of the joint can be expressed with simple algebraic equations of the receptance matrix, which were found with either experimental modal analysis or the finite element method. By doing that, the proposed approach requires less effort for mathematical processes (owing to RC) and increases the accuracy of identified joint dynamics (owing to EMA) compared to other identification methods (refer to section 2.3). Therefore, to identify the assembled dynamics, the receptance coupling method is used at every increment of frequency, along with the experimental measurements and FE data.

Figure 3-1 depicts the proposed joint identification approach. The identification method consists of two steps. The first step is to identify analytically the dynamics at Substructure A (i.e. tools), either through FE analysis or beam formulas, and the rotational dynamics of Substructure B (i.e. collet and spindle assembly). It is rather difficult to experimentally measure the dynamics of angular displacements by applying moments and forces at Substructure B; therefore, the rotational dynamic response of Substructure B is determined by substituting the direct and cross FRF measurements taken at the free end of the assembly and the rigid cylinder in the receptance coupling expressions, as explained in Park's work [Park 2003]. The second step is to acquire joint dynamics of the fastener joint by comparing the FRFs of the rigid system and the joined system. The joined system consists of two substructures: a spindle and a short rigid tool (Substructure B), whose dynamics are obtained experimentally through experimental modal analysis (EMA); and, an arbitrary tool (Substructure A), whose dynamics are obtained analytically through FE (finite element) analysis.

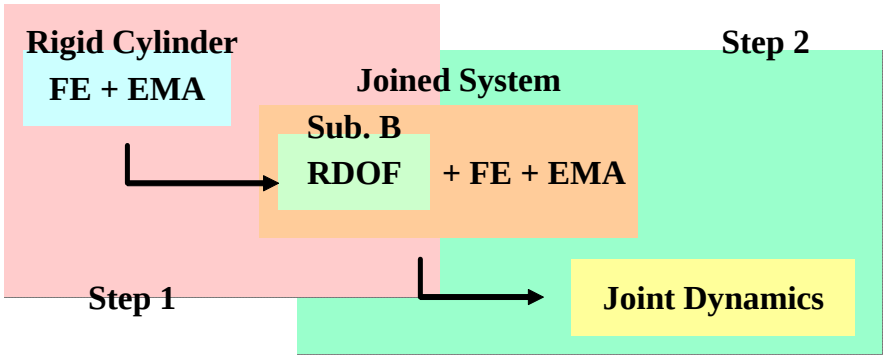

Figure 3-1 the Proposed Joint Identification Method

3.1.1 Receptance Coupling

Receptance is the relationship between the displacement, $x(\omega)$, of the system and the force, $F(\omega)$, in frequency domain based on the assumption that the response of the system is linearly elastic [Harris 1997]. The receptance coupling method enables two substructures to be joined, as shown in Figure 3-2 where f_1, f_2, f_3 and f_4 are applied forces; x_1, x_2, x_3 and x_4 are displacements; f_2^J, f_3^J, M_2^J and M_3^J are forces and moments at joint; and, k_x, k_θ, c_x and c_θ are stiffness and damping constants in TDOF and RDOF [Schmitz 2002][Song 2004]. Substructures A and B can represent any substructures that are connected by a joint. The relationship of the displacement and the force is characterized by the system FRF. The responses of the unassembled Substructures A and B are given by:

$$\begin{bmatrix} x_1 \\ x_2 \end{bmatrix} = \begin{bmatrix} H_{11} & H_{12} \\ H_{21} & H_{22} \end{bmatrix} \begin{bmatrix} f_1 \\ f_2 + f_2^J \end{bmatrix}$$
$$\begin{bmatrix} x_3 \\ x_4 \end{bmatrix} = \begin{bmatrix} H_{33} & H_{34} \\ H_{43} & H_{44} \end{bmatrix} \begin{bmatrix} f_3 + f_3^J \\ f_4 \end{bmatrix} \quad (3\text{-}1)$$

where, H_{ij} is the FRF of the substructures. Subscripts i and j indicate the location of the displacement and force, respectively.

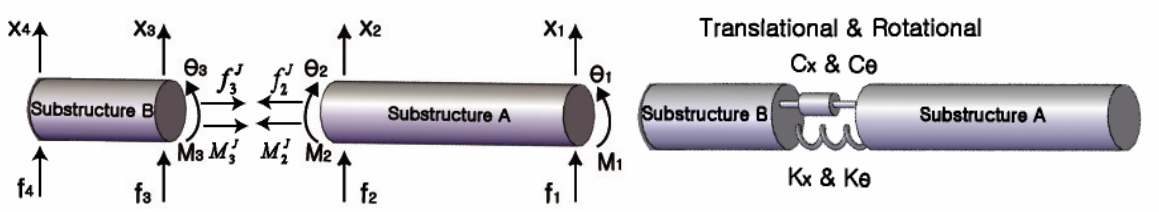

Figure 3-2 Receptance Coupling of Two Substructures

Two substructures are assembled together by a joint, which is expressed by stiffness, damping, and mass elements. The assembled system is displayed in Figure 3-2. The equilibrium and compatibility conditions at the joint must be satisfied in the assembled structure, as shown in Equations (3-2) and (3-3), respectively.

$$f_2^J + f_3^J = 0, \;\; M_2^J + M_3^J = 0 \tag{3-2}$$

$$\begin{aligned} m(\ddot{x}_3 - \ddot{x}_2) + c(\dot{x}_3 - \dot{x}_2) + k(x_3 - x_2) &= f_2^J, \\ m(\ddot{\theta}_3 - \ddot{\theta}_2) + c(\dot{\theta}_3 - \dot{\theta}_2) + k(\theta_3 - \theta_2) &= M_2^J \end{aligned} \tag{3-3}$$

where, m or J, k and c represent the mass, stiffness, and damping matrices of the joint, respectively. By applying the Laplace transform to Equation (3-3), we can obtain Equation (3-4) as:

$$\begin{aligned} \begin{bmatrix} (x_3 - x_2) \\ (\theta_3 - \theta_2) \end{bmatrix} &= \begin{bmatrix} \dfrac{1/m}{s^2 + 2\zeta_{ff}\omega_{n,ff} + \omega_{n,ff}^{\;2}} & 0 \\ 0 & \dfrac{1/m}{s^2 + 2\zeta_{mm}\omega_{n,mm} + \omega_{n,mm}^{\;2}} \end{bmatrix} \begin{bmatrix} f_2^J \\ M_2^J \end{bmatrix} \\ &= \begin{bmatrix} h_{ff}^J & 0 \\ 0 & h_{mm}^J \end{bmatrix} \begin{bmatrix} f_2^J \\ M_2^J \end{bmatrix} = \left[H^J\right] \begin{bmatrix} f_2^J \\ M_2^J \end{bmatrix} \end{aligned} \tag{3-4}$$

where, H^J represents the translational and rotational joint dynamics. In this research, cross-coupled properties (i.e. h_{fm}^J and h_{mf}^J) of the joint between TDOF and RDOF dynamics are assumed to be zero. It has already been verified by Wang [Wang 1990] through simulations that the cross-coupled terms of joints (i.e. h_{fm}^J and h_{mf}^J) have no significant effect on the response of the assembled system. The performance of the proposed algorithm can

effectively be improved by excluding the cross-coupled properties of the joint and reducing the computational time on the analysis of the dynamics of the machine tool system.

Substituting Equations (3-1) and (3-2) into Equation (3-4) leads to Equation (3-5):

$$f_2 = -B^{-1}H_{21}f_1 - B^{-1}H_{22}f_2 + B^{-1}H_{33}f_3 + B^{-1}H_{34}f_4 \tag{3-5}$$

The matrix $B = (H_{22} + H_{33} + H^J)$ must be invertible, which suggests the determinant of the matrix is not zero. By substituting Equation (3-5) into Equation (3-1), the FRF matrices for the assembled structure are constructed as:

$$\begin{bmatrix} X_1 \\ X_2 \\ X_3 \\ X_4 \end{bmatrix} = \begin{bmatrix} G_{11} & G_{12} & G_{13} & G_{14} \\ G_{21} & G_{22} & G_{23} & G_{24} \\ G_{31} & G_{32} & G_{33} & G_{34} \\ G_{41} & G_{42} & G_{43} & G_{44} \end{bmatrix} \begin{bmatrix} F_1 \\ F_2 \\ F_3 \\ F_4 \end{bmatrix}$$
$$= \begin{bmatrix} H_{11} - H_{12}B^{-1}H_{21} & H_{12} - H_{12}B^{-1}H_{22} & H_{12}B^{-1}H_{33} & H_{12}B^{-1}H_{34} \\ H_{21} - H_{22}B^{-1}H_{21} & H_{22} - H_{22}B^{-1}H_{22} & H_{22}B^{-1}H_{33} & H_{22}B^{-1}H_{34} \\ H_{33}B^{-1}H_{21} & H_{33}B^{-1}H_{22} & H_{33} - H_{33}B^{-1}H_{33} & H_{34} - H_{33}B^{-1}H_{34} \\ H_{43}B^{-1}H_{21} & H_{43}B^{-1}H_{22} & H_{43} - H_{43}B^{-1}H_{33} & H_{44} - H_{43}B^{-1}H_{34} \end{bmatrix} \begin{bmatrix} F_1 \\ F_2 \\ F_3 \\ F_4 \end{bmatrix} \tag{3-6}$$

where, G_{ij} represents the FRF of the assembled system.

From Equation (3-6), the FRF matrix of any points in Figure 3-2 can be determined. As a result, the FRF matrices of each substructure are required to construct the matrix of Equation (3-6). The FRF matrix can be acquired by experimental modal analysis (EMA) or the FE (finite element) method. In the receptance coupling, the FRF in RDOF is a critical element [Park 2003]; therefore, the FRF matrix of the each substructure is represented by translational displacement (x) as well as rotational displacements (θ) with force (f) and moment (M), as shown in Figure 3-2. Therefore:

$$\begin{bmatrix} x_1 \\ \theta_1 \end{bmatrix} = \begin{bmatrix} h_{11,ff} & h_{11,fm} \\ h_{11,mf} & h_{11,mm} \end{bmatrix} \begin{bmatrix} f_1 \\ M_1 \end{bmatrix} \Rightarrow \{X_1\} = [G_{11}]\{F_1\} \tag{3-7}$$

$$\begin{bmatrix} x_1 \\ \theta_1 \end{bmatrix} = \begin{bmatrix} h_{12,ff} & h_{12,fm} \\ h_{12,mf} & h_{12,mm} \end{bmatrix} \begin{bmatrix} f_2 \\ M_2 \end{bmatrix} \Rightarrow \{X_1\} = [G_{12}]\{F_2\}$$

By substituting Equation (3-7) into Equation (3-6), the FRF of Locations 1 and 2, which includes the translational and rotational degrees-of-freedom, are obtained as:

$$\begin{bmatrix} G_{11,ff} & G_{11,fm} \\ G_{11,mf} & G_{11,mm} \end{bmatrix} = \begin{bmatrix} h_{11,ff} & h_{11,fm} \\ h_{11,mf} & h_{11,mm} \end{bmatrix} - \begin{bmatrix} h_{12,ff} & h_{12,fm} \\ h_{12,mf} & h_{12,mm} \end{bmatrix} \begin{bmatrix} b_{ff} & b_{fm} \\ b_{mf} & b_{mm} \end{bmatrix}^{-1} \begin{bmatrix} h_{21,ff} & h_{21,fm} \\ h_{21,mf} & h_{21,mm} \end{bmatrix}$$
$$\begin{bmatrix} G_{12,ff} & G_{12,fm} \\ G_{12,mf} & G_{12,mm} \end{bmatrix} = \begin{bmatrix} h_{12,ff} & h_{12,fm} \\ h_{12,mf} & h_{12,mm} \end{bmatrix} - \begin{bmatrix} h_{12,ff} & h_{12,fm} \\ h_{12,mf} & h_{12,mm} \end{bmatrix} \begin{bmatrix} b_{ff} & b_{fm} \\ b_{mf} & b_{mm} \end{bmatrix}^{-1} \begin{bmatrix} h_{22,ff} & h_{22,fm} \\ h_{22,mf} & h_{22,mm} \end{bmatrix} \quad (3\text{-}8)$$

where,

$$\begin{bmatrix} b_{ff} & b_{fm} \\ b_{mf} & b_{mm} \end{bmatrix}^{-1} = \left\{ \begin{bmatrix} h_{22,ff} & h_{22,fm} \\ h_{22,mf} & h_{22,mm} \end{bmatrix} + \begin{bmatrix} h_{33,ff} & h_{33,fm} \\ h_{33,mf} & h_{33,mm} \end{bmatrix} + \begin{bmatrix} h_{ff}^J & 0 \\ 0 & h_{mm}^J \end{bmatrix} \right\}^{-1} \quad (3\text{-}9)$$

where, h_{ff}^J (translation) and h_{mm}^J (rotation) describe the dynamic characteristics of the joint.

The assembled dynamics, which have the joint dynamics in TDOF and RDOF, are formulated with the receptance matrix of each substructure (A, B) based on the equilibrium and compatibility conditions. As a result, the joint dynamics can be calculated from the above equations with the dynamics of each substructure and the assembled structure.

3.1.2 Finding the RDOF Responses at Substructure B

When the assembled structure is excited, inertia is expected due to the rotation or bending around the joint; therefore, RDOF at the assembled joint cannot be neglected for accurate receptance coupling [Park 2003]. To determine RDOF responses experimentally is very difficult [Song 2004][Hanss 2002], due to the inability to measure rotational displacements accurately. Often, designers ignore the rotational dynamics during the substructure coupling process; however, this negation of RDOF responses leads to severe inaccuracy in the coupled dynamics. To overcome the difficulties associated with

measuring the RDOF responses, the authors have proposed indirect methods to obtain the rotational dynamics at Location 3 in Figure 3-2, based on gauge blank cylinders as described in [Park 2003]. This identification first considers the joint between the substructure as rigid by assuming the h^J_{ff} (translation) and h^J_{mm} (rotation) terms are equal to zero and, then, indirectly identifies the rotational dynamics at the free end of Substructure B ($h_{33,fm} = h_{33,mf}, h_{33,mm}$), as illustrated in [Park 2003]. Consequently, the FRFs (the h_{33} term in Equation (3-9)) of Location 3 in Figure 3-2 can be completed after acquiring $h_{33,ff}$, by performing an impact hammer test at that location. Therefore, the RDOF responses become as:

$$\begin{aligned} h_{33,mf} &= b_{mf} - h_{22,mf} \\ h_{33,mm} &= b_{mm} - h_{22,mm} \end{aligned} \tag{3-10}$$

3.1.3 Finding Joint Dynamics

In Equation (3-9), all the FRF matrix elements in the RDOF and TDOF responses for Substructures A and B, except the joint dynamics, are obtained through either EMA or the FE method. The elements in the first row and first column of matrices $[G_{11,ff}]$ and $[G_{12,ff}]$ can be measured directly from the EMA of the assembled system. By doing so, there are two equations (Equations (3-11) and (3-12)) and two unknown parameters (b_{ff} and b_{mm} in Equation (3-9)):

$$G_{11,ff} = \frac{x_1}{f_1} = h_{11,ff} - \frac{1}{b_{ff}b_{mm} - b_{mf}b_{fm}}[(h_{12,ff}b_{mm} - h_{12,fm}b_{mf})h_{21,ff} + (-h_{12,ff}b_{fm} + h_{12,fm}b_{ff})h_{21,mf}] \tag{3-11}$$

$$G_{12,ff} = \frac{x_2}{f_2} = h_{12,ff} - \frac{1}{b_{ff}b_{mm} - b_{mf}b_{fm}}[(h_{12,ff}b_{mm} - h_{12,fm}b_{mf})h_{22,ff} + (-h_{12,ff}b_{fm} + h_{12,fm}b_{ff})h_{22,mf}] \tag{3-12}$$

Using the symbolic nonlinear analytical toolbox [Matlab™ 2001], b_{ff} and b_{mm} can be identified based on the following two equations:

$$u = a + \frac{f(-\beta\sigma + ek) + c(-\beta e + \delta\sigma)}{\beta^2 - \delta k} \tag{3-13}$$

$$v = \sigma + \frac{g(-\beta\sigma + ek) + d(-\beta e + \delta\sigma)}{\beta^2 - \delta k} \tag{3-14}$$

where, $G_{11,ff} = u,\ G_{12,ff} = v,\ h_{11,ff} = a,\ h_{12,ff} = \sigma,\ h_{21,ff} = c,$
$h_{22,ff} = d,\ h_{12,mf} = e,\ h_{21,mf} = f,\ h_{22,mf} = g,\ b_{ff} = k,\ b_{mf} = \beta,\ b_{mm} = \delta$

From Equations (3-13) and (3-14), $b_{ff} = k$ and $b_{mm} = \delta$ can be derived. As a result, the dynamics of the joint, h_{ff}^J (TDOF) and h_{mm}^J (RDOF), can be obtained as:

$$H^J = \begin{bmatrix} h_{ff}^J & 0 \\ 0 & h_{mm}^J \end{bmatrix} = \begin{bmatrix} b_{ff} - (h_{22,ff} + h_{33,ff}) & 0 \\ 0 & b_{mm} - (h_{22,mm} + h_{33,mm}) \end{bmatrix} \tag{3-15}$$

The joint dynamics are considered to be time-invariant parameters, which can be described by the FRF. Then, a curve-fitting algorithm is employed to identify the modal parameters of the joints that can be stored in a database for coupling of arbitrary dynamics in the FE analysis. Using modal analysis, the dynamic responses shown in Equation (3-16), such as modal mass, damping ratio and stiffness, can be obtained.

$$\begin{aligned} h_{ff}^J(j\omega) &= \frac{x}{F} = \sum_{i=1}^{kk} \frac{1/m_i}{j\omega^2 + 2\zeta_{ff,i}\omega_{n,ff,i} j\omega + \omega_{n,ff,i}^2} = \sum_{i=1}^{kk} \frac{\omega_{n,i}^2 / k_i}{j\omega^2 + 2\zeta_{ff}\omega_{n,i,ff} j\omega + \omega_{n,i,ff}^2} \\ h_{mm}^J(j\omega) &= \frac{\theta}{M} = \sum_{i=1}^{kk} \frac{1/J_i}{j\omega^2 + 2\zeta_{mm,i}\omega_{n,mm,i} j\omega + \omega_{n,mm,i}^2} = \sum_{i=1}^{kk} \frac{\omega_{n,i}^2 / k_i}{j\omega^2 + 2\zeta_{mm,i}\omega_{n,mm,i} j\omega + \omega_{n,mm,i}^2} \end{aligned} \tag{3-16}$$

Consequently, we are able to understand how the joint may affect the response of the assembled structure, when forces excite the assembled structure. Figure 3-3 depicts the algorithm of the proposed joint identification approach. At first, RDOF at the joint of Substructure B are obtained by coupling receptances of two blank cylinders. The receptance coupling method then extracts joint dynamics from the measured dynamics of the assembled cylinder from EMA with FRFs of Substructure A from FEM.

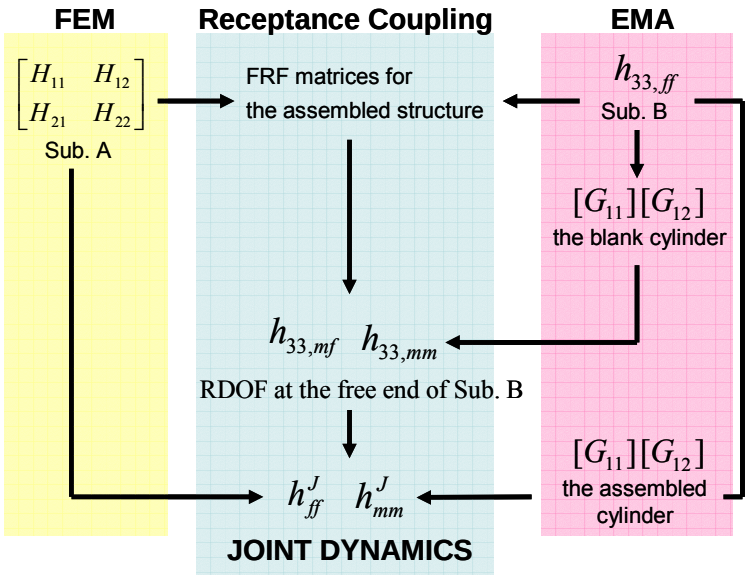

Figure 3-3 Algorithm of the Joint Identification Method

3.2 Experiment and Results

To demonstrate the feasibility of the joint identification algorithm, EMA was performed to acquire the FRFs by impacting the structure and measuring the vibration responses. In addition, FE analysis (Timoshenko beam theory) was performed to acquire the information on arbitrary Substructure A. Based on that information, an analytic extraction of rotational dynamics at the interface of the modular component was executed; and, the dynamic characteristics of the joint were retrieved (Figure 3-3).

The test structures were fabricated with aluminum (6061T6511; Young's modulus: 6.89E9 N/m^2; density: 2700 kg/m^3; damping coefficient: 0.012; diameter: 19.95 mm) and steel (ASTM A108; Young's modulus: 200E9 N/m^2; density: 7872 kg/m^3; damping coefficient: 0.012; diameter: 19.95 mm). The dimensions of the cylinders, with and without the joint, were identical. The joint used was a fastener, which is one of the most common joining methods in mechanical structures. In order to increase the joint effect in the dynamic characteristics of the assembly, a steel washer was inserted between the substructures.

In order to define the dynamics of the joints, the FRF sets were required. Figure 3-4 illustrates the experimental setup to acquire the FRFs of a machine tool assembly. The tests

were performed under two different boundary conditions: free-free, and machine tool assembly. These experiments were able to show the accuracy and effectiveness of the proposed algorithm. For the free-free boundary condition, the test configuration is identical to that shown in Figure 3-4, except for the collet and spindle.

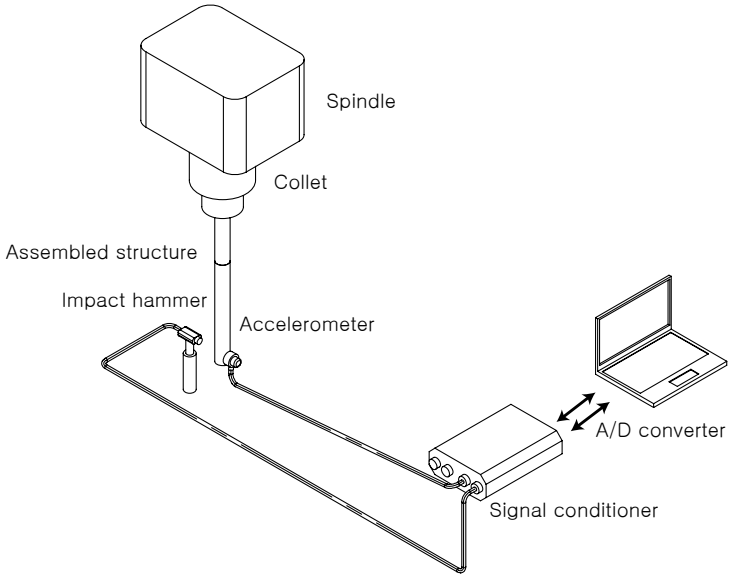

Figure 3-4 Experimental Test Setup

The structure was excited with an impact hammer (Dytran 58008L), and the response was measured by an accelerometer (Kistler 8778A500) with a mass of 0.29 g. The mass of the accelerometer may affect the measured natural frequencies of the system; therefore, the size of the accelerometer was chosen carefully.

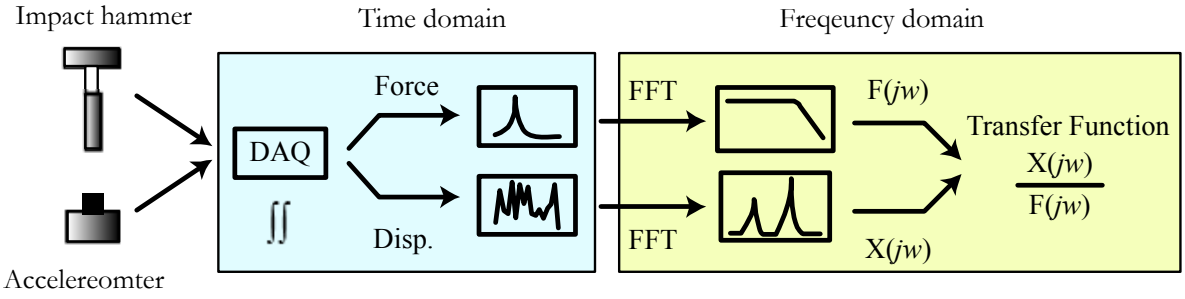

Figure 3-5 Block diagrams of Experiment Modal Analysis (EMA)

Figure 3-5 shows the procedures of the dynamic identification of the system using

EMA. Both signals were fed to a signal conditioner, which had an anti-aliasing filter. The filtered signals were converted from continuous to discrete type by an A/D converter. In this test, only two channels were used to acquire the signals from force and displacement transducers. The converted signals were transformed from the time domain to the frequency domain by the discrete Fourier transform algorithm. From the acquired signals, the transfer functions could be obtained in the frequency domain [Altintas 2000][Harris 1997]:

$$H(j\omega)_{pq} = \frac{F(j\omega)_q}{X(j\omega)_p} \tag{3-15}$$

where, p and q represent the locations of the displacement and force transducers.

The inherent measurement noise can affect the joint dynamics that are to be identified [Wang 2004]. Further, the inconsistent pole position during measurement can make the prediction very irregular; therefore, consistency in pole positions is necessary. These problems are corrected by the methods of curve fitting and averaging the fitted data [Tsai 1988]. To minimize the measurement noise (errors), the impact hammer tests were performed at the same location, at least seven times, and averaged. The measurement data were acquired under a specific sampling rate (100 kHz). By choosing a high sampling rate and the anti-aliasing filtering, the aliasing effect could be eliminated. The minimum-phase frequency region of the structure dynamics may also decrease the accuracy of the proposed method due to non-minimum phase zeros in the transfer function [Spector 1990].

The experiments are able to show the accuracy and effectiveness of the proposed algorithm. The joint dynamics is identified by the proposed identification method with data from the experiments and the analytical FE method. Based on the obtained joint dynamics, Substructure B can be mathematically coupled with the new Substructure A, which has arbitrary dimensions and materials.

3.2.1 Free-free Boundary Condition

The impact hammer test under free-free boundary conditions is able to show the role of joint dynamics in the dynamic characteristics of the whole structure and to verify the method proposed in this research, by predicting the dynamic characteristics of another substructure assembled with the same joint conditions. Substructure B (152.4 mm in

length) was suspended in air by two flexible strings at Location 4 (Figure 3-2). A fastener, with a steel washer applied, was used to assemble to Substructure A (127 mm in length). Three different test configurations were prepared for impact hammer tests: i) a Substructure B for H_{33ff}; ii) a rigid cylinder without any joint, in order to extract analytically the rotational dynamics at the free end of Substructure B ($h_{33,fm} = h_{33,mf}$, $h_{33,mm}$); and, iii) a cylinder with a fastener joint for $[G_{11}]$ and $[G_{12}]$. Through Equations (3-12) and (3-13), the joint dynamics were identified. After that, a 152.4 mm rod replaced the 127 mm rod as Substructure A and the FRF of [G11] was measured for comparison with the predicted FRF.

In this experiment, the effects of the joint on the assembled structure were examined. The dynamic responses of each cylinder, one blank cylinder (152.4 mm in length, Substructure B) and two assembled cylinders (152.4 mm and 127 mm in length, Substructure A), were obtained with the impact hammer test under identical test configurations. The joint dynamics extracted from the assembled cylinders (127 mm in length, Substructure A) was used to predict the dynamic responses of the assembled cylinder (152.4 mm in length, Substructure A; dash-dot lines) at Location 1 (G_{11}) shown in Figure 3-6.

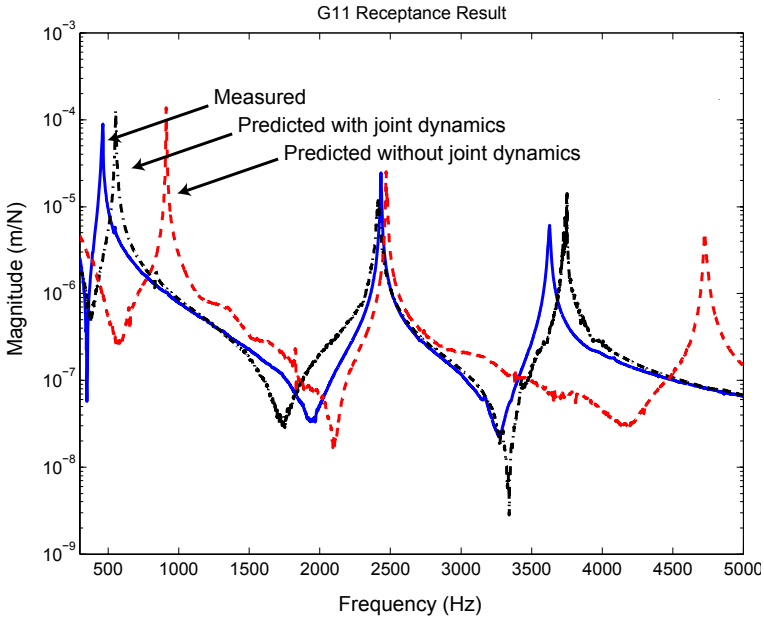

Figure 3-6 Comparisons between Measured Frequency Responses of each Cylinder at G_{11}

The deviations of the dynamic responses of each cylinder were observed. The solid lines are the experimentally measured FRF results of the assembled cylinder. The

differences (over 100 % at the first mode, around 450 Hz; about 33 % at the third mode, around 3500 Hz) in the dynamic responses between the blank cylinder (predicted without joint dynamics – dashed lines) and the assembled cylinder (predicted with joint dynamics – dash-dot lines) were caused by the dynamic characteristics of the joint. The blank cylinder had a higher natural frequency than the assembled cylinders.

The result suggests that the presence of the joint reduced the stiffness (k) of the system. Further, deviations in the magnitude ($1/(2k\zeta)$) at the mode of FRF were also observed. The system with the higher damping (ζ) had the lower magnitude in dynamic response; therefore, the bolted joint had higher damping, because the interfaces between two substructures were not fully connected. When the bolted joint was forced, slippage at the contact area occurred and friction, which results in energy loss, was generated. Thus, the joint plays a significant role in the dynamic characteristics of the assembly especially for that prediction. However, the experimental results have shown errors in the prediction of the assembly dynamics with the identified joint dynamics (Figure 3-6). They may have been caused by some noise from equipment, measurement techniques or the assumptions that the joint dynamics are linear.

3.2.2 Fastener Joint Dynamics Identification

To show that the proposed method is viable, another experiment was carried out under new boundary conditions. Considering the particular test environment in this work, the system can represent a machine tool; therefore, Substructure A can represent a drill, end mill, etc.; and, Substructure B can represent a tool holder or spindle of a computer numerically controlled (CNC) machine. The length of the cylinder structure without a joint was 304.8 mm, including the segment (30 mm) inserted in the collet of the mechanical chuck, as shown in Figure 3-7. The fastener was positioned firmly with sufficient torque to prevent the hysteresis effect [Kim 2001], so that the effect of the joints would reflect on the differences of the FRF of the structures.

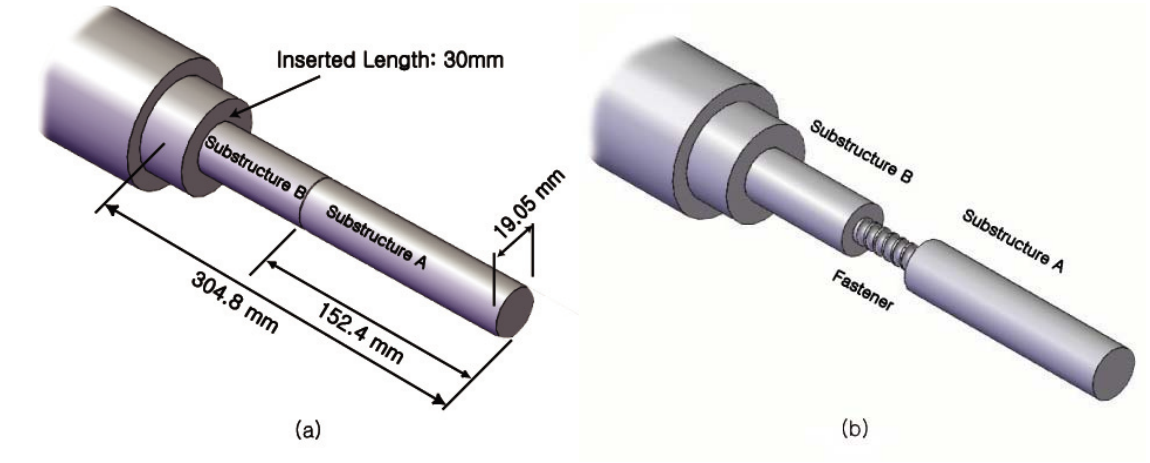

Figure 3-7 Dimensions and Joint method of the test structures: (a) dimensions of the system, (b) fastener joint

It is impractical to measure the FRF of Substructure B at Location 4 ($\frac{x_4}{f_4}$) in this boundary condition because it is inserted into the spindle, as shown in Figure 3-7. Fortunately, the proposed joint identification does not require a full set of FRFs of each substructure (Equations (3-10)-(3-14)). However, RDOF responses ($h_{33,mf}$ and $h_{33,mm}$) at Location 3 were required prior to the evaluation of the joint dynamics. EMA were performed at Location 3 in Substructure B, and the element, $h_{33,ff}$ (Figure 3-1), in the transfer function matrix was obtained. In the same manner, in Equation (3-6), [G_{11}] and [G_{12}] of the rigid cylinder without a joint were measured. It led to RDOF of Location 3 of Substructure B. Similarly, the impact tests were performed on the assembled cylinder (127 mm, Substructure A). Locations 1 and 2 of the assembled structure were excited by the impact hammer to acquire [G_{11}] and [G_{12}] (with joint), which were substituted into Equations (3-10) and (3-11) with Equation (3-9). As a result, from Equations (3-12) and (3-13), the dynamics of the joint, h^J_{ff} (TDOF) and h^J_{mm} (RDOF), were determined. With the identified dynamic characteristics of the joint, the FRFs of the newly assembled cylinder (152.4 mm, Substructure A) were predicted.

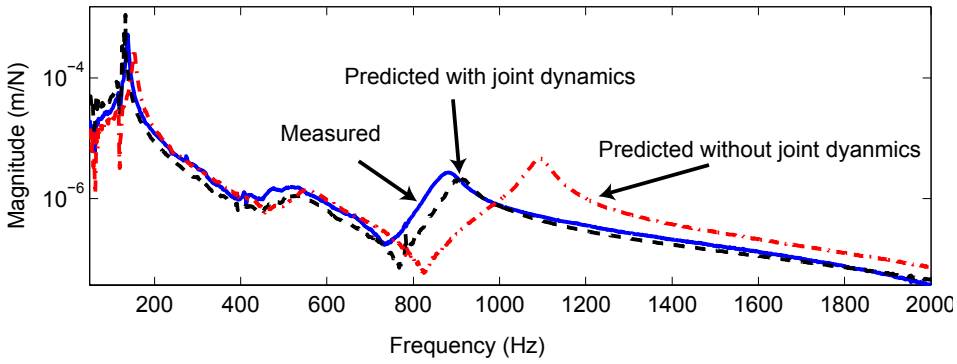

Figure 3-8 The comparison of FRFs at Location1: steel rod

Figure 3-8 presents a good match (less than 5% at the natural frequencies) between the measured and predicted FRF responses of the new assembled cylinder. It also depicts that the prediction without joint dynamics generates a deviation with the measured FRF, especially at high frequency regions (around 1000 Hz). This may be caused by neglecting of the mass effect of the joint [Tsai 1988][Wang 2004]. Figure 3-8 also shows a distinct feature that the system with the joint had a higher magnitude than the blank cylinder at the dominant mode in this particular system. This phenomenon may be due to the machine tool. The damping at the joint was too small to change the dynamic characteristics of the system; therefore, the stiffness as well as the mass of the joint became more dominant in the overall dynamic characteristics of the assembly in this particular test. The identified joint dynamic characteristics are shown in Figure 3-9.

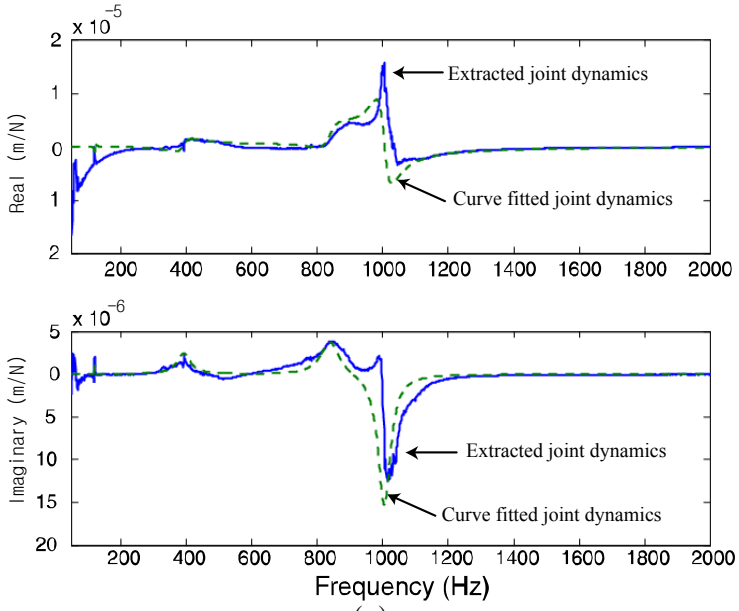

(a)

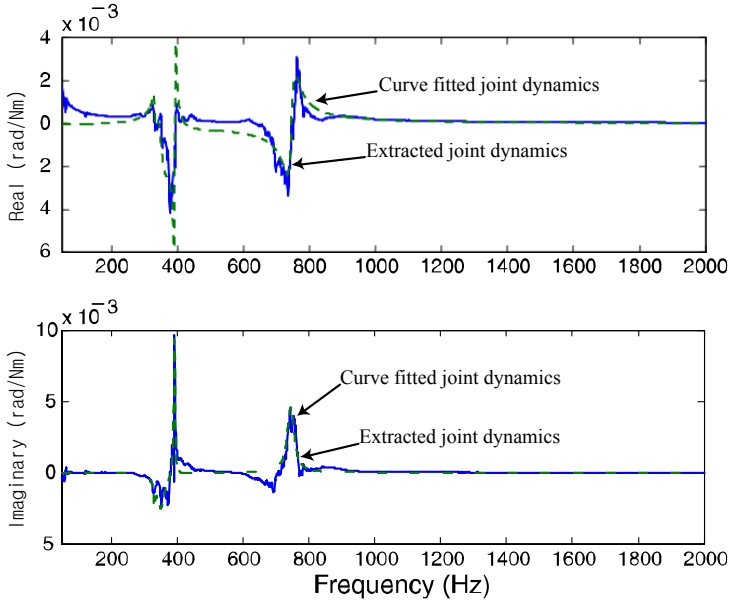

(b)

Figure 3-9 Identified Frequency Response of the Steel Fastener Joint: (a) TDOF: h_{ff}^{J}, (b) RDOF: h_{mm}^{J}

Four dominant modes of the joint FRF were selected. The upper and lower boundaries and the algorithm were nonlinearly curve fitted using the algorithm [Harris 1997].**Error! Reference source not found.** depicts the identified modal parameters of the fastener joint dynamics. The parameters are identified based on an identification algorithm developed in-house [Altintas 2000].

Table 3-1 The Identified Joint Dynamics expressed in Modal Mass, Modal Stiffness, and Modal Damping

	TDOF: h_{ff}^{J}				RDOF: h_{mm}^{J}			
Natural frequency ω_n (Hz)	121.5	393	840	1005	331	351	392	745
Modal stiffness k (N/m), (J/θ)	3.25e6	6.25e7	2.97e6	1.4e6	3.33e4	4.87e3	8.63e3	6.39e3
Modal Damping ratio ζ	0.064	0.004	0.042	0.023	0.01	0.041	0.006	0.017

3.2.3 Utilization of the Identified Joint Dynamics

In order to show the example for the utilization of the identified joint dynamics, the FRF of the assembled aluminum cylinder (152.4 mm, Substructure A) was predicted with

the identified joint dynamics from the steel cylinder assembly. The dynamic differences in the assembled cylinders depend also on the material properties of the substructures. The assembled aluminum cylinder (152.4 mm in length, Substructure A) consisted of the same joint (fastener) and boundary condition (machine tool assembly). In this case, only RDOF were extracted from the measured FRFs of the blank aluminum cylinder with the measured element, $h_{33,ff}$, of aluminum Substructure B. Figure 3-10 depicts the predicted and measured frequency response functions of the assembled aluminum cylinder (152.4 mm, Substructure A).

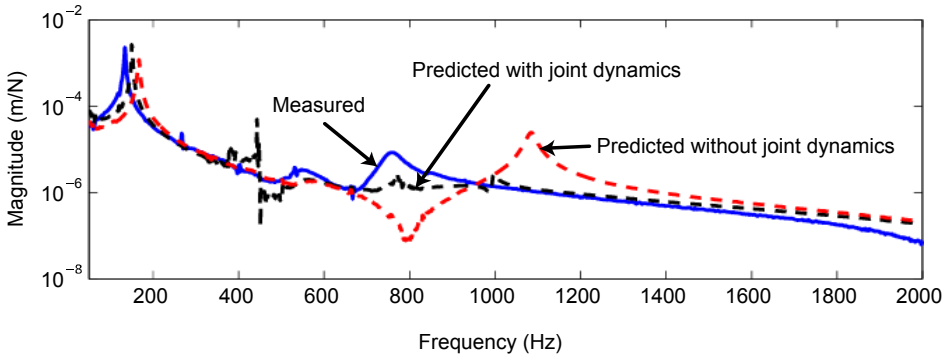

Figure 3-10 Predicted Frequency Response of the Aluminum Assembled Cylinder (152.4 mm, Substructure A)

The deviations of FRF in frequency and magnitude at the first mode between the predicted and measured values were approximately 3% and 15%, respectively. It can be seen that the agreement of the magnitude deteriorates at high frequency (around 800 Hz). However, the frequency of the assembled aluminum cylinder with the joint dynamics was predicted well compared to the cylinder without the joint dynamics at that frequency region. These differences were mainly caused by measurement errors, which may have been amplified during the inversion processes. Since the proposed joint identification method is based on experimental data, the existence of measurement noise is inevitable; hence, the filtering algorithm (i.e. Savitzky-Golay filter [Flannery 1992]) or curve fitting of individual FRF data may be necessary. However, it is very difficult to curve fit these curves at low frequencies, if the noise plays an important role in that region [Duarte 2000]. Also, manufacturing errors at the interface with the fastener joint between the steel rod and

aluminum rod may have led to discarding of the data from the analytical FE method. In addition, the linear assumption for the joint dynamics contributes to this error, since the friction between the two surfaces may be nonlinear and may induce a hysteresis phenomenon [Shen 2000].

3.2.4 Applications

Today's manufacturing industries are faced with many challenges in order to respond to diverse market demands. Cutting tools are becoming more complex to accommodate demand, and their life cycle periods are getting shorter. To preserve competitive performance in machining processes, the tool manufacturers have introduced a modular cutting tool (Figure 3-11).

Figure 3-11 Modular Cutting Tool (Mitsubishi Materials Co.)

The prediction of modular structure dynamics is important, especially for machining operations where identification of chatter-free cutting conditions are paramount to productivity. The proposed method is able to evaluate the dynamic properties of the modular machine tool. Once the joint dynamics of a modular cutting tool are identified by the proposed approach, the dynamic characteristics of the modular structure with cutters of any size can be accurately predicted. The interchangeable cutters in Figure 3-12 and the carbide cylinder blank (120 mm in length) in Figure 3-11 were used as Substructures A and B, respectively, to demonstrate the application of the proposed method. Each Substructure A without a joint (fastener part) was divided into 10 disk elements for the FE model. The carbide cylinder blank was inserted 40 mm into the collet.

(a) (b) (c)

Figure 3-12 Interchangeable Calibration Cutters and Cutting Cutter: (a) 50 mm length, 13 mm diameter calibration cutter; (b) 30 mm length, 13 mm diameter calibration cutter; (c) two-fluted cutting cutter with 16 mm tool diameter**.**

Using the 50 mm calibration cutter (Figure 3-12 a), the joint dynamics were identified through the algorithm of the proposed joint identification method (Figure 3-3). In order to extract RDOF at the free end of Substructure B (120 mm length), the carbide cylinder blank (170 mm length) was used as the blank cylinder in Figure 3-3.

Because the proposed method directly uses the measured translational FRF, small measurement errors may result in large disagreement between the measured and predicted FRFs of the modular machine tool assembly. In this case, the Savitzky-Golay filter was used to minimize measurement errors, which are represented as noise in frequency data. This filter is also called a digital smoothing polynomial filter or a least squares smoothing filter [Matlab^{TM} 2001]. The identified joint dynamics are depicted in Figure 3-13.

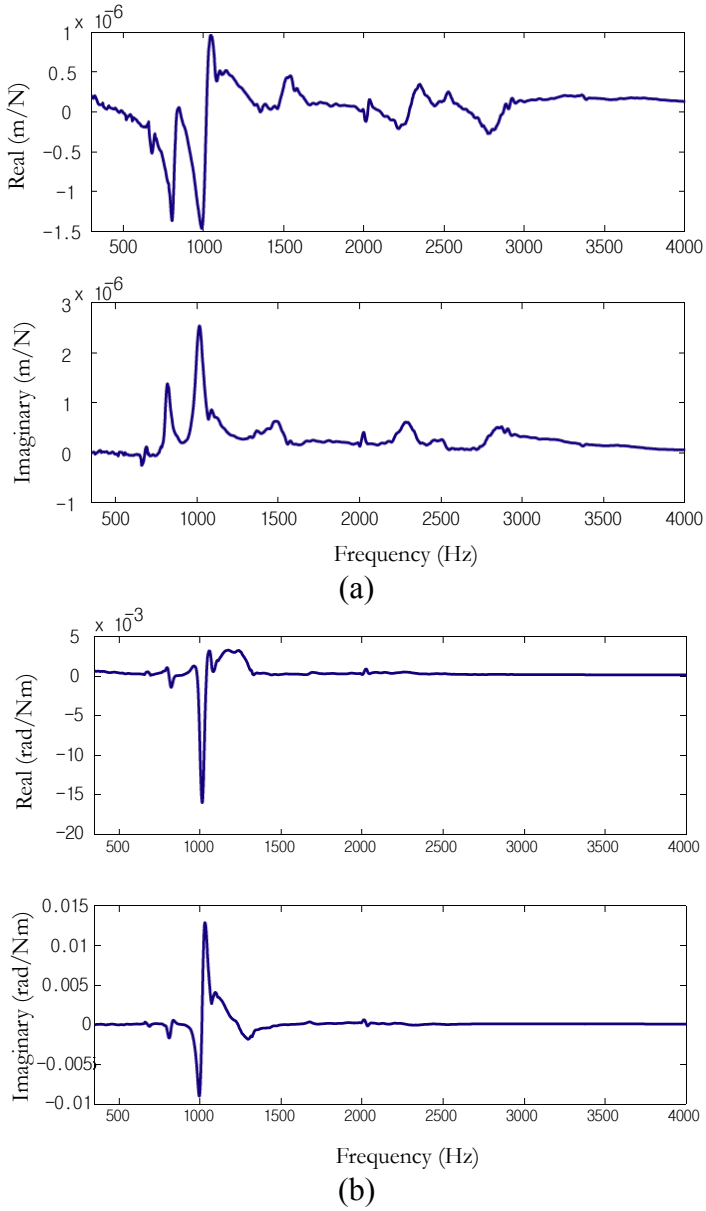

Figure 3-13 Identified Frequency Response of Modular Tool Joint from 50 mm Calibration Cutter ((a) in Figure 3-12): (a) TDOF: h_{ff}^{J} , (b) RDOF: h_{mm}^{J}

Using the identified joint dynamics from the 50 mm calibration cutter (Figure 3-12a), the dynamics of the modular tool assembly, with the 30 mm calibration cutter (Figure 3-12b) at the cutter end (G_{11}), were predicted, as shown in Figure 3-14. The accuracy of the prediction is good for the entire frequency range. The dominant mode was around 1250 Hz.

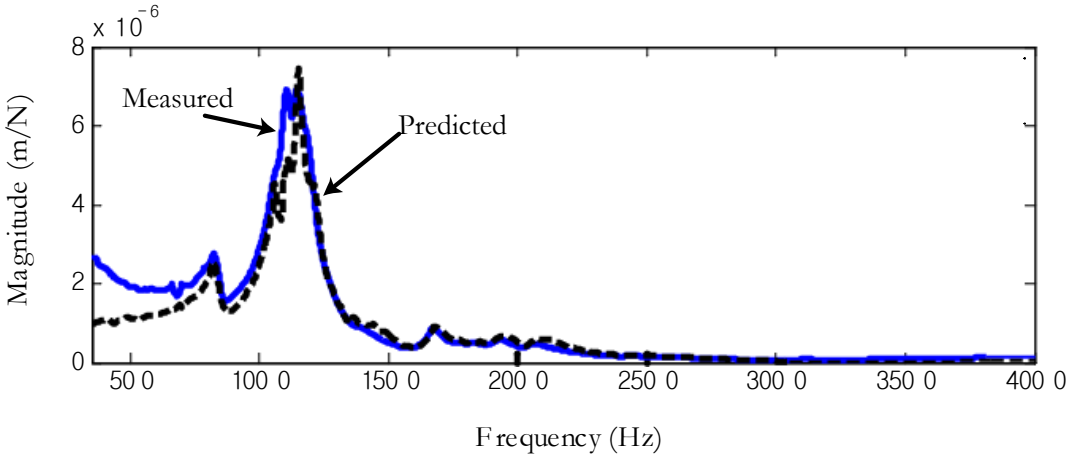

Figure 3-14 Predicted and Measured FRFs of the Modular Tool Assembly with 30 mm Calibration Cutter (Figure 3-12b) when the identified joint dynamics are considered

A two-fluted cutter (Figure 3-12c) of 16 mm in diameter, consisting of two rotating inserts (APX3000, Mitsubishi Materials Japan Co.), was assembled with a carbide cylinder blank that was inserted 40 mm into the collet. The modeling of this cutter for the FE analysis is very difficult, due to its complex geometry such as flutes, coolant holes, and various other features. Using a 3D scanner, this cutter can be converted to a solid model, and a commercial FE analysis program (i.e. ANSYS^{TM}) can import the solid model to generate its FRF. However, this process requires a lot of time and cost. Therefore, in this study, the diameter of the cutter was considered to be 65.6 % (10.5 mm) of the maximum diameter in the FE model [Park 2003]. The predicted FRF of the modular machine tool with the two-fluted cutter also utilized the identified joint dynamics from the 50 mm calibration cutter, shown in Figure 3-13. Figure 3-15 shows the comparison between the measured and predicted FRFs of the assembled system at the cutter's tapered end.

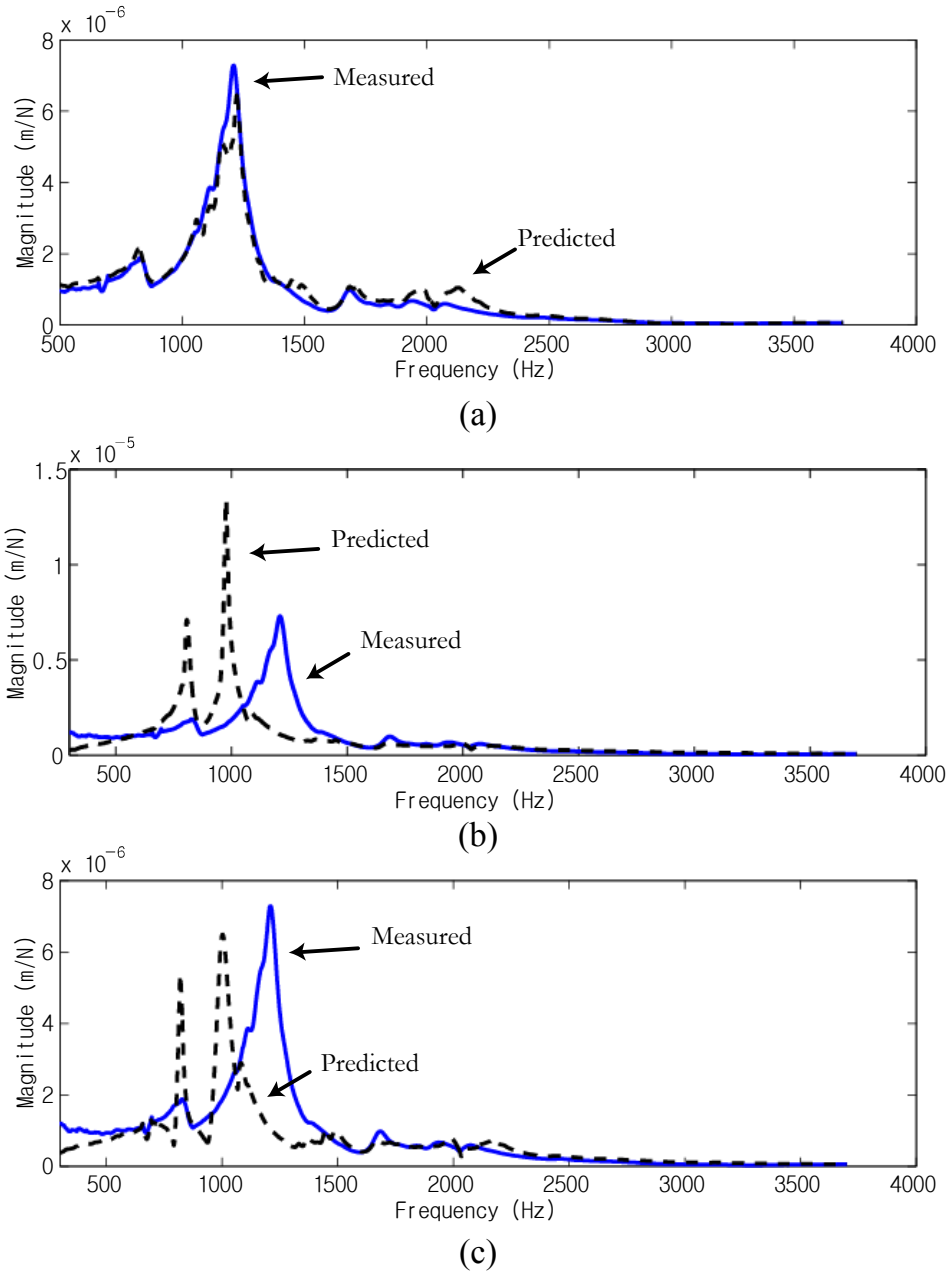

Figure 3-15 Predicted and Measured FRFs of the Modular tool assembly with Cutting cutter (Figure 3-12c); when the Identified Joint Dynamics are considered (a), without the identified joint dynamics (b), when the Identified Joint Dynamics are considered without RDOF (c).

Although a couple of peaks are observed at a higher frequency (approximately 2000 Hz), reasonable agreement is seen at the dominant mode (1200 Hz). Therefore, the

experiment's results show that the identified joint dynamics can be used to predict the dynamics of the assembly with the new geometry of modular cutting tools.

3.3 Summary

Engineers/machinists can evaluate and increase the performance of machine tools with their dynamics, which can be used to investigate stability lobe in order to minimize chatter vibration. The identification of joint dynamics is essential for an accurate evaluation of the assembly of substructures. Therefore, the performance of the machining processes depends on the dynamics of the machine tools as well as joint dynamics. In this investigation, the joints were modeled as linear mass, spring and damping elements in the system. Relative equations were derived by improved receptance coupling techniques in combination with the FE method and experimental tests in RDOF and TDOF responses.

Several assumptions need to be made in order to utilize the proposed method; the dynamics of the system is invariant, the dynamics of the joint is linear, and there is no nonlinear and hysterisys phenomena, which is caused by slippage and friction at the joint. The dynamic characteristics of a fastener joint in a mechanical system were identified and verified by the proposed method in experimental analyses. Based on the obtained joint dynamics, designers can predict the overall dynamics of either micro or macro machine tools, which consists of various substructures with joints, in order to minimize instability, such as chatter, in machining operations. The proposed method also predicted the dynamic properties of the modular micro machine tool (i.e. micro factory) with the identified joint dynamics. These advantages of this method have already begun to be explored in predicting the dynamics of the micro tool's tip of micro machining tools [Mascadelli 2006].

The progress in joint identification advances micro and macro machine tool performance towards a cost-effective industry. This process offers higher accuracy in machining and productivity and, consequently, fulfills the expeditious demand in manufacturing requirements.

CHAPTER 4. DEVELOPMENT OF THE MICRO CNC MACHINING

The capabilities and precision of a machine tool are vital to micro product requirements, such as size, accuracy, surface roughness and dimensional repeatability. There are two kinds of machine tool setups for micro mechanical machining processes; precision machine tools and micro machine tools (Chapter 2). Precision machine tools in the macro domain can produce micro-scale parts within desired tolerances and precision. Also, micro machine tools are an alternative way to fabricate micro parts using mechanical material removal process. In particular, various laboratories and academic institutes have been studying and utilizing the micro machine tools more than precision machine tools owing to economic benefits such as energy consumption, less materials, and significant reductions of the occupied space [Okazaki 2004]. However, thus the knowledge to develop such tools has been lacking. Therefore this research has undertaken the task of developing micro machine tools to further the micro domain's design experience and knowledge. The micro CNC machine was developed with the spindle assembly (air spindle and electric motor) capable of high speeds (500 – 80,000 rpm). The machine used two different positioning systems, one based on stepping motor, the other using a piezoelectric actuator. The size of the micro tools for milling operation was 50 μm to 2 mm. In this chapter, the development of the micro machining centre (see Figure 4-1) at the University of Calgary's Micro Engineering, Dynamics and Automation Laboratory (MEDAL) is discussed.

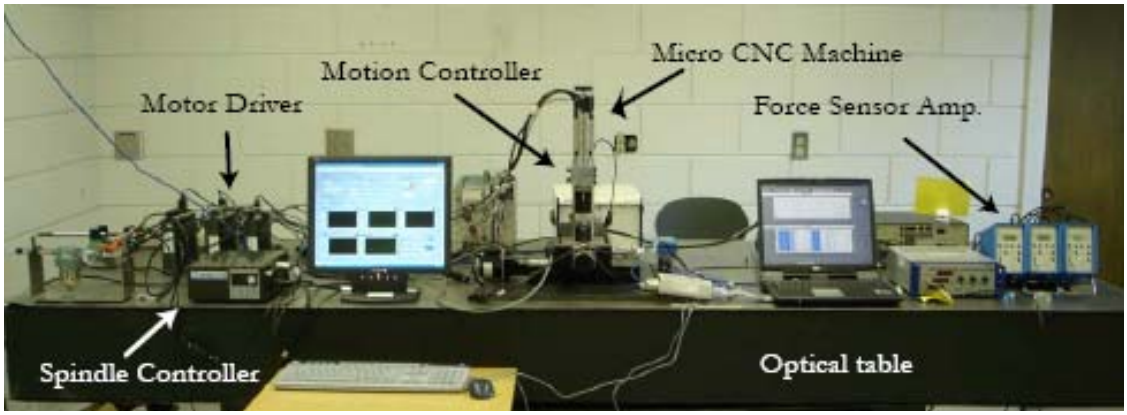

Figure 4-1 Micro CNC machine at the University of Calgary's MEDAL

The design configuration of the micro CNC machine at MEDAL is similar to the

conventional design. The micro CNC machine consists of a spindle, stages, frames and various control systems. It has been specified to meet functional requirements for travel, minimum resolution, velocity, accuracy and load capacity. In addition, the ratio of the micro CNC machine to the produced micro parts is much smaller than the precision machine tool. Therefore, various aspects (i.e. thermal deformation, dynamic stability from internal source and external source) must be considered in the design stage in order to ensure micro CNC machine performance. The weight of the micro CNC machine is much less compared to a conventional CNC machine. It is also easily excited by the external forces such as vibration from the base of the system. Therefore, the developed micro CNC machine was installed on an optical table (Ealing 4' x 8' air isolation)

This chapter is organized as follows: the first section describes the requirements for a micro CNC. The design of conventional vertical CNC machine was used to gain an idea for a concept design of the micro CNC machine. Various components; micro cutting tools, precision tables, and spindle, are selected for the micro CNC machine tool. Next section introduces the design of the micro CNC machine using 3D CAD software (Solidwork^{TM}). The actual design process considered various issues such as a maximum load, torque, minimum movement, stiffness of the structure due to the reduction of the size of machine. Using FEA, spindle holder and vertical structure are analyzed with different materials and the results are shown. Section 4.6 provides the operation of a micro CNC machine, mechanism of the stage and controller, and discussion for the future research directions.

4.1 Design of Micro CNC machine

The design of the micro CNC machine was based on the conventional column-and-knee-type machines due to their simplicity and inherent rigidity [Kalpakjian 2002]. The micro CNC machine is basically a three-axis vertical milling machine (Appendix B.1.) that can be used in various operations such as face and end milling, boring and drilling. Thus, it must have the same functionality and resolution as an ultra-precision machining system.

The design of the micro CNC machine is shown as illustrated in Figure 4-2. The structure consists of operating and stationary parts. The operating parts include air-spindle, electric motor, and precision linear tables. The selections of the operating parts are critical

to machining accuracy and the motion trajectory of micro tools according to the design of the produced micro parts. The stationary body represents spindle holder, base, and vertical structure (column). It is important to select proper materials for these components to minimize thermal deformation and size for the suitable configuration of the micro CNC machine.

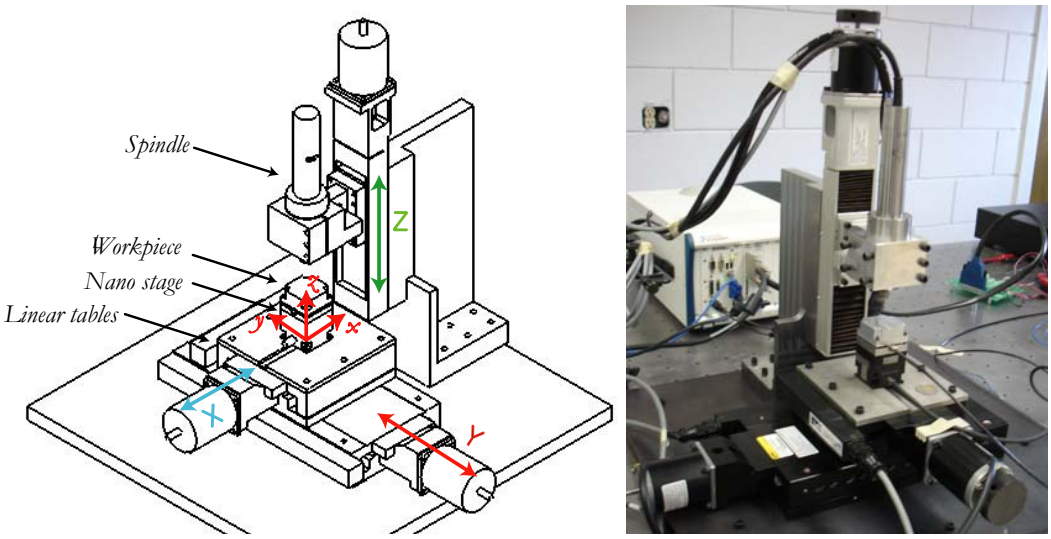

Figure 4-2 Designed Micro CNC machine at MEDAL

4.1.1 Spindle and Motor

Since the feedrate in micro machining is relatively smaller than macro machining, a spindle used in the micro CNC machine must be able to rotate the micro tools at a very high speed with a low run-out in order to increase the volumetric material removal rate (MRR) of the micro cutting tool.

Majority of researchers are using small and commercially available air turbine spindles, which have non-contact type bearings. They are capable of rotational speeds up to 200,000 rev/min (rpm). These spindles have a very low run-out (less than 1 μm). However, the air turbine spindles are not suitable to fabricate realistic 3D structures in steel, aluminum, or brass due to insufficient torque as well as low stiffness. In this study, we employ a 300 W electric air-motor spindle (NSK Astro 800E), which is capable of rotational speeds up to 80,000 rpm, is used for this micro CNC machine to achieve adequate torque requirements in order to machine various materials including steel,

aluminum and other alloys. In addition, the weight of the spindle assembly (include the motor) is only 1.05 kg, which is below the loading capacity of the linear table for Z-axis. Figure 4-3 is the image of the air spindle and electric motor for the micro CNC machine. The outside diameter of this spindle is 50 mm. The run-out of the spindle maintains within 1 μm. The air-cooling system is utilized to prevent heat buildup for both systems. It allows long continuous operation. The regulator between air supply and spindle assembly removes the moisture of air and control the pressure of air to 5 psi.

.

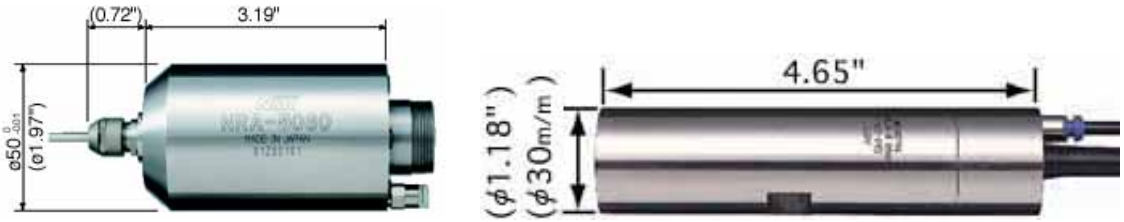

(a) (b)

Figure 4-3 Spindle assembly; (a) Air spindle (NSK Astro NRA-5080) (b) Electric motor (NSK Astro EM-805)

There are two ways to control and monitor the actual spindle speed, when the micro tool rotates at a certain speed. The LCD window on the spindle controller indicates the spindle speed and the spindle controller generates analog outputs according to the spindle speed (i.e. 6.5V = 65,000 RPM). By utilizing these two monitoring methods, user can control the spindle with desired speed precisely.

4.1.2 Precision Stages

The size and accuracy of the machined micro structures depends on the capability of the precision table. Therefore, the position tables require a high resolution and low repeatability errors to achieve high accuracies in micro-structure fabricating. Linear drive motors are commonly used in typical ultra precision machine tools. Compared to conventional drive mechanisms such as ball screws, linear motors have no accumulative errors from friction and the motor-coupling, no loss of accuracy due to wear and no back-lash. They can also provide very high accelerations. However, linear motors requires

feedback loop, which consists of either an encoder or high resolution position sensor, to locate the tables in the desired position.

Piezoelectric drives are also used for the precision table. Several advantages of the piezoelectric drives are fast response, high resolution and driven force. Piezoelectric materials generate strain according the electric voltage. In order to achieve a large displacement, the piezoelectric drives are made by bonding multiple piezoelectric materials together as shown in Figure 4-4. The voltage is applied to the surface of the thin actuators; the expansion of the thickness is used to perform work. This condition generates trajectory errors know as hysteresis effect, which is a non-linear relationship between input and output. The piezoelectric drives are suitable for low displacement movement with a small increment (under micrometer).

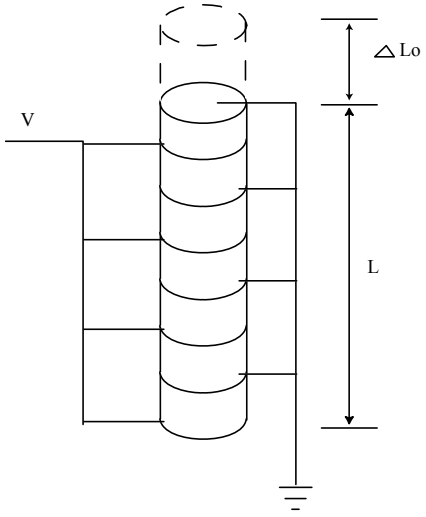

Figure 4-4 Stack Piezoelectric Actuator

The moving mechanism of the micro machine tool in this project is a dual-control stage system; linear table and nano-stage. The three linear tables used for coarse control incorporate cross roller linear bearings (Parker Daedal 10600, 402LN, ζ Drives) and stepping motors for the X, Y, and Z axes. The linear tables move the workpiece to the desired location with a resolution of 8 μm at relatively high speed. The position accuracy of these tables is ± 1.3 μm. The motion controller then operates the nano stage in order to locate the workpiece to the exact location.

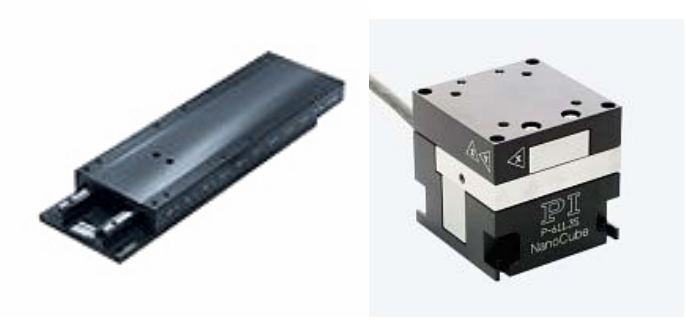

(a) (b)

Figure 4-5 Precision tables; (a) Cross roller linear table (b) Nano-Stage

Table 4-1 shows the specification of the linear table. This table requires the size 23 frame motor. The used motors for the micro CNC machine are controlled by the Paker's zeta4-240 driver. Using various combination of the dip switch on the driver, the motor is allows to generate 50,000 steps per revolution. This high number of steps minimizes the impact of movement, which generates by the stepping motor and linear bearing on the table. The motion controller sends digital signals (0V or 5V) according to the number of steps, which means the rotation angles of the stepping motor, to the driver. Based on the configuration of the stepping motor, (series or parallel), the driver sends the appropriate currents to the alternative in the motor, in order to rotate the shaft.

	Specification	Unit
Max screw speed	25	Rev/sec
Max acceleration	1200	mm/sec^2
Axial loading	24.9	Kgf/m^2
Directing loading	108	Kgf/m^2
Max running torque	0.106	N-m

Table 4-1 Specification of cross roller linear bearing table

In addition, the nano-stage (PI P-611.3SF) can be attached on the X-Y axis linear table (Appendix C.4) for fine control, and has a resolution as low as 25 nm. This high resolution stage is necessary for most micro mechanical machining operations owing to the small diameter of the typical micro cutting tool (> 50 μm).

4.1.3 Machine Structures

The machine structure provides the mechanical support for moving and stationary parts. This Micro CNC machine is the structure with the vertical spindle. It provides the operator with an easily accessible work zone. For research purposes, it is very important for the operator to monitor the cutting conditions and change the work zone environment.

Therefore, there are two main structures; one is a vertical structure for a Z-axis linear table, another is a spindle holder attached on the linear table in Z-axis. The main considerations for these structures are the geometry configuration, high static and dynamics stiffness.

Dynamic properties of the structures also refer to dynamic rigidity / stability and can be influenced by the size, damping characteristics, effective mass and static stiffness of the structures. In general, systems are considered as mass-spring-damper systems to represent its dynamic behavior such as mode shapes at the natural frequency. When the spindle reaches a certain speed, the level of the vibration can be very severe. The combination of the number of the flutes and the spindle speed can become a resonant frequency of the system. For example, two flute micro tools at 80,000 rpm have 2667 Hz as a tool passing frequency. Therefore, natural frequencies of the structures limit to a certain spindle speed.

The maximum magnitude of vibration is proportional to $1/2k\zeta$. Where, k and ζ represents stiffness and damping ratio. Therefore, the structure must have high natural frequencies because the natural frequency is also proportional to the stiffness and high damping ratio. High natural frequency of the structure represents that structure has high stiffness.

Using receptance coupling (refer to chapter 3), the micro-end mill tool tip dynamics are predicted. The resulting predicted curve-fit tool tip dynamics are seen in Figure 4-6. The identified modal parameters of the micro-end mill tool tip dynamics are seen in Table 4-2 [Mascardelli 2006, A].

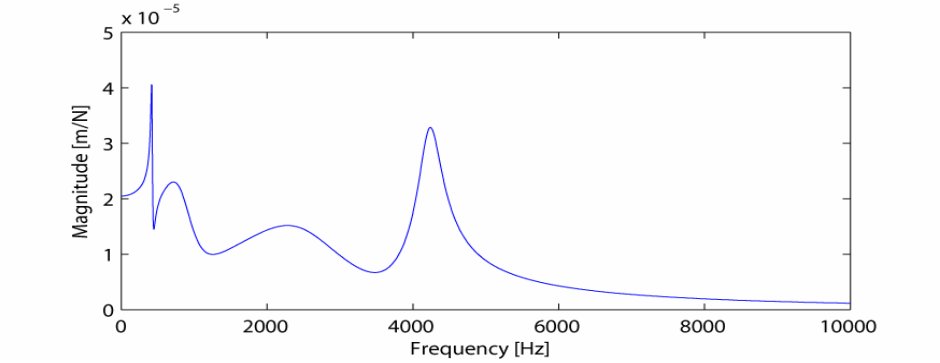

Figure 4-6 Predicted micro-end mill tool tip dynamics (Dia. 200 μm) [Mascardelli 2006, A]

Mode	Frequency, f_n [Hz]	Damping, ζ	Stiffness, k [N/m]
1	423	0.028	$6.686x10^5$
2	865	0.029	$1.172x10^5$
3	2580	0.30	$1.246x10^5$
4	4230	0.040	$4.114x10^5$

Table 4-2 Tool tip modal parameters [Mascardelli 2006, A]

In addition, thermal stiffness must be considered. The tolerance of the micro machined features is the order of micro range. During a long period of machining time, either room temperature or heat produced from the motor or spindle may increase the temperature of structures. It can deform the support structures. As a result, the location of micro cutting tool is relocated as much as the deformation of the structures.

There are two main parameters; material and design, which we can manipulate, in order to increase the machine performance. In this study, finite element analysis (CosmosWork™) was performed in order to show the performance of the structures with materials. On the other hand, the design of the structures depends on the interaction with other systems such as the diameter of the spindle, the thickness of workpiece and X-Y linear tables. The vertical structure and spindle holder are modeled by considering the above criteria using computer modeling CAD (SolidWork™).

4.1.3.1 Spindle Holder

The spindle holder attaches the spindle-motor assembly to the z- axis linear table by using eight M5 bolts. The dimensions of the holder are determined by considering several

aspects; the distance between z axis and the center of x-y tables (Appendix B.3). By doing so, the yaw, pitch, and rolling effects of the x-y tables can be minimized. The outside diameter and recommended clamping area of spindle also determine the shape, height and diameter of the hole on the spindle holder. In order to clamp the spindle, three fasteners are used as shown in Figure 4-7. If the screws push directly on the spindle, it could damage the housing and may result in failure of rotation, or overheating. In addition; this holder must be light due to the load limitation of the z-axis linear tables.

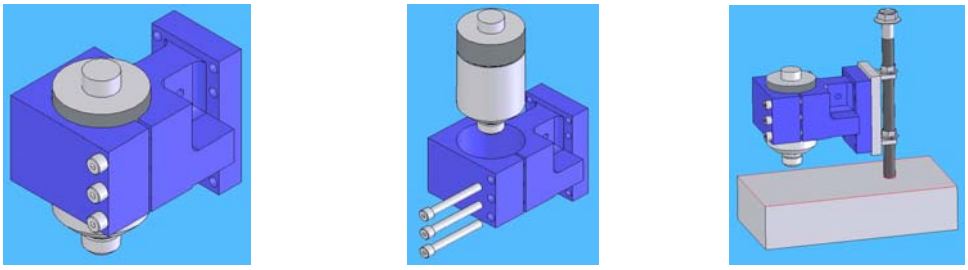

(a) (b) (c)

Figure 4-7 Spindle holder; (a) Assembly with spindle (b) Exploded view (c) Z-axis elevation mechanism

Without constriction, heat generates the strain on the structure without stress. Using the CAD and FE software packages, the thermal strain analysis was performed. Thermal expansion mainly depends on material properties rather than its geometry shape. In this project, several common materials were considered and their material properties are shown in Table 4-3.

Material	Steel 1020	Steel 1080	Al 7075	Al 6061
Density (Kg/m3)	7870	7850	2810	2700
Thermal Conductivity (W/m-k)	52	48	130	166.9
Modulus of Elasticity (GPa)	2.05E+02	205	71.7	69

Table 4-3 Material Properties [Kalpakjian 2002]

Steel 1080 has relatively the lowest thermal conductivity. This represents a low thermal deformation. However, the weight of spindle holder with steel and air spindle-motor assembly is close to the load limitation of the Z-axis table. Figure 4-8 shows the simulated thermal deformation of the holder. The source of heat is spindle and its temperature is assumed to be 328 K in this case because the maximum temperature on the

spindle is 50 °C during operation. The maximum displacements of the structure are about 0.5 μm for the aluminum case and 0.3 μm for the steel case. The difference of two cases is about 0.2 μm, which is less than the roughness of many micro-machined surfaces. Therefore, we can use aluminum for this particular spindle holder.

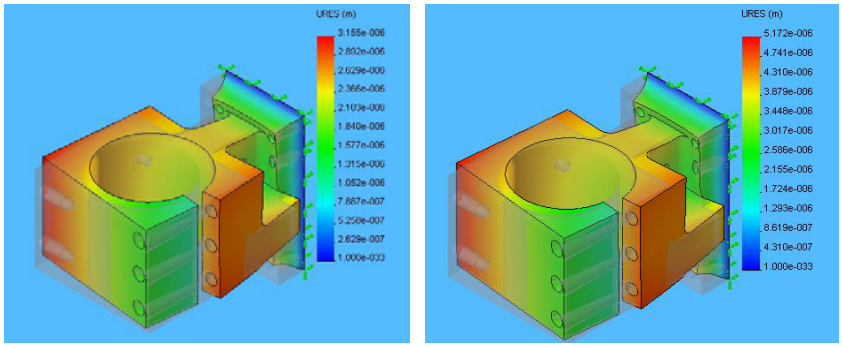

(a) (b)

Figure 4-8 Results of Thermal deformation of the Spindle holder; (a) Steel 1080, (b) Aluminum 6061

Modal analysis for the spindle holder has been performed using CosmosWork™. One of the dynamics characteristics of the system is the natural frequency. If the operating spindle speed is identical to the one of the natural frequencies, the excessive vibration on the structure will occur. Therefore, the purpose of this analysis is to evaluate the natural frequency of the structure so that the spindle speed can be optimized.

In this project, the range of the spindle speed is from 5,000 RPM to 80,000 RPM, which are from 166.67 Hz to 2666.67 Hz with two-flute micro tool. Three modes are in the range of spindle speed. Therefore, the spindle speed must be selected beside three natural frequencies (840.26 Hz – 25207 RPM, 1644.8 Hz – 49344 RPM, 2294.5 Hz – 68805 RPM) during the machining operation.

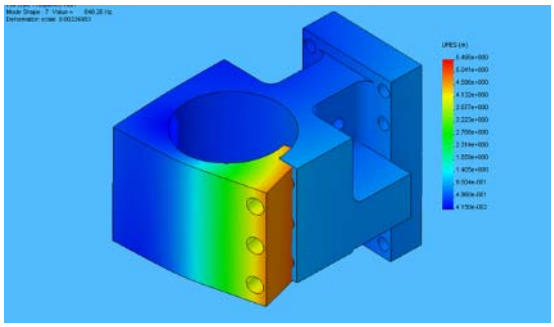

Figure 4-9 First Mode Shape of Spindle holder

Figure 4-9 shows mode shape of the spindle holder at the first natural frequency. It is clearly shown that the maximum deformation occur at the location for the three tighten screws. When the spindle is assembled with this holder, the screws play a role as supporting structures. As a result, it will minimize the deformation, which is caused by first natural frequency, which is generally a dominant mode.

4.1.3.2 Vertical Structure

The objective of the vertical structure is positioning and supporting the Z-axis linear table. The location of the Z–axis table creates the machine working zone with X-Y tables, which has 100 mm high. In addition, this structure directly links the micro tools to the base of the machine tool, which means that external forces will deliver the micro tools through the vertical structure. Therefore, the design of the vertical structure (Appendix B.2) is important in order to ensure the performance of the micro CNC machine.

The vibration of tool tip can decrease the quality of the fabricated micro structure because vibration of the vertical structure directly delivers to the micro tool tips. Also, the size of the vertical structure is relatively bigger than any other structure in this micro CNC machine. Therefore, the deformations of this structure are relatively larger than those of other structures due to either heat or resonance frequency.

The material for the structures can be chosen based on the comparison of the properties of the material (Table 4-3). The steel 1080 can minimize the thermal effect and increase the rigidity of the system. However, in reality, ANSI 1018 is used for the vertical structure because it is easy to fabricate and purchase it and it has similar material properties with steel 1080. The system must have a high natural frequency to achieve high stiffness. In order to increase the stiffness of the structure, this vertical structure was machined from one piece of block steel instead of assembling several pieces with various joints. The typical assembly methods in mechanical structures are welding and fasteners. These types of joints represent discontinuities of the strcuture, which reduce the stiffness of the structure (Chapter 3). Considering machine volume, size of the moving parts, machining working volume and relative displacement between workpiece and micro tools, the dimension and

shape of the vertical structure is designed and evaluated through the FE analysis.

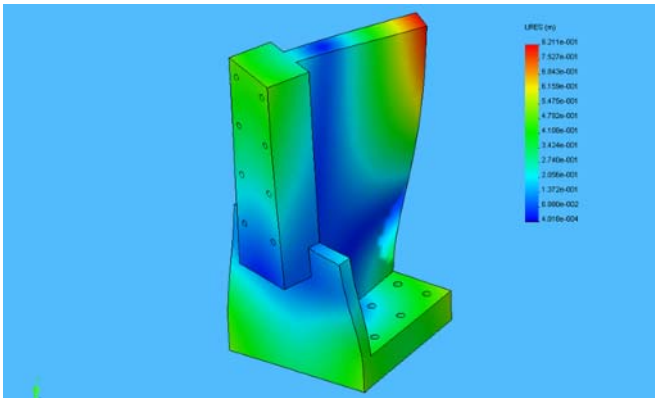

Figure 4-10 First Mode shape of First version of Vertical structure

The mode shape shows how the structure will vibrate at the natural frequency. The vertical structure can be redesigned to restrict the vibrations at the upper regions, where the level of the vibration is relatively high. However, the actual displacement is under sub-micron range, which will not affect the accuracy of the micro-mechanical machining because the diameter of machine tool is already over 100 μm. As a result, the vertical structure satisfies the requirements; low thermal deformation, high rigidity and the suitable configuration for the micro machining process.

4.2 Control Algorithms

Several aspects need to be investigated for micro CNC machine in order to perform the same functionality and high resolution as the ultra precision machining tools. The system should be able to interface the geometry information from CAD system with actual command signals for stages and spindle. In order to do so, the system must be controlled on the personal computer platform. In addition, the user must be able to control spindle speed, feed rate, axial depth of cut, locations of the X-Y table.

This micro CNC machine system requires seven simultaneous control signals; six control signals for the dual stages and one for the spindle speed. This is implemented through a National Instrument motion controller (PXI 7240) and AD/DA (PXI 1250)

system, which are operated by a personal computer. The motion controller is also able to link the micro CNC machine to CAD/CAM software. The typical part geometry consists of points, lines, and curves. Once the geometry is designed on the CAD system, the motion controller feeds velocity and position control inputs to all axes as well as the spindle speed after a certain pre-process (Appendix C). This is based on the linear interpolation code from the CAM system.

The interface between the CAM information (i.e. tool paths) and the hardware is linked by NI Motion Assistant™ software. The motion controller and the software carry out the specific operations to actuate the motors to move the stages to desired locations through following steps:

a. System initialization and updating profiles based on user defined position
b. Trajectory generation, an interpolation component, or spline engine based on user defined profiles; calculating set points.
c. Performing control loop to maintain position, velocity, and trajectory on one or more axes.

For this particular micro CNC machine system, the control loop generates steps as a command signal, which is an analog output from the motion I/O (the part of the motion controller), for the drive. The motion I/O is also able to react to limit switches and create initial position for the movement (Appendix C). Figure 4-11 shows the schematic of the micro CNC machine. However, most tests in this thesis were performed, when the set-up of the micro CNC machine was without the nano cube because the measurement of forces is prime interest rather than the accurate fabrication of micro structures.

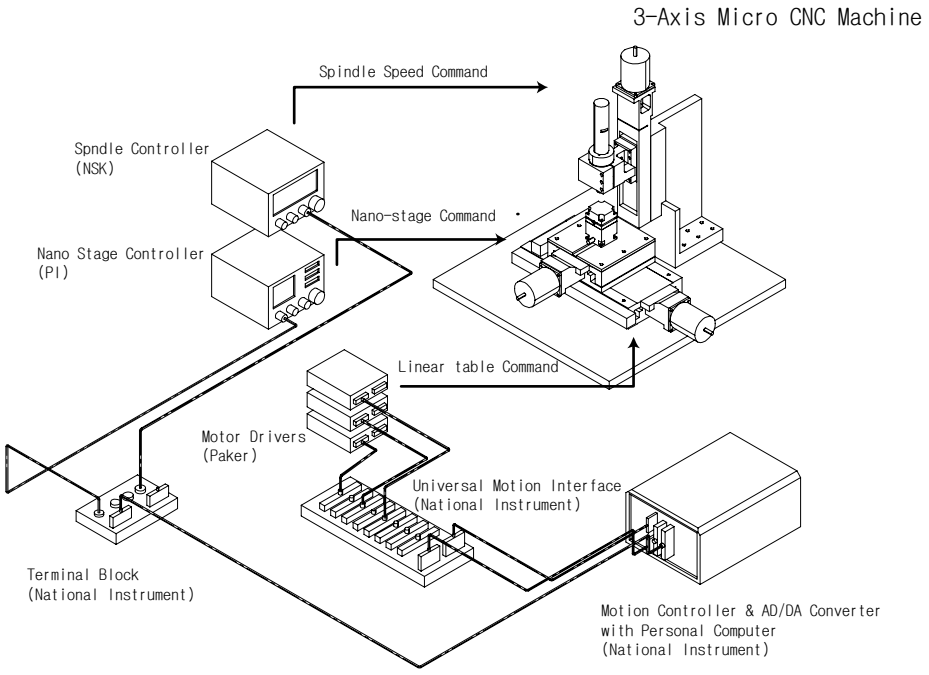

Figure 4-11 Micro CNC machine with nano cube

4.3 Cutting Process Monitoring System

In order to increase the efficiency of the micro machining operation, the cutting conditions must be monitored. In conventional machining, cutting force is usually used for monitoring the cutting condition (refer to chapter 2). Accurate measurement of the cutting forces indicates the state of a machining operation and allows process engineers to select the optimal process parameters to achieve productivity goals and to monitor machining operations. In this study, a commercial miniature three-axis piezo-electric force sensor and an accelerometer are utilized to measure cutting forces accurately.

The force sensor has three pairs of quartz plates (like piezoelectric material; refer to 4.2.2) for X, Y, Z direction. Depending on the direction of the force, positive or negative charges are generated from the plates. These charges produce voltages, which we are monitored with a Data acquisition system, with charge amplifier.

The force sensor is located between workpiece and the dual stage tables to measure cutting forces during the machining operation, similar to a conventional CNC machine (Exploded view in Figure 4-12). The nano stage is limited to a load capacity of 15 N,

therefore a small three-axis force sensor (Kistler, 9017B, diameter: 16 mm, thickness: 9 mm) was utilized to measure micro cutting forces. To get the full capability of the force sensor, preloading is essential prior to use because, the forces are transmitted between sensor and the workpiece. Micro-gap between two objects can reduce the frequency bandwidth of the force sensor. In this particular configuration, the preload is set to be 10 KN with torque wrench. The charge signals generated from the force sensor are fed into the charge amplifiers (Kistler 9025B), which convert the charge signals into voltage signals.

In the machining process, the location of the actual cutting force is separated from the force sensor by a distance equal to the workpiece thickness. Therefore, a scaling factor, which is the ratio between the actual cutting force and the measured force, must be calculated. This is typically accomplished by generating a force with an impact hammer at the actual cutting force location. A scaling factor can then be extracted from two measured forces (impact hammer and force sensor). This process was repeated for each of the three axes. Whenever a workpiece is changed, this scale factor must be updated to reduce the measurement error. Once a scaling factor is available, the micro cutting force can be obtained from the cutting force measurement system.

The micro machining requires inexpensive sensing devices for the measurement of various quantities. The advantage of using another sensor is to provide more information about the micro cutting condition by measuring and analyzing more than one type of signal. An accelerometer is attached on the workpiece in order to monitor the micro cutting forces indirectly. The advantage of using accelerometer is reducing set-up time for the cutting force monitoring system. Whenever the workpiece is changed, the force sensor requires the calibration to find the sensitivity factor out. However, the sensitivity factor of the accelerometer does not depend on the workpiece. Signals from force sensor and accelerometer are fed to the data acquisition system (National Instrument). Two analog signals can be acquired with various sampling rate and number of data.

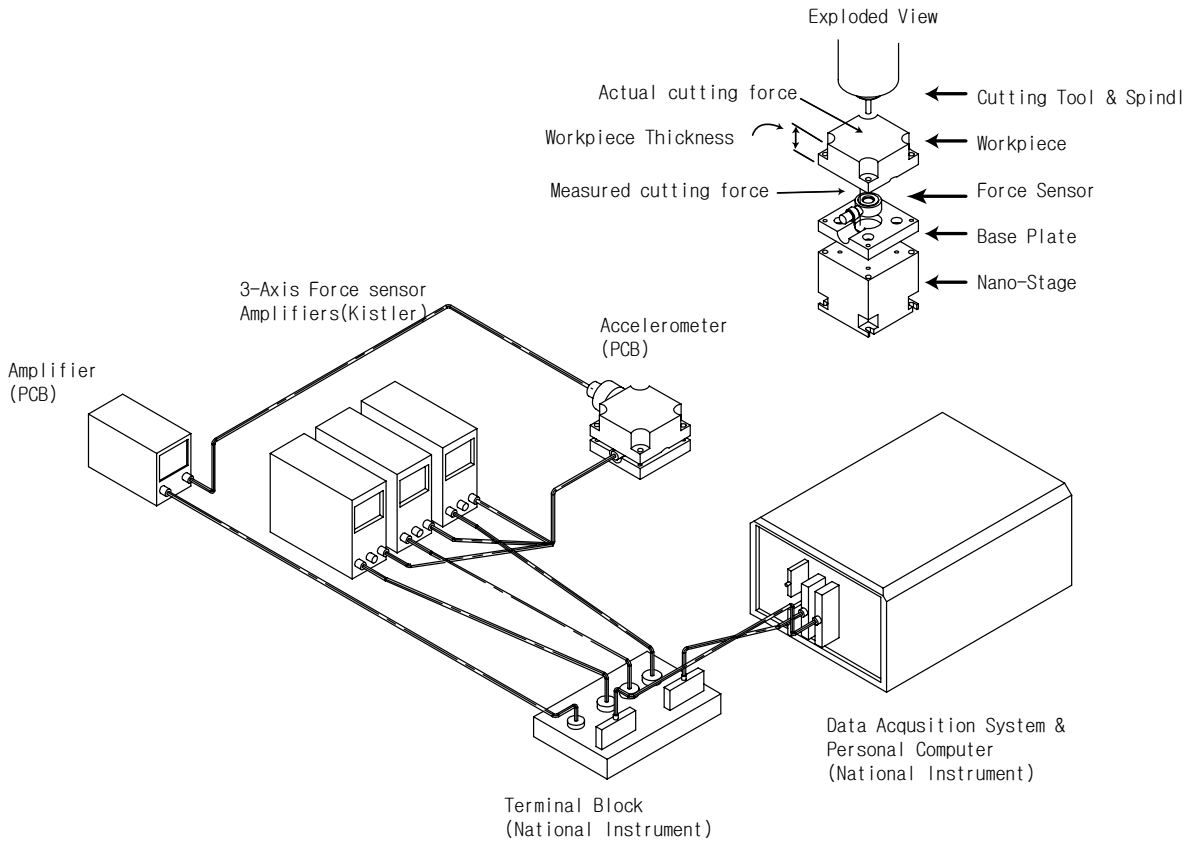

Figure 4-12 Cutting Force Measurement System

4.3.1 Calibration and Modal Analysis of Sensors

Since the three-axis piezo-electric force sensor (Kistler 9017B) is sandwiched between the workpiece and the X-Y stage with the preloads, the calibration of the force sensor is imperative. The calibration is performed using a force gauge (Omega DFG51-2), as shown in Figure 4-13(a). The force gauge is in contact with the workpiece, measures the movement and then translates it to forces.

The linear X-Y stage is moved 50 μm at every 800 ms interval, in order to have a stair-step profile as shown in Figure 4-13(b). The data acquisition system measures the two analog signals from the force gauge and the piezo-electric force sensor. The sensitivity of the piezo-electric force sensor is found to be 28.6 pC/N and 35.26 pC/N for the X- and Y-axes, respectively. The cross-talk between the axes is found to be less than 9.9%. The comparison of two force measurements using the force sensor and the force gauge in X-

direction is shown in Figure 4-13 (b). In addition, the modal impact hammer test is performed to verify the force measurement of the force sensor, where the output is measured from the force sensor.

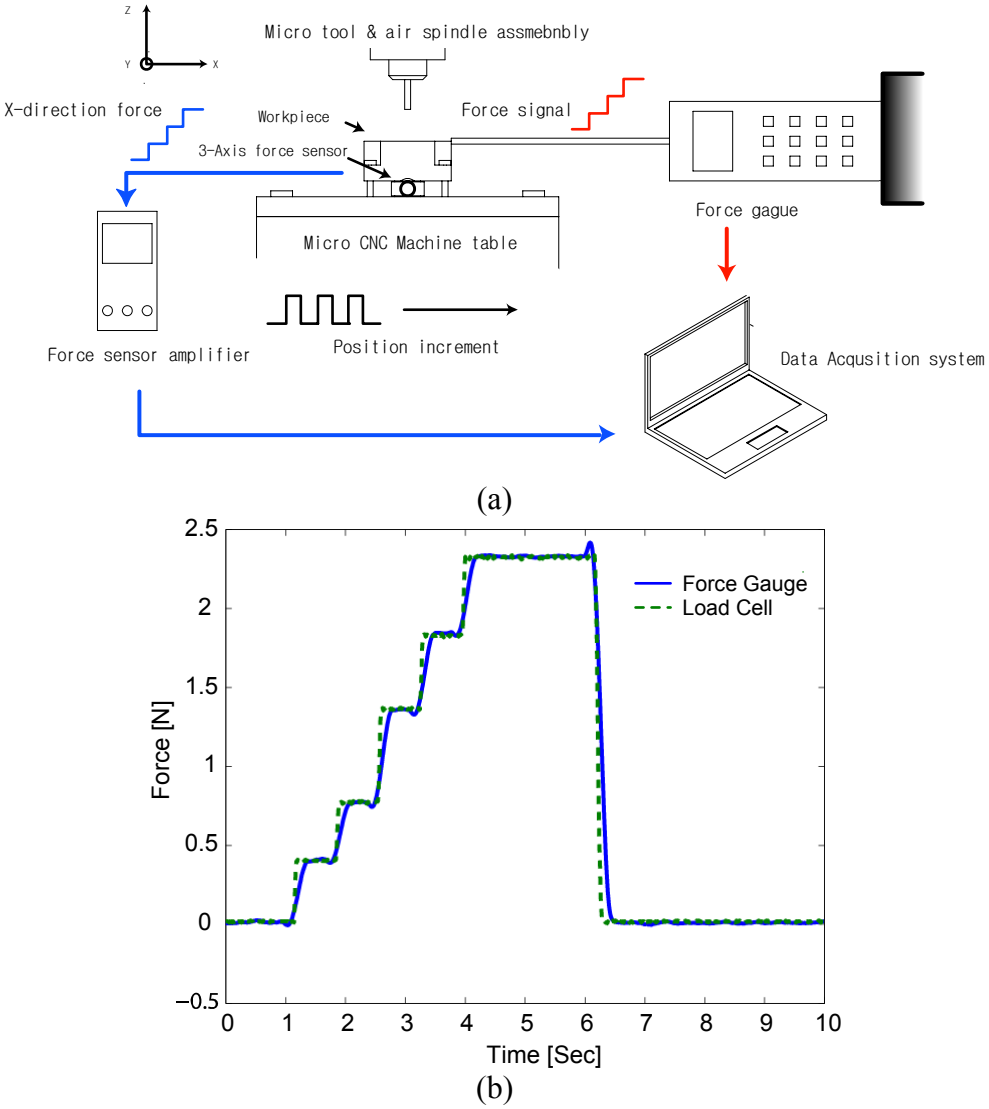

Figure 4-13 Static Calibration of the Force Sensor (a) Setup and (b) Calibration

The frequency response function (FRF) between the applied force from the impact hammer and the force sensor is acquired to have the unity gain shown in Figure 4-14(a). With the verified scale factor, the micro cutting forces are measured from the cutting force measurement system. In order to measure the different dynamics of the micro cutting condition, the vibration measurements are obtained through the use of an accelerometer (Kistler 8778A500). The accelerometer is attached to the workpiece to measure vibration

signatures, which are then used to fuse the signals from the force sensor and accelerometer to reconstruct accurate high-bandwidth cutting forces (Chapter 5). The dynamics of the sensing structure are measured using the instrumented impact hammer (Dytran 58008L) and the accelerometer. The impact hammer provides sufficient energy, up to 10 kHz, simulating the actual cutting forces; and, the resulting response is measured by the accelerometer. From the acquired signals, the transfer functions can be obtained in the frequency domain. The experimental FRF is obtained from the experimental modal analysis in Figure 4-14(b).

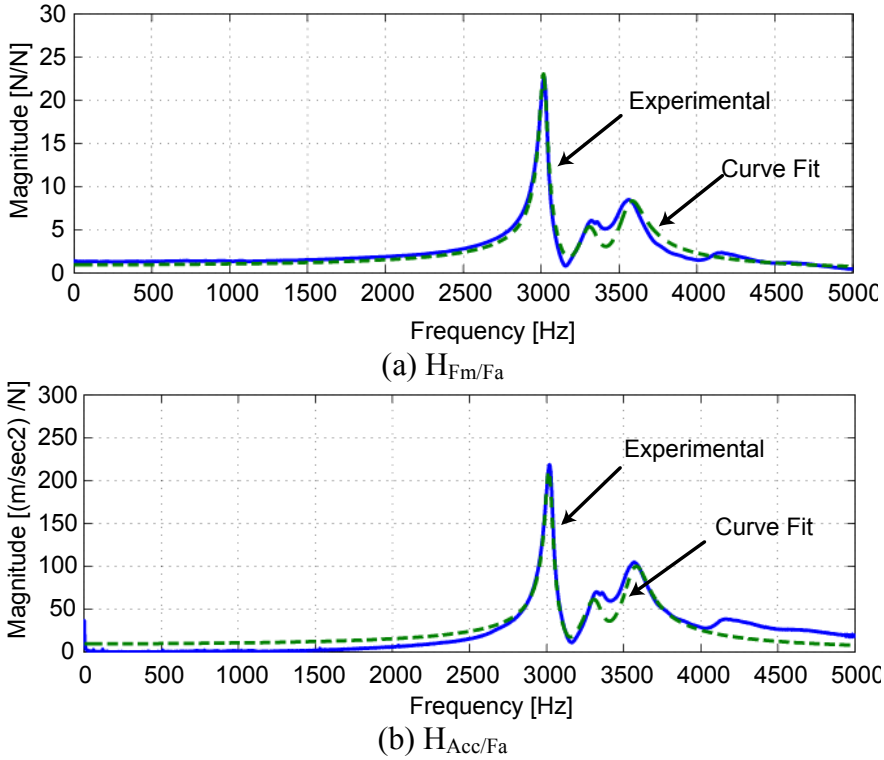

(a) $H_{Fm/Fa}$

(b) $H_{Acc/Fa}$

Figure 4-14. Identified Frequency Response of the Force Measurement Mechanisms

The experimental FRFs from the force sensor and the accelerometer can be curve fitted using a nonlinear fitting method [Atintas 2000]. The transfer functions can be acquired from Equation (4-1), where the modal parameters are depicted in Table 4-4. We observe three dominant modes at 3017, 3312, and 3571 Hz, and we curve fit these three modes. The measured and curve fitted transfer functions are in good agreement, as can be seen in Figure 4-14.

$$H_{Fm/Fa} = \frac{F_m(s)}{F_a(s)} = \sum_{m=1}^{3} \frac{\omega_{n,m}^2 / k_{f,m}}{s^2 + 2\xi_m \omega_{n,m} s + \omega_{n,m}^2} \quad , \quad H_{Acc/Fa} = \frac{Acc(s)}{F_a(s)} = \sum_{m=1}^{3} \frac{\omega_{n,m}^2 / k_{A,m}}{s^2 + 2\xi_m \omega_{n,m} s + \omega_{n,m}^2} \qquad (4\text{-}1)$$

where k is the number of modes, Acc is the acceleration measured by the accelerometer, F_m is the measured force from the force sensor, and F_a is the actual force acting on the workpiece.

$H_{Fm/Fa}$		Natural frequency ω_n (Hz)	Modal Damping ratio ζ	$k_{f,m}$
	mode 1	3017	0.009	2.4874
	mode 2	3312	0.019	6.008
	mode 3	3571	0.024	2.749
$H_{Acc/Fa}$		Natural frequency ω_n (Hz)	Modal Damping ratio ζ	$k_{A,m}$ N/(m/sec^2)
	mode 1	3017	0.009	2.635e-1
	mode 2	3312	0.019	5.398e-1
	mode 3	3571	0.024	2.241e-1

Table 4-4 Identified Modal Parameters

The 3-axis force sensor is carefully calibrated with the force gauge and verified by experimental modal analysis using the impact hammer. An accurate measurement of the cutting forces will provide an effective monitoring of tool wear, breakage and deflection, all of which are important considerations in the development of micro machining applications.

4.4 Experimental Cutting Tests

The cutting test results for the various cutting speed (2, 4, 6, and 8 μm/tooth) are given in Figure 4-15 (a, b, c, d). Due to the dynamics of the force sensor (Figure 4-14), the spindle speed is set to be 5000 rpm (166.7 Hz) for monitoring cutting force precisely. The cutting force signals for each case were measured with a sampling rate; 100 K Hz, number data 20 K, and low path filter; cutoff frequency 10 K Hz. The tool is made by tungsten carbide with two flutes, 30 degree of helix angle, and 4 mm shank diameter. Aluminum 7075 was used as the workpiece. Table 4-5 depicts the cutting conditions.

Cutting Conditions		Tool Information	
cut depth	0.1 mm	tool diameter	0.5 mm
spindle speed	5000 rpm	number of flutes	2
feed rate [mm/ flute]			
0.002, 0.004, 0.006, 0.008, 0.01			

Table 4-5 Cutting condition with Dia.500 μm end milling tool

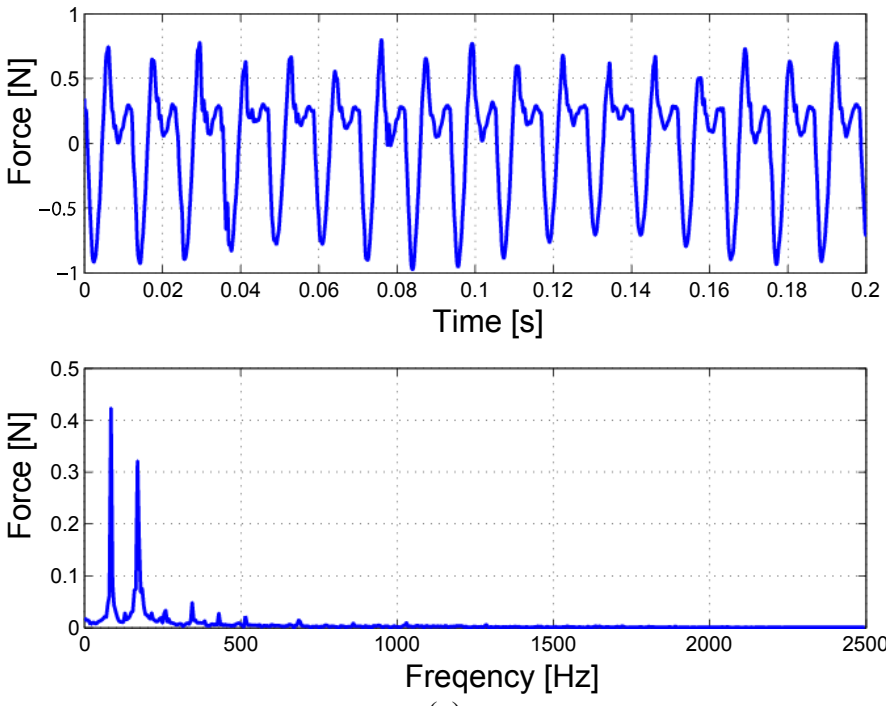

(a)

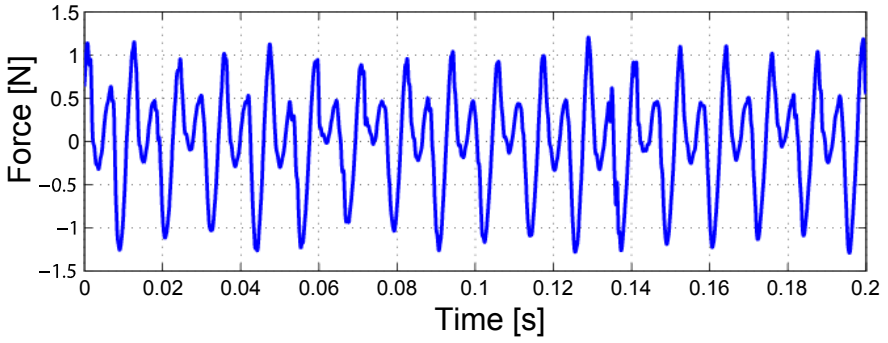
Force [N]
Time [s]

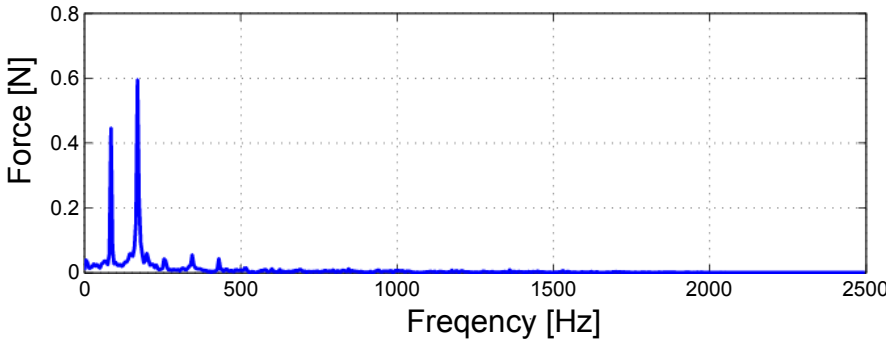
Force [N]
Freqency [Hz]

(b)

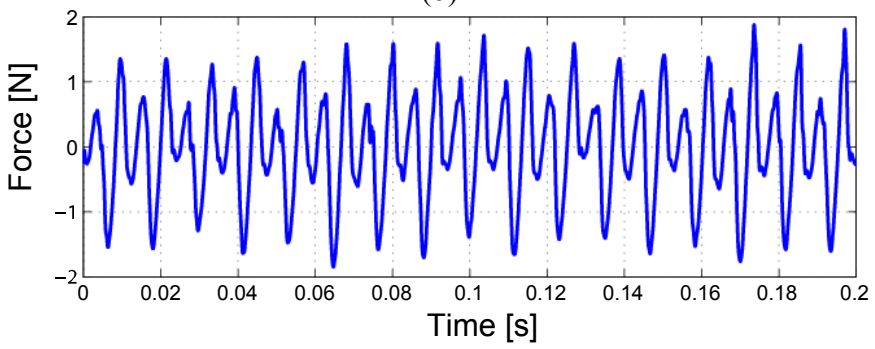
Force [N]
Time [s]

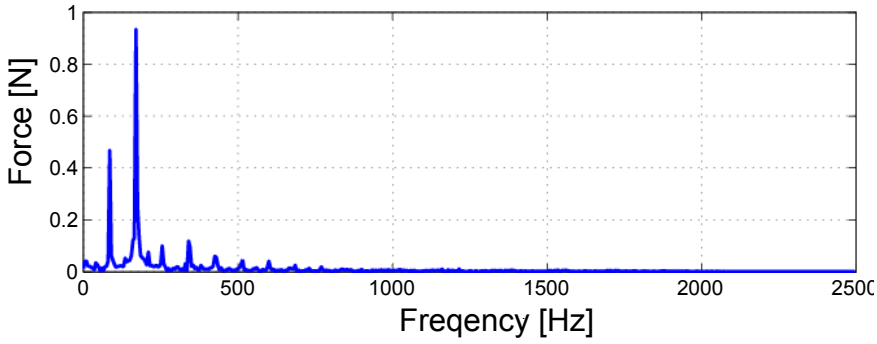
Force [N]
Freqency [Hz]

(c)

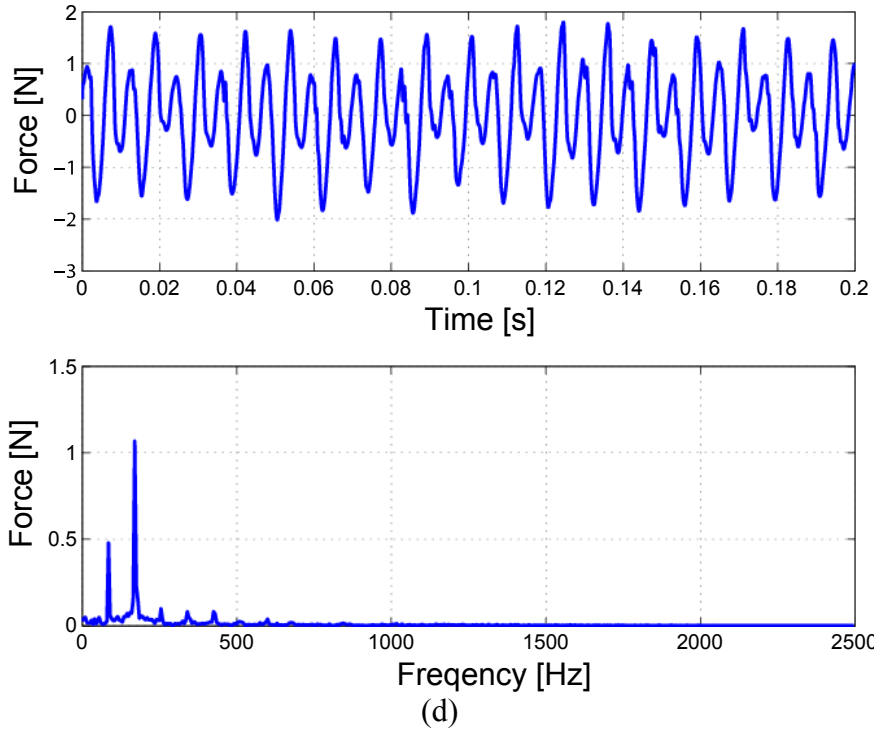

(d)

Figure 4-15 Micro cutting force with various cutting speed: (a) 0.2 μm/tooth, (b) 0.4 μm/tooth, (c) 0.6 μm/tooth, (d) 0.8 μm/tooth

Contrasting with the macro cutting model, the cutting forces are not proportional to the feed rate in micro cutting. The feed rate is increased 4 times (from 0.2 μm/ tooth to 0.8 μm/ tooth). However, the cutting force is only increased about 2 times. Through these cutting tests, it is obvious that the sharp edge theorem is no longer reliable for the micro cutting force prediction. Also, when the feed rate is 0.2 μm/tooth, the cutting force at spindle frequency (85 Hz) is higher than at tooth path frequency (170 Hz). The micro tool for this experiment has two teeth. Therefore, only one of two teeth is engaging with the workpiece more than the other. This phenomenon typically occurs due to run-out of the tool or tool misalignment.

Figure 4-16 shows the comparison between the measured and theoretical cutting forces using generalized cutting coefficients [CutPro^{TM}]. The theoretical cutting forces consist of shearing forces and edge forces. In this test, the feed rate is higher than the edge radius of the micro cutting tool in order to match the conditions in macro cutting, except for the size of the cutting tool. Therefore, area of shearing zone in this cutting is similar to those in macro machining. However, the differences between the measured and theoretical

cutting forces are shown in Figure 4-16. Therefore, it can be assumed that the edge forces between micro cutting and macro cutting contribute to the differences.

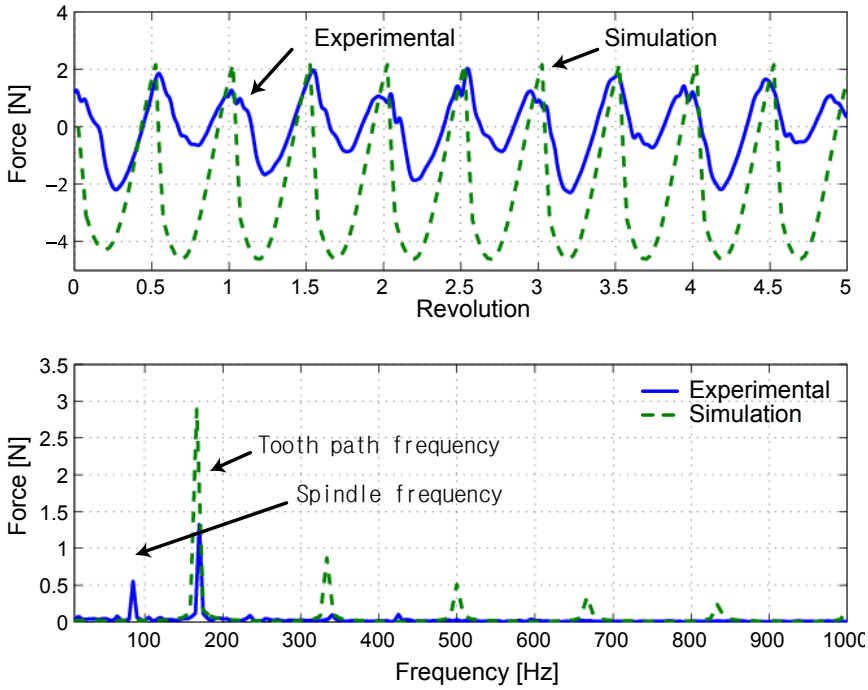

Figure 4-16 Cutting Force Measurement at 5000 rpm with 10 μm / flute.

4.5 Tool wear and breakage after micro machining

The importance of tool monitoring has been introduced in Chapter 2. This section attempts to monitor the edge of the micro tool with a digital vision system at MEDAL in off-line. The setup for the vision system and micro tool for monitoring is shown in Figure 4-17.

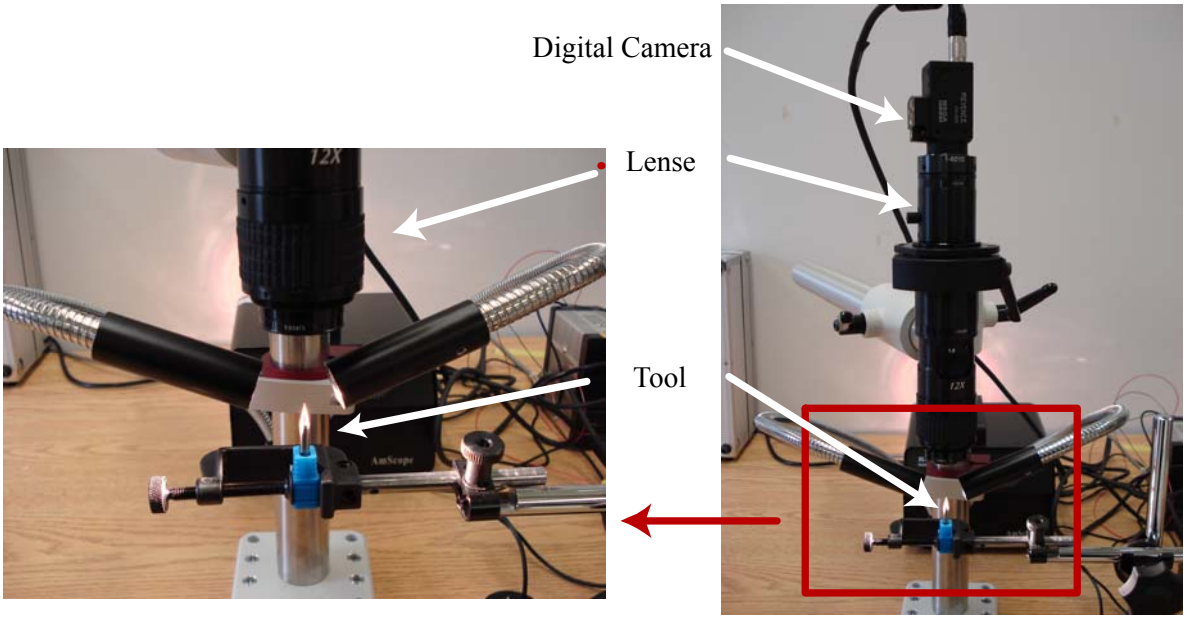

Figure 4-17 Vision system; Digital camera (Keyence, CV2600), Lenses (Navitar, Zoom12X), micro tool (Mitsubishi Material Co.)

The condition of various tools under dry cutting was observed after machining Al-7075. The cutting speed varied from 5000 rpm to 80,000 rpm. A typical axial depth of cut is 100 μm in this case. Figure 4-18 depicts that the tool wear occurs at the end cutting edge. It is clear that both cutting edges of the tool did not wear non-uniformly. This can be the evidence that only one tooth engages the workpiece more than the others, which is discussed in previous section. Debris of workpiece material adhere to the surface of the cutting edge (built-up edge).

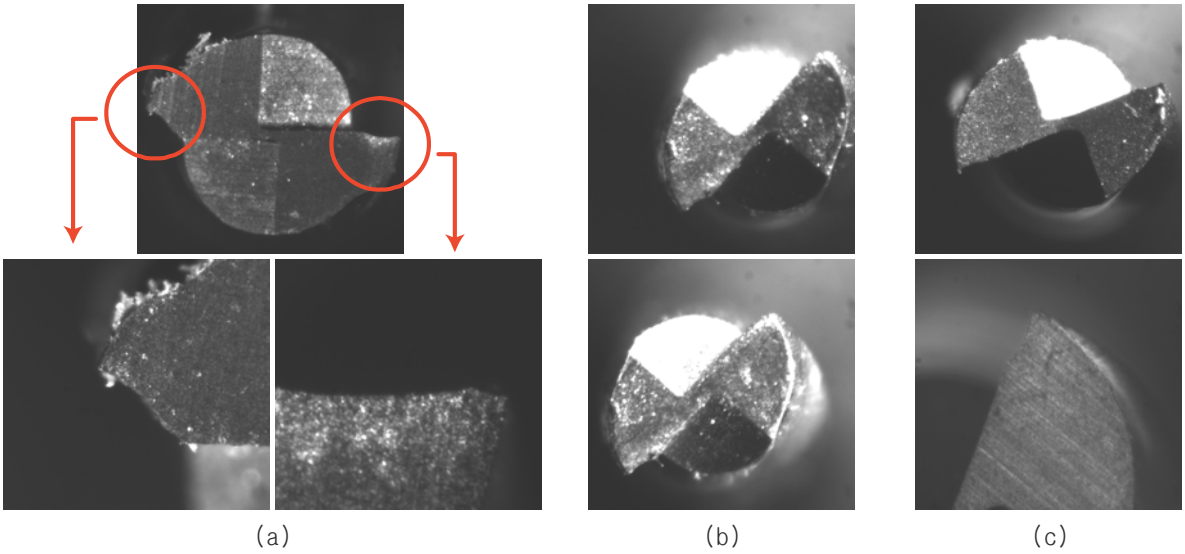

Figure 4-18 the wear of micro carbide tool after machining Al7075; (a) broken cutting edge of tool of Dia. 2mm, (b) flank wear of tools of Dia. 0.5mm, (c) new tool of Dia. 0.5mm (upper), new tool of Dia. 1 mm (lower)

The life of the micro tool cannot be estimated with bare eyes prior to operation. During machining operations, many tools used to cut the workpiece failed before they finished the operation. There are two broken patterns of the micro tools; at the end of taper parts from shank, cutting area along to the helix angle. Figure 4-19 shows the typical broken patterns of the micro tools.

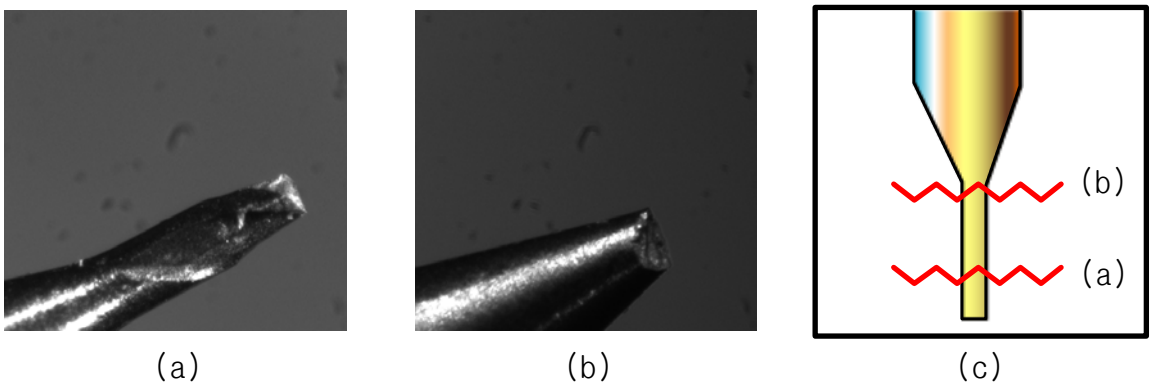

Figure 4-19 typical broken pattern of the micro tools; (a) cutting area along to the helix angle, (b) at the end of taper, (c) schematic of micro tool

It may be caused by that the diameter of micro tool tip are significantly reduced from Φ 4 mm shank because the overall geometry of the cutter will influence tool rigidity, as well

as the stress and strain experienced [Uhlmann 2005] [Mascadelli 2006].

4.6 Run-Out / Unbalance

Problems that are generally minor in the macro-domains, such as tool run-out, are amplified in the micro-domain. Tool run-out and unbalance is usually a minor problem in macro-machining operations; however, the problem is severely amplified when the diameter of the tool decreases and spindle speed increases significantly. Tool run-out is caused by a misalignment of the axis of symmetry between the tool and the tool holder or spindle. In macro-machining it often ignored, as the diameter of cutting tools is relatively large compared to the tool run-out and the speed is relatively slow compared to micro-machining.

Using laser displacement (Keyence; LKG-32), the runout of the micro CNC machine tools at MEDAL is measured. The laser displacement can only measure the object, which is bigger than 500 μm. therefore; the laser focuses on the shank of the micro tool not the tip of the micro tool. According to the specification of the installed spindle at the micro CNC machine, the maximum spindle runout is within 1 μm. However, the measured runout of the shank of the micro tool is varying between 2 μm and 6 μm, which means the tool runout depends on especially the alignment between the spindle axis and the center of the micro tools.

The unbalanced component of the rotating spindle can contribute significant noise to force measurements, especially at high rotating speeds. Like run-out, this noise is caused by the eccentricity (or unbalance) of the rotating spindle that exerts centrifugal forces. Unbalance forces are modeled as Equation (2-3), where the right hand side of the equation is the centrifugal force acting on the unbalanced mass, m_o, with a distance of the center of the unbalanced mass from the rotational axis, e, and a spindle rotational speed denoted ω_r:

$$M\ddot{x} + C\dot{x} + Kx = m_o e\omega_r^2 \sin\omega_r t \qquad (4\text{-}1)$$

Thus, the unbalanced forces are a function of the square of the rotational speed, and severe vibration can occur for high-speed micro-machining operations. This unbalance can

be also caused by the deflection of the tool due to cutting forces; however, no work has been reported in this area for micro-cutting. This oversight has perhaps contributed to difficulties in measuring micro-cutting forces, as they are severely distorted by the run-out and unbalance.

Several researchers [Dow 2004] [Bao 2000] [Ikua 2001] have investigated tool run-out by investigating cutting forces during cutting and non-cutting. They also investigated different type of tool holders, and concluded collet-type holders are superior to the set-screw type for reducing run-out. Liu *et al.* [Liu 2004, A] [Liu 2004, B] used a capacitance sensor to examine tool run-out. Capacitance sensors, however, are inaccurate on round surfaces with the displacement measurement becoming non-linear [Vallance 2004].

Tool deflection due to cutting also affects its accuracy. Lee [Lee 2001] showed that cutting marks due to tool run-out contribute to surface roughness. These cutting marks had a period of twice the chip load, indicating that one cutting edge is deeper than the other cutting edge. That is, the radius of one cutting edge appears larger than the others. Novel tool holder design may improve micro-tool run-out, and deserves more study. Rivin [Rivin 2000] surveyed tool holders, but active or passive control of tool holders using actuators may be required to compensate for any unbalance and minimize tool run-out. New geometric designs for tools may also be required in micro-machining operations where the spindle speed is very high.

4.7 Summary

This chapter has addressed the development of the micro CNC machine, cutting forces monitoring system, and application of vision system for tool monitoring system. The qualities and size of the micro products depend on the performance of the micro CNC machine. The micro CNC machine was designed and realized using 3D CAD based on the Cartesian coordinate (X, Y, Z axis) system. Due to the reduction of the size of the machine tool, various aspects such as external and internal vibration, movement resolution, and loading limitation of the system were incorporated in design stage.

The micro CNC machine tool at MEDAL consists of three fundamental units; machine tools, motion control and cutting force measurement system. The motion control

system interacts between the geometry of the micro products and the micro CNC machine tools. The micro CNC machine tool is capable of the fabrication of 3-D features on the micro scale with various engineering materials. The positioning systems in the machine have two moving mechanism; stepping motor with lead screw and a piezoelectric actuator. The combination of two mechanisms is able to achieve high resolution movement under 25nm.

Dry cutting tests were performed with various cutting conditions. The cutting force measurement system is utilizing the miniaturized 3-axis force sensors due to the load capacity of the nano cube. In order to measure the cutting forces accurately, the force sensor is calibrated using an external force gauge. Using cutting force measurement system, it was verified that the micro cutting forces are not proportional to the feed rate through the cutting tests due to the minimum chip thickness effect. In addition, Vision system checked the tool wear and tool breakage in off-line. In most cases, one of tool edge is worn out more than the other. It is caused by the tool runout or misalignment between the micro tool axis and spindle axis. Also, the sudden changing of the tool diameter from shank to tool tip reduce the rigidity of the micro tools. As a result, we often monitored the broken tools at the micro tool tip.

CHAPTER 5. COMPENSATION OF DYNAMICS OF THE FORCE SENSOR USING SENSOR FUSION

In micro machining processes, cutting forces in tools and workpieces generate high-frequency signals because of high spindle speed. One of the difficulties associated with the verification of micro cutting forces is that existing table dynamometers are limited to a small signal frequency bandwidth; and, this difficulty grows as the rotational spindle increases. For example, the spindle speed can increase up to a half million rpm. In that case, if the micro tool has a two-fluted cutter, the tooth passing frequency is 16,667 Hz. In addition, sub-Newton force measurements can easily be distorted by external noise. Commercially available table dynamometers or force sensors do not meet the requirement for measuring micro cutting forces of high-speed micro machining operations. Therefore, new methods must be applied. This chapter proposed a method which is able to monitor the micro cutting force in broadband frequency without distortion. The method was verified through various micro cutting tests.

The monitoring system in micro cutting process requires subsidiary sensors in order to compensate the distorted force signal in high frequency. Various transducers, capacitor sensors, accelerometers, or laser sensors can be used to monitor the micro cutting conditions simultaneously. The Kalman filter (KF) technique is utilized in order to reconstruct the cutting forces with the measured data from both the force sensor and the accelerometer. The delivered signals from transducers can be then superimposed on force signal by the Kalman Filter. This measuring technique is known as sensor fusion. In this particular case, the KF has two roles: to compensate for unwanted dynamics of the measuring system; and, to fuse two signals together to increase the frequency bandwidth. The following sections describe the theorem, experiment, and results.

5.1 Methodology

The KF typically consists of the system dynamics model, how the error state vector changes over time, and the measurement model between the error state vector and any measurements. Two assumptions must be considered prior to use of the KF for this

particular system. First, the actual process and measurement noise must be a zero-mean white noise. Second, the natural frequencies and damping ratios of the measuring systems are assumed to be the same. By doing so, the denominator of two transfer functions (Equation (4-1)) become the same. This means the two systems has the same system dynamics model (A_s in Equation (5-2)). The sensor dynamics can be formulated into the state space form as:

$$\dot{x} = A_s x + B_s u \ , \ z = C_s x \tag{5-2}$$

where x is the state vector, u is the input, and z is the measurement vector, consisting of measured force from the force sensor and acceleration from the accelerometer $z = \{F_m \ Acc. \}^T$. The main goal of this reconstruction scheme is the estimation of the actual cutting force, which will be $u = F_a$. The curve fitted transfer functions shown in Equation (4-1) can be reverted to the state space form using the direct programming method.

$$\begin{bmatrix} \dot{x}_1 \\ \dot{x}_2 \\ \vdots \\ \dot{x}_n \end{bmatrix} = \underbrace{\begin{bmatrix} -a_1 & -a_2 & \cdots & -a_n \\ 1 & 0 & \cdots & 0 \\ 0 & \ddots & 0 & \vdots \\ 0 & \cdots & 1 & 0 \end{bmatrix}}_{A_s} \begin{bmatrix} x_1 \\ x_2 \\ \vdots \\ x_n \end{bmatrix} + \underbrace{\begin{bmatrix} 1 \\ 0 \\ \vdots \\ 0 \end{bmatrix}}_{B_s} F_a \quad , \quad \begin{bmatrix} F_m \\ Acc \end{bmatrix} = \underbrace{\begin{bmatrix} b_0 & b_1 & \cdots & b_m \\ c_0 & c_1 & \cdots & c_m \end{bmatrix}}_{C_s} \begin{bmatrix} x_1 \\ x_2 \\ \vdots \\ x_n \end{bmatrix} \tag{5-3}$$

The matrices $\boldsymbol{A_s}$ and $\boldsymbol{C_s}$ contain both very large and very small numbers, which often results in poorly conditioned matrix conditioning with respect to inversion and eigenvalue analysis (refer to Appendix D.1). In order to cope with the problem, the system is transformed into an equivalent system using a similarity transformation [Robert 2005]:

$$A_n = T A_s T^{-1}, \quad B_n = T B_s, \quad C_n = C_s T^{-1} \tag{5-4}$$

where T is the similarity transformation matrix (refer to Appendix D.2), which balances the state space model as A_n, B_n, and C_n by equalizing maximum row and column norms across the entire matrix.

$$T = diag\left(\begin{bmatrix} 5.12e2 & 3.35e7 & 1.1e12 & 3.6e16 & 2.95e20 & 2.42e24 \end{bmatrix}\right)$$

Equation (5-2) can be rearranged as:

$$\dot{x}_n = A_n x_n + B_n u \ , \ z = C_n x_n \tag{5-5}$$

Sometimes, all of the states may not be measurable with the sensor, because the state space model is not a physical variable of the system. The observability can be checked by the rank of the observability matrix, which is defined by:

$$W^T = [C_n^T \quad A_n^T C_n^T \quad \cdots \quad (A_n^{n-1})^T C_n^T] \tag{5-6}$$

We found that the observability matrix, W, is full rank in this application (i.e. observable). The KF will estimate the posteriori state (x_n). Therefore, the state matrix (x_n) in Equation (5-5) needs to be modified into the following expanded state equation, where the input becomes a part of the state vector:

$$\begin{bmatrix} \dot{x}_{n(n\times 1)} \\ \dot{F}_{a(1\times 1)} \end{bmatrix} = \begin{bmatrix} A_{n(n\times n)} & B_{n(n\times 1)} \\ o_{(1\times n)} & 0 \end{bmatrix} \begin{bmatrix} x_{n(n\times 1)} \\ F_{a(1\times 1)} \end{bmatrix} + \Gamma_{((n+1)\times 1)} w_{(1\times 1)} \ , \ z_{(2\times 1)} = \begin{bmatrix} C_{\mathbf{n}(2\times n)} & 0_{(2\times 1)} \end{bmatrix} \begin{bmatrix} x_{n(n\times 1)} \\ F_{a(1\times 1)} \end{bmatrix} + v_{(2\times 1)} \tag{5-7}$$

where w represents noise disturbance for input, Γ is the system noise matrix, and v represents measurement noise (or sensor noise).

$$\begin{aligned} \dot{x}_{e((n+1)\times 1)} &= A_{\mathbf{e}((n+1)\times n)} \ x_{e((n+1)\times 1)} + \Gamma_{((n+1)\times 1)} \ w_{(1\times 1)} \\ z_{(2\times 1)} &= C_{\mathbf{e}(2\times(n+1))} \ x_{e((n+1)\times 1)} + v_{(2\times 1)} \end{aligned} \tag{5-8}$$

Therefore, the expanded state vector includes the cutting force (F_a):

$$x_{e((n+1)\times 1)} = \begin{bmatrix} x_n^{T}{}_{(1\times n)} & F_a^{T}{}_{(1\times 1)} \end{bmatrix}^T, \ u_e = [0] \tag{5-9}$$

The optimal estimator is given by:

$$\begin{aligned}\dot{\hat{x}}_e &= A_{\mathbf{e}}\,\hat{x}_e + \underline{K}(z-\hat{z}) = A_{\mathbf{e}}\,\hat{x}_e + K(z - C_{\mathbf{e}}\,\hat{x}_e) = (A_{\mathbf{e}} - KC_{\mathbf{e}})\hat{x}_e + K\,z \\ \hat{z}_o &= C_{\mathbf{o}}\,\hat{x}_e = \hat{F}_a, \quad with\ C_{\mathbf{o}} = \begin{bmatrix} 0_{(1\times n)} & 1 \end{bmatrix}\end{aligned} \tag{5-10}$$

where K is the Kalman filter gain matrix, and $\hat{F}_a$ is an estimate for the actual cutting force F_a. The optimal K gain matrix is defined by minimizing the error $(\hat{x}_e - x_e)$ covariance matrix P, which is the solution of the algebraic Riccati equation.

$$\dot{P} = A_{\mathbf{e}}\,P + P\,A_{\mathbf{e}}^{\mathbf{T}} + \Gamma\,Q\,\Gamma^{\mathbf{T}} - P\,C_{\mathbf{e}}^{\mathbf{T}}\,R^{-1}\,C_{\mathbf{e}}P \quad , \quad K = P\,C_{\mathbf{e}}^{\mathbf{T}}\,R^{-1} \tag{5-11}$$

It is assumed that white Gaussian zero-mean processes with known covariance are as given below:

$$Q = E[w\ w^T] > 0, \quad R = E[v\ v^T] \geq 0, \text{ and } E[w\ v^T] = 0 \tag{5-12}$$

The KF relies on either the system model or the measurements for estimates. It depends on the level of the noises (R and Q). When the measurement is good (R is small) and Q is larger, it results in a fast filter with high bandwidth. For this study, the measurement covariance R is obtained based on the electronic and air cutting noise from the force sensor and accelerometer. A data acquisition system measured the magnitudes of each sensor signal during air-cutting (no cutting). The RMS values of the measured signals are used as the measured covariance. The system covariance Q is acquired through tuning (trial and error), and Γ is:

$$R = diag[0.001 \quad 0.25];\ Q = [1.0e10];\ \Gamma = \begin{bmatrix} 0_{(1\times 6)} & 1 \end{bmatrix}^T \tag{5-13}$$

The gain, K, is obtained as:

$$K = \begin{bmatrix} 2.14e4 & 1.29e4 & 1.343e3 & -5.32e2 & 3.28e2 & 1.045e2 & 2.59e6 \\ 9.32e2 & 5.489e2 & 1.27e2 & 4.84e1 & -2.94e1 & -9.48 & 1.15e5 \end{bmatrix}^T$$

The continuous Kalman filter transfer function can be derived from Equation (5-13) as:

$$\hat{F}_a = \left\{ \frac{C_0\ adj[sI - (A_e - KC_e)]}{\det[sI - (A_e - KC_e)]} K \right\} \cdot z = G_F \cdot F_m + G_A \cdot Acc \tag{5-14}$$

$$G_F = \frac{2.59e6s^6 + 5.69e9s^5 + 3.37e15s^4 4.76e18s^3 1.45e24s^2 + 9.85e26\,s + 2.05e32}{s^7 + 2.3e5s^6 + 2.78e10s^5 + 1.78e15s^4 + 2.53e19s^3 + 1.38e24s^2 + 5.7e27s + 2.81e32}$$

$$G_A = \frac{1.15e5s^6 + 2.6e8s^5 + 1.5e14s^4 + 2.2e17s^3 + 6.3e22s^2 + 4.6e25s + 8.9e30}{s^7 + 2.3e4s^6 + 2.78e10s^5 + 1.78e15s^4 + 2.53e19s^3 + 1.38e24s^2 + 5.7e27s + 2.81e32}$$

There are two measured signals; 'Z' from the force sensor and accelerometer, and two optimal KF gains; 'K' in Equation (5-14). Therefore, the two TFs have the same denominator and two different nominators. However, the output matrix 'C_o' in optimal estimator (Equation (5-10)) only produce the optimal estimated cutting forces. For digital signal processing, Equation (5-14) is transformed into an equivalent discrete transfer function using continuous-to-discrete-transformation and zero-order-hold:

$$\hat{x}_e(k+1) = \exp\{(A_e - KC_e)\,t_d\}\hat{x}_e(k) + \left(\int_0^{t_d} \exp\{(A_e - KC_e)\,\tau\}\,K\,d\tau \right) z(k)\ ,\ \hat{F}_a(k) = C_o\,\hat{x}_e(k) \tag{5-15}$$

The FRFs of the model, Kalman filters, and cascaded systems are depicted in Figure 5-1 for the force sensor and accelerometer. The compensated sensor systems have constant gains at wide frequency regions; therefore, the micro cutting force is measured at the high frequency without distortion by the dynamics of the measurement systems. A similar approach can be used to compensate in Y and Z directions (Appendix D).

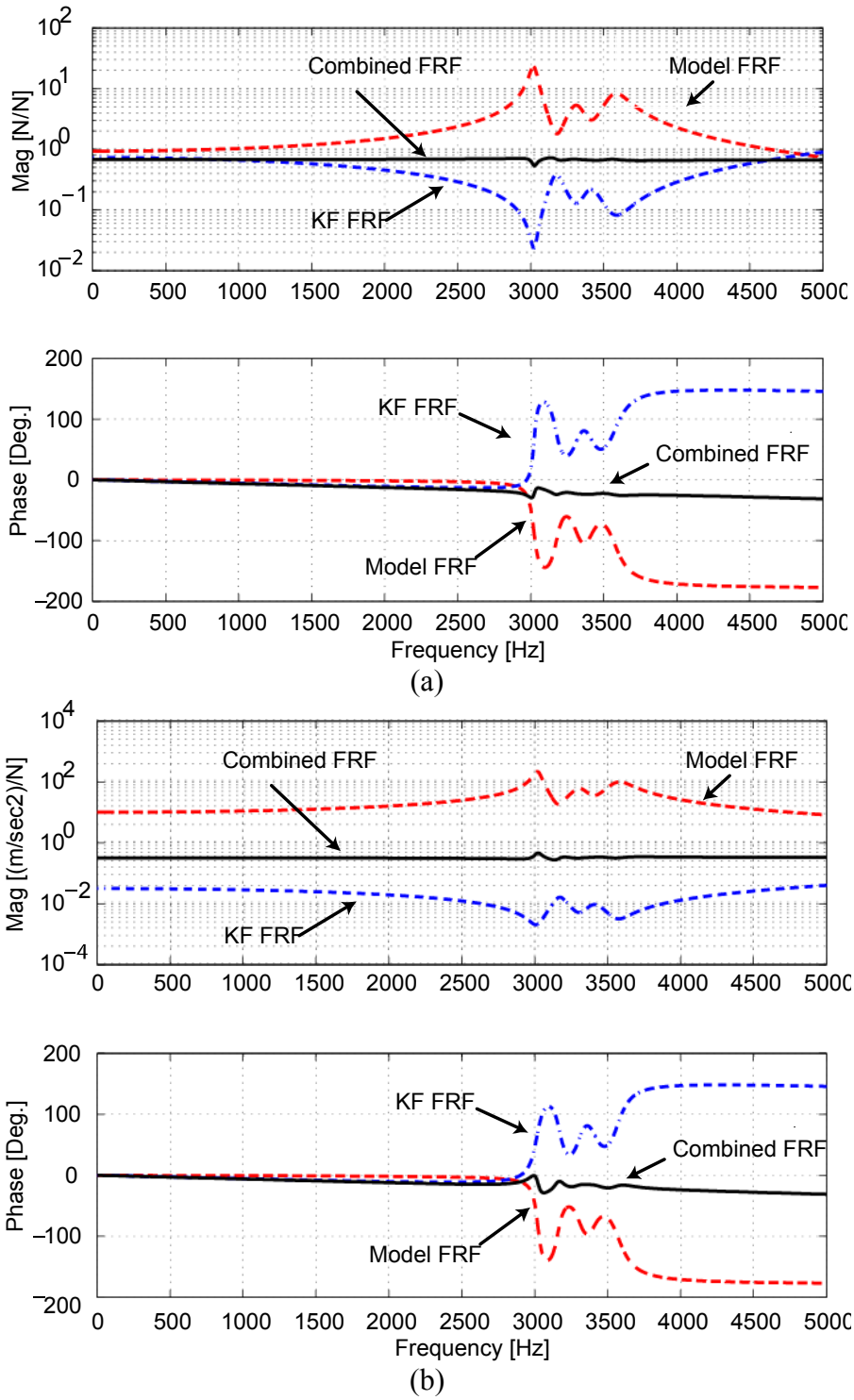

Figure 5-1 FRFs of the Model, Kalman Filter and Cascaded System for: (a) Force Sensor and (b) Accelerometer System

5.2 Experiment and result

Various cutting tests with different tools and cutting conditions are performed with the developed micro machining centre. The accurate cutting force signals are reconstructed via the proposed compensation scheme based on fusion of the force and acceleration signals and compensation of unwanted dynamics. Through experimental cutting tests, the performance of the precision micro machining centre is also examined. The spindle speed and the movement of the precision table are monitored by voltages from the spindle controller and steps from the motion controller respectively.

The cutting force and acceleration signal are acquired through the data acquisition system with a sampling rate of 100 kHz. Since the frequency range of interest is up to 10 kHz, the signals are passed through the anti-aliasing filters (Kron-Hite 3364), where the cut-off frequency is 10 kHz and 4^{th} order Butterworth filters are used.

5.2.1 Preprocessing

In order to measure the force signals accurately, the cutting force signals are pre-processed by subtracting the air cutting signals where the force signals are measured without engagement of the tool to the workpiece. The air cutting force signals are mainly contributed to from the eccentricity of the tool (i.e. tool run-out), feed drive noise due to bearings, and inherent ground noise. The vibration caused by the spindle at high rotational speeds is transmitted to the force sensor.

The air cutting force signals are quite observable when the spindle rotational speed is at 80,000 rev/min. The subtraction of the air cutting forces from the measured force requires synchronization of the spindle at each revolution. This is achieved by using the high frequency bandwidth laser sensor (Keyence LK-G32) to measure the micro tool: a small piece of tape is attached on to the shank of the micro tool to measure each revolution. The measured cutting forces (F_c) and the air cutting forces (F_{air}) are synchronized at each revolution of the spindle and pre-processed prior to the KF compensation.

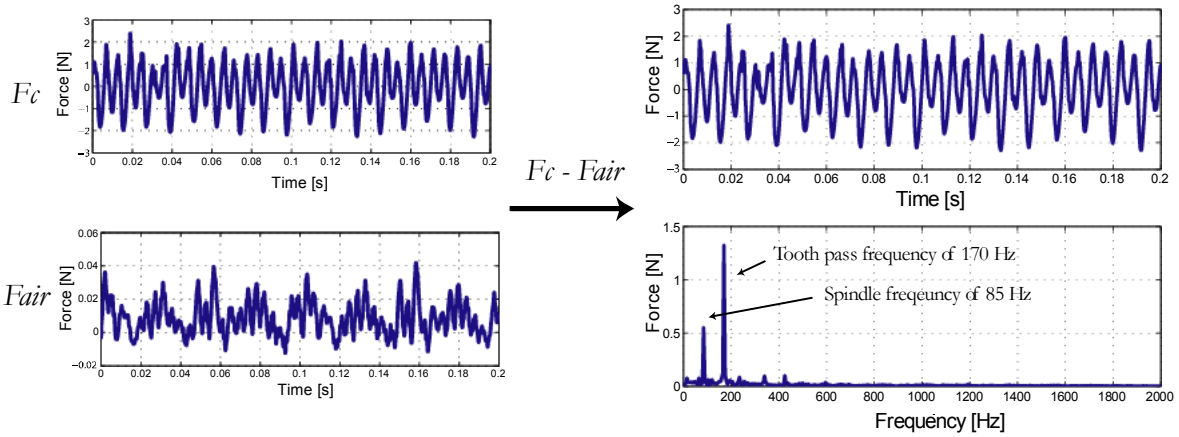

Figure 5-2 Pre-Processed Micro Cutting Force Data

5.2.2 Micro Cutting Force Compensation

The tools used in the tests are two-fluted end mills made of fine-grain tungsten carbide (WC). The diameter of the tools is 200 μm; the helix angle is 30 degrees; and, the shank diameter is 4 mm. The workpiece used in the tests is aluminum 7075. The cutting condition is full-emersion slot milling, where the feed rate is 0.5 μm per tooth and the axial depth of cut is 50 μm. The spindle speeds were chosen at 5000, 40,000, and 80,000 rev/min. The corresponding tooth passing frequencies are 167, 1333, and 2667 Hz, respectively. We expect that the force measurements at the high rotational speeds of 40,000 and 80,000 rev/min are distorted, due to the dynamics shown in Figure 5-1(a), since the bandwidth of the sensor is approximately 1000 Hz when we consider less than 10% errors in magnitudes. This means, therefore, that the micro cutting forces with a two-fluted micro end mill can be measured without distortion when the spindle speed is below 30,000 rev/min. The maximum distortion occurs at the first natural frequency (3021 Hz), which corresponds to a spindle speed of 90,630 rev/min.

In this study, forces at 5000 rev/min are utilized as the reference force measurements to verify the proposed method. It is assumed that the cutting forces at higher rotational speeds should exhibit the same force magnitudes, and the effect of thermal softening of workpiece is neglected due to very small chip loads. The experimentally measured uncompensated cutting forces at various rotational speeds are exhibited in Figure 5-3, where the top figure depicts the time domain and the bottom figure illustrates the frequency

domain signals. The peak-to-peak values of the reference forces are approximately ± 0.2 N. As expected, force measurements at 40,000 and 80,000 rev/min exhibit distortions, since the tooth passing frequencies come close to the first natural frequency of the measuring system. Especially at 80k rev/min, the peak-to-peak values are approximately ± 0.5 N (250 % deviation); therefore, the uncompensated force signals at high rotational speeds need to be compensated.

The experimentally measured forces are reconstructed based on the proposed Kalman filter approach using Equation (5-14). The compensated cutting forces at 40k and 80k rev/min are exhibited in Figure 5-3(b), based on the fused signals from the force sensor and accelerometer. The compensation method performed well at both speeds, and the deviations between the reference forces and the compensated force decreased significantly. This verifies that the proposed KF compensates for unwanted dynamics of the measuring system and fuses two signals together to increase the frequency bandwidth.

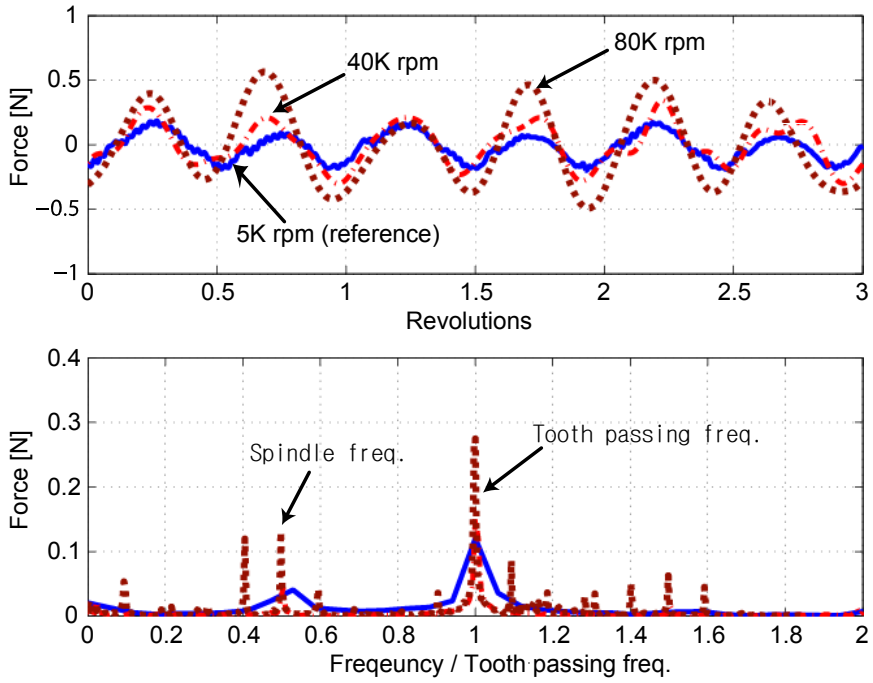

(a)

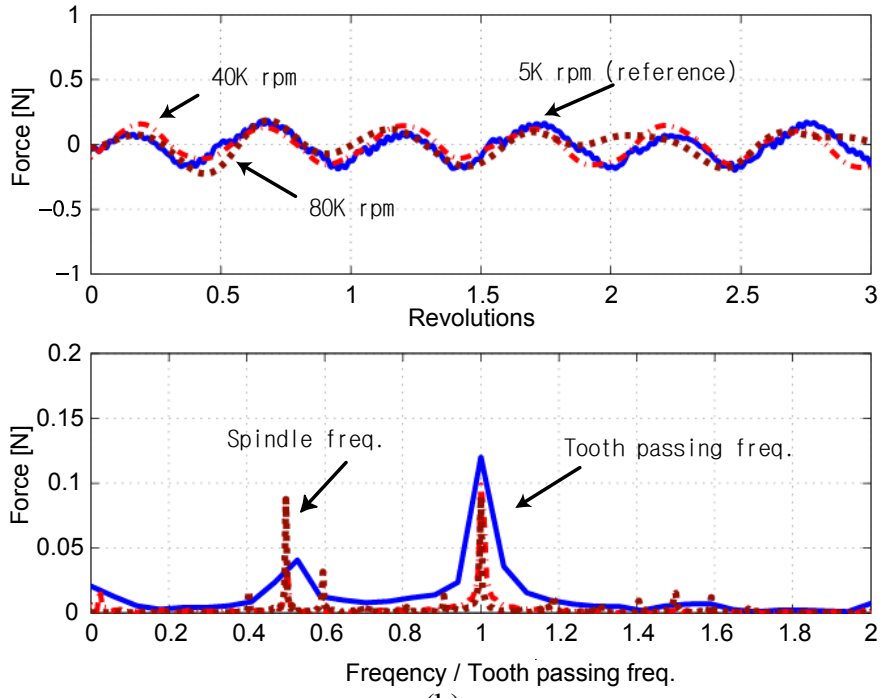

(b)

Figure 5-3 Cutting Force Measurements: (a) Without Compensation and (b) With Compensation

In this study, we utilize the expanded Kalman filtering scheme, which compensates for unwanted dynamics by fusing the force and acceleration signals. The various cutting tests are performed using 200 μm diameter micro end mills to machine an aluminum 7075 workpiece. The compensation scheme effectively compensates for unwanted dynamics. This will provide the basis for accurately monitoring of micro machining operations.

There are several assumptions in this proposed scheme are required to investigate more in-depth analyses in micro machining operations. We are not able to measure the tool run-out accurately: since the diameter of the tool is 200 μm with the sculpted surfaces, the laser cannot be properly focused. The inertial effects due to movements of the stage are neglected, owing to the small mass and constant velocity during machining. Also, the gravity centre of the acceleration is equal to the acceleration of any point of the workpiece by neglecting the rotation. The change in dynamics of the measurement system is assumed to be negligible, since the amount of material removed from the workpiece is miniscule compared with the overall mass of the workpiece.

The accurate measurement of cutting forces can also be obtained using the force sensor [Park 2004]. Even accelerometer signals provide cutting forces [Spiewaks 1995].

Unlike the force sensor system where the calibration is required whenever workpiece is changed, the accelerometer can be easily placed on the workpiece. Nevertheless, the sensor fusion of force and accelerometer signals provides redundant information about micro cutting conditions which increases reliability. In this work, the effects of accelerometer play a secondary role compared with the force sensor to obtain the high frequency cutting forces based on the inertance graph in Figure 5-1(b).

5.3 Summary

One of the limitations of the typical micro cutting force monitoring system is the low bandwidth due to the dynamics of the sensors. However, the tool passing frequency of the micro machining process is typically higher than the bandwidth of the table dynamometer or force sensor due to the high spindle speed (i.e. from 10,000 rpm to 500,000 rpm). Using sensor fusion with the Kalman filter, the high bandwidth cutting force measurement system is developed and verified through the experiment based on several assumptions such as linear models, and the error characteristics of each sensor have zero-mean, Gaussian noise. Accelerometer and force sensor are utilized and 350 % bandwidth of the micro cutting force monitoring system are increased. As a result, we are able to monitor the micro cutting forces accurately at 80,000 rpm.

This proposed method is able to improve the performance of the micro cutting process. For instance, when tool wear or breakage occurs, the magnitude of micro cutting forces will increase unexpectedly. In addition, the micro cutting forces in frequency domain should match with a tool passing frequency or its harmonic responses. The forces at different frequencies indicate that the micro cutting operation is experienced by a forced vibration such as chatter vibration. Therefore, operators/engineers can optimize micro cutting conditions based on the measured cutting forces in off-line or on-line. By doing that, the tool wear and tool breakage can be minimized and chatter vibration can be analyzed.

CHAPTER 6. CONCLUSION AND FUTURE WORK

6.1 Conclusion

The precision micro milling operation has been studied in depth. The micro milling operation is one of the emerging fabrication processes for micro structures owing to the demand in various industries such as MEMS and the bio-medical arena. However, there is insufficient knowledge and experience for micro mechanical machining operations to meet demands to fabricate functional 3D systems. Various aspects of micro-mechanical machining operations have been researched; literature review of state-of-art micro milling operations, joint identification methods, development of the micro CNC machine, and a high bandwidth cutting force measurement system in order to improve the performance of micro milling operations. The identified joint dynamics with the proposed method can increase the accuracy of the dynamic prediction of micro machine tools and the accurately measured micro cutting forces can determine the status of micro cutting tool indirectly. This information (micro machine tool dynamics and tool conditions) can be utilized for engineers/operators to set up the optimal conditions for machining operations.

The precision micro CNC machine is also realized from a design stage to actual micro cutting tests. Various issues especially dynamic problems are considered and addressed during the fabrication process. Joint identification method and sensor dynamics compensation method are proposed and verified through the experiment in order to overcome the limitations (i.e. bandwidth of force measurement and dynamics prediction of the assembly) in micro machining process as well as the system consisting of several sub-systems.

The contributions in this thesis are summarized as follows:

a. The state of the art survey of micro-milling operations is conducted. The micro milling operations are found to be an appropriate method for fabricating 3D structure with various engineering materials. The work also finds that there are similarities between the micro and macro operations related to tool wear, tool breakage, cutting forces, instability. However, there are significant differences in the cutting force models, monitoring, etc. Many research topics, which are using conventional theories

in order to understand the micro cutting conditions, are introduced in this thesis because the principals of micro machining are similar to conventional machining. Several new issues such as effect of workpiece material (grain size), minimum chip thickness, handing, testing, and assembly problem, which are caused by its significant size reduction, are described. The work is published in the Int. Journal of Machine Tools and Manufacture [Chae 06.A].

b. The dynamics of machine tools are obtained accurately with less experiment efforts owing to receptance coupling method with the identified joint dynamics. A novel method, which couples receptance matrix of substructures from EMA and FE analysis, was also presented in order to identify joint dynamics in this thesis. This proposed method is verified by performing the impact hammer test with a fastener joint. In addition, using an interchangeable cutter with a conventional machine tool, the proposed method shows feasibility in the real world. The work has been presented at two conferences [Chae 05A] [Chae 05B] and submitted to International Journal of Advanced Manufacturing Technology [Chae 06C]

c. Owing to many advantages such as space, energy, portability, and cost, the miniaturized machine tools are recently focused on fabricating the micro products. In this thesis, the 3-axis micro CNC machine at the MEDAL was developed based on the conventional column-knee type milling machine. The machine consists of high speed electric motor, air-turbine spindle, precision tables and controllers. Using the CAD software, several structures; spindle holder, vertical support, base plate, workpiece are designed with considering various issues such as materials, size, and thermal effects. The micro CNC machine is capable of fabricating 3D micro structures such as micro channels and micro holes. A portion of the work is presented and published in the 2006 CSME conference [Mascardelli 06].

d. It is impractical for human to control the micro machining operations because the parts cannot be observed with human’s bare eyes. Therefore, the micro machine tool must be controlled and operated by some kind of automation system in order to increase machining accuracy and its performance. In this thesis, the control unit was developed at the MEDAL to automate and control the micro CNC machine. The control unit consists of a personal computer, a motion controller and Motion

Assistant™ [National Instrument Co.] in order to interface the geometry of parts and the micro CNC machine tool. The interface generates pulse signals, which are fed to the stepping motor controllers, move the linear tables in X, Y, and Z axis according to desired locations. By doing so, the micro tool tip can locate to any location on a workpiece in 3D. In addition, spindle speed is controlled by the D/A converter. As a result, the cutting conditions; feed rate, axial depth of cut, spindle speed, and X, Y, Z locations of tool tip can be set by a user.

e. The micro cutting monitoring system was developed in order to monitor the micro cutting process using various sensors; miniaturized 3-axis small force sensor, an accelerometer, and laser sensor. A data acquisition system captures all signals from the sensors with various sampling rates and numbers of data. In addition, the force sensor is precisely calibrated using a force gauge. For the verification process, the micro cutting forces are simulated with impact hammer and dynamics of force sensor and accelerometer was found. The signals from force sensor and accelerometer under various cutting conditions can be also correlated and compared by using laser sensor signals, which are generated at every revolution of the micro tool.

f. The high bandwidth of the cutting force measurement system was developed using sensor fusion with the expanded Kalman filter in order to overcome the limitation of the conventional force sensor. The measurement system is also verified through various cutting test experiments. The expanded Kalman filter plays two roles; fusing two signals from the force sensor and the accelerometer, and estimating the actual micro cutting forces. This system increased about 350 % bandwidth of the micro cutting force monitoring system for this particular system. Therefore, it is able to measure accurately the micro cutting force at the spindle speed 150,000 rpm. In this thesis, the micro cutting forces at 80,000 rpm were measured without distortion from sensor's dynamics. The work is presented in the 2006 CIRP-HCP Conference [Chae 06B] and submitted to the Int. Journal of Machine Tools and Manufacture.

Through this research, some macro domain knowledge (joint identification method using RC and high frequency bandwidth cutting forces measurement system) has been translated to the micro domain in order to increase the performance of micro mechanical

machining. This thesis covers various aspects of the development of the micro CNC machine from theory to application, and was originally based on conventional CNC machine design. A couple of methods are proposed to overcome the limitation of the current micro mechanical techniques. These methods are also applicable to any other micro mechanical process, such as micro lathe and micro drilling, including conventional machining process.

6.2 Future Work

Micro-mechanical machining provides a niche opportunity to bridge the gap between the micro/nano- and macro-domains. This is especially true for providing functional devices and assemblies that are made out of a variety of materials. This section suggests future research directions for mechanical micro-fabrication methods to create 3D components. There are still a lot of issues requiring attention especially prediction of cutting forces, on-line micro tool monitoring, minimum chip thickness detection, and measurement of dynamics of the micro tools as well as the fabricated parts.

Identification of the axial distance of the micro tool from the workpiece

Due to the small size of micro tools, the tools are very fragile. Many tools are damaged prior to actual machining during the setup stage. For example, the engineer /operator must know the axial distance (Z-axis) of the micro tool from the workpiece. It is also affected by the insert length of the micro tool into the spindle. The current micro CNC machine moves Z axis to the workpiece with small increments (10 μm) step by step while the spindle is rotating. As soon as the micro tool is engaging with the workpiece, the operator stops Z-axis and resets the locations of X, Y, Z axis as zero. The micro tool then machines the surface of the workpiece by moving only Z and Y axis to make a reference datum on the workpiece. This pre-process is very critical to micro machining. Based on the micro cutting experiences, this process generates tool wear as well as tool breakage. Therefore, the methods, which can solve this problem, must be studied [Bourne 2006].

Prediction of micro cutting forces and minimum chip thickness

Many improvements to micro-cutting can be achieved by advancing models for the accurate prediction of the micro-cutting process. The accurate prediction of micro-cutting forces enables the selection of an optimal feed rate to provide maximum chip removal without instability. This will also permit tool deflection compensation and minimize tool wear and built-up edge. Accurate prediction of the minimum chip thickness is also important. Various researchers have developed chip formation models to quantify the minimum chip thickness necessary for chip formation instead of elastic deformation. A consolidated model for the minimum chip thickness is required for various materials and cutting conditions. Detailed investigation is needed to determine the effects such as built-up edge, deflection, elastic-plastic behavior, run-out, tool wear and thermal expansion. Limited research has been performed for these individual effects; however, the combined effects need to be addressed to further understand the micro-machining phenomena.

Preprocess for workpiece material

To improve uniformity and consistency of micro-components, the workpiece materials need to be uniform. Since the material costs for micro-components are relatively small compared with the macro-processes, better treatment of workpiece materials is required. Further studies are required to explore various workpiece materials including engineering alloys, composites, plastics, and ceramics. Developing appropriate machining and post-processing techniques to reduce and remove burrs and residual chips on the fabricated part also warrants additional investigation.

Real-Time Monitoring

At very high spindle speeds, measurement and monitoring becomes critical. Since the maximum rotational speed for the developed system at MEDAL is only 80,000 rev/min in this particular system, we are not able to excite the system at the first, second or third modes of the cutting force measurement system. If we perform highly intermittent cuttings (i.e. small immersion), the harmonics of the signals will excite three modes and

compensation becomes vital. Further study is also required to predict micro cutting forces accurately; and, the real-time monitoring scheme based on the proposed method needs to be implemented to detect tool wear and breakage.

At present, micro-machined products and tools are generally monitored off-line using the special instruments such as vision system and SEM which are expensive and trained technicians. As a result, developing new inspection and testing techniques will have significant impact. Online monitoring of micro-machining processes is becoming essential. For example, online monitoring of tool breakage and wear detection, chatter suppression and adaptive control will increase tool life, minimize tolerance violation, and improve quality and productivity. The real-time monitoring of machining processes is possible when you have accurate and reliable high-bandwidth sensor signals. The fusion of various sensor signals also holds promise to capture and monitor micro-machining processes robustly.

Testing and Assemblies

Experimental modeling and testing of micro-components will be important for the assembly of functional devices. Due to the miniature size of micro-components, the human eye alone is not sufficient to observe micro-component defects or micro-system performance. Sophisticated vision and optical systems are needed to examine the accuracy and surface finish of finished components. It is anticipated that the production of 3D shapes that micro-machining makes possible will also make their testing and handling quite difficult. Optimal pre- and post-processing techniques and features are needed when developing micro-components to provide handling, clamping and interfaces. Assembly techniques are also required with requisite precision in monitoring, sensing and actuation.

Some macro-phenomena have been translated to the micro-domain, but not without difficulties. Adapting macro-machining knowledge, and shifting its paradigm where appropriate, is essential to making micro-machining processes more flexible, robust and productive. The unique ability of micro-mechanical cutting to fabricate 3D shapes cost effectively using variety of materials provides new opportunities and applications. The integration of design, fabrication, assembly and testing of functional, finished 3D micro-systems still remains a challenge.

REFERENCE

[Adams 2001] D.P Adams, M. J. Vasile, G. Benavides, A. N. Cambell, Micromilling of metal alloy with focused ion beam-fabricated tools, J. Int. Societies of Precision engineering and nanotechnology 25 (2001) 107-113.

[Alting 2003] L. Alting, F. Kimura, H.N. Hansen, G.Bissacco, Micro engineering, Annals of CIRP Keynote (2003) STC-O.

[Altintas 1989] Y. Altintas, I. Yellowley, The process detection of tool failure in milling using cutting force models, ASME J. of Eng. for Industry 111 (1989) 149-157.

[Altintas 1992] Y. Altintas, Prediction of cutting forces and tool breakage in milling from feed drive current measurements, ASME J. of Eng. of Ind. 114 (1992) 386-392.

[Altintas 2000] Y. Altintas, Manufacturing Automation: Metal Cutting Mechanics, Machine Tool Vibrations, and CNC Design, Cambridge University Press, 2000.

[Atre 2004] A. Atre, Dynamic response of surface micro machined horizontal beam flexure actuator, Proc. ASME International Mechanical Engineering Congress and Exposition. Anaheim California, 13-20 Nov, 2004.

[Bang 2004] Y.B. Bang, K. Lee, S. Oh, 5-Axis Micro Milling Machine for Machining Micro Parts, Advanced Manufacturing Technology (2004).

[Bao 2000,A] W. Y. Bao, I. N. Tansel, Modeling micro-end-milling operations. Part1: analytical cutting force model, International Journal of Machine Tools & Manufacture 40 (2000) 2155-2173.

[Bao 2000,B] W. Y. Bao, I. N. Tansel, Modeling micro-end-milling operations. Part2: tool run-out, International Journal of Machine Tools & Manufacture 40 (2000) 2175-2192.

[Benavides 2001] G.L. Benavides, D.P. Adams, P. Yang, Meso-Machining Capabilities, Sandia Report (2001).

[Bergman 2001] MA, X., Bergman, L., Vakakis, A., Identification of bolted joints through laser vibrometry, Journal of Sound and Vibration, 246, (2001) pp. 295-316.

[Berktold 1993] W. Konig A. Berktold, K.-F. Koch, Turning versus grinding-A comparison of surface integrity aspects and attainable accuracies, Annals of CIRP 42 (1993) 39-43.

[Bourne 2006] K. Bourne, M. Jun, S. G. Kapoor, R. E. Devor, An acoustic emission-based method for determining relative orientation between a tool and workpiece at the

micro-scale, Univerisy of Illinois at Urbana-Champaign, 2006.

[Breguet 1997] J. M. Breguet, S. Henein, R. Mericio, R. Clavel, Monolithic piezoceramic flexible structures for micromanipulation, Proc. of the 9th Int. Precision Engineering Seminar (1997) 397-400.

[Budak 2000] E. Budak, Improving productivity and part quality in milling of titanium based impellers by chatter suppression and force control, Annals of CIRP 49 (2000) 31-36.

[Byrne 1995] G. Byrne, D. Dornfeld, I. Inasaki, W Konig, R. Teti, Tool condition monitoring (TCM) – The status of research and industrial application, Annals of CIRP 44(2) (1995) 541-567.

[Byrne 2003] G. Byrne, D. Dornfeld, B. Denkena, Advancing Cutting Technology, Annals of CIRP (2003) 483.

[Chae 2006A] J. Chae, S.S. Park and T. Freiheit, "Investigation of Micro-cutting Operations", International Journal of Machine Tools & Manufacture, 46, 2006, pp. 313-332.

[Chae 2006B] J. Chae, S.S. Park, "High Frequency Bandwidth Measurements of Micro Cutting Forces", CIRP 2nd International Conferences High Performance Cutting, Jun 12-23, 2006.

[Chae 2005A] J. Chae, S.S. Park and S. Lin, "Substructure Coupling with Joint Identification for Reconfigurable Manufacturing Systems", The International Conference on Design Education (CDEN), Kananaskis, Alberta, Canada, July 18-20, 2005.

[Chae 2005B] J. Chae, S.S. Park, "Joint Identification Method using Receptance Coupling Techniques", Western Manufacturing technology show, Edmonton, Alberta, Canada, June 14-16, 2005.

[Chae 2006 C] J. Chae, S.S. Park, "Joint Identification using a novel Receptance Coupling method", International Journal of Advanced Manufacturing Technology, Submitted at 19th April, 2006

[Choi 1999] D. Choi, W.T. Kwon, C.N. Chu, Real time monitoring of tool fracture in turning using sensor fusion, Int. J. of A. Mfg. Tech. 15(5) (1999) 305-310.

[Constantinides 1987] N. Constantinides, S. Bennett, An investigation of methods for on line estimation of tool wear, International Journal of Machine Tools & Manufacture 27 (2) (1987) 225-237.

[Corbet 2000] J. Corbett, P. A. McKeon, G. N. Peggs, R. Whatmore, Nanotechnology: International developments and emerging products, Annals of CIRP 49 (2000) 523-546.

[Cox 2004] D. Cox, G. Newby, H. W. Park, S. Y. Liang, Performance evaluation of a Miniaturized machining center for precision manufacturing, Proc. ASME International Mechanical Engineering Congress and Exposition. Anaheim California, 13-20 Nov, 2004.

[Darwish 2003] Darwish, S.M., Chrateristics of weld-bonded commercial aluminum sheets (B.S. 1050), International Journal of adhesion & adhesives 23 (2003) pp. 169-176,

[Davies 1995, B] M. A. Davies, Y. Chou, C. J. Evans, On chip morphology, tool wear and cutting mechanism in finish hard turning, Annals of CIRP 45 (1995) 77-82.

[Davies 1995,A] M. A. Davies, C. J. Evans, K. K. Harper, Chip segmentation in machining AISI 52100 steel, ASPE 11th (1995) 235-238.

[Dimla 1999] D. E. Dimla, Tool wear monitoring using cutting force measurements, 15th NCMR, University of Bath (1999) 33-37.

[Dimla 2000] Snr. D.E. Dimla, Sensor Signals for tool wear monitoring in metal cutting operations – a review of methods, Int. J. Mech. Sci. 40 (2000) 1073-1098.

[Dornfeld 1990] D. A. Dornfeld, Neural network sensor fusion for tool conditioning monitoring, Annals of CIRP 39(1) (1990) 101-105.

[Dow 2004] Thomas A. Dow, Edward L. Miller, Kenneth Garrard, Tool force and deflection compensation for small milling tools, Precision Engineering 28 (2004) 31-45.

[Dugas 2002] A. Dugas, J. Lee, J. Hascoet, An enhanced machining simulator with tool deflection error analysis, Journal of Manufacturing Systems 21(6) (2002) 451-463.

[El-Fatatry 2003] A. El-Fatatry, EUSPEN Vision Online: Transferring Microsystems Technology, NEXUS report (2003).

[El-Wardany 1996] T. I. El-Wardany, D. Gao, M. A. Elbestawi, Tool condition monitoring in drilling using vibration signature analysis, International Journal of Machine Tools & Manufacture 36 (6) (1996) 687-711.

[Fang 2003] F. Z. Fang, H. Wu, X. D. Liu, Y. C. Liu, S. T. Ng, Tool geometry study in micromachining, Journal of Micromechanics and Microengineering 13 (2003) 726-

731.

[Fearing 1995] R. S. Fearing, Grasping for macro-scale and micro-scale, IROS 95 Workshop on Working in the micro-world: Systems to enable the manipulation and machining of micro-objects (1995) 13-40.

[Furukawa 1988] Y. Furukawa and N. Moronuki, Effect of material properties on ultra precise cutting process, Annals of CIRP, 37(1) (1988) 113-116

[Furuya 1990] Y. Furuya, H. Shimada, Shape memory actuators for robotic applications, in engineering Aspect of Shape Memory Alloys, Butterworth Heinemann (1990) 338-355.

[Gialamas 1996] Gialamas, T., Tsahalis, D., Bregant, L., Otte, D., H. Van der Auweraer., Substructuring by means of FRFs: some investigations of the significance of rotational DOFs, 14th IMAC Vol 1 (1996)

[Greitmann 1996] G. Greitmann, R. A. Buser, Tactile micro gripper for automated handling of micro parts, Sensors and Actuators 53 (1996) 410-415.

[Grum 2003] J. Grum, M. Kisin, Influence of microstructure on surface integrity in turning-part 2: the influence of a microstructure of the workpiece material on cutting forces, International Journal of Machine Tools & Manufacture 43 (2003) 1545-1551.

[Hanss 2002] Hanss, M., Oexl, S., Gaul, L., Identification of a bolted-joint model with fuzzy parameters loaded normal to the contact interface, Mechanics Research Communications 29 (2002) pp. 177-187

[Hart 2000] M. Hart, R. Conant, K. Lau, R. Muller, Stroboscopic interferometer system for dynamic MEMS characterization, Journal of Microelectromechanical Systems 9(4) (2000) 409-418.

[Hesselbach 2004] J. Hesselbach, A. Raatz, J. Wreg, H. Herrman, S. Illenseer, H Weule, J Fleischer, C. Buchholz, M. Knoll, J. Elsner, H. Tritschler, F Klocke, M Weck, J. Bodenhausen, A Klitzing, International state of the art of micro production technology, Production Engineering 11(1) (2004) 29-36.

[Howe 2003] R.T. Howe, Micro Systems Research in Japan, World Technology Evaluation Center (WTEC), (2003).

[Ibrahim 2005] Ibrahim, R.A., Pettit, C.L., uncertainties and dynamic problems of bolted joints and other fasteners, Journal of Sound and Vibration 279 (2005) pp. 857-936.

[Ikua 2001] B. W. Ikua, H. Tanaka, F. Obata, S. Sakamoto, Prediction of cutting forces and machining error in ball end milling of curved surfaces -I theoretical analysis, J. Int. Societies of Precision engineering and nanotechnology 25 (2001) 266-273.

[Jardret 1998] V. Jardret, H. Zahouani, J. L. Loubet, T. G. Mathia, Understanding and quantification of elastic and plastic deformation during a scratch test, Wear 218 (1998) 8-14.

[Jorgensen 1996] B. R. Jorgensen., Y. C. Shin, Dynamics of machine tool spindle/bearing systems under thermal growth, DSC 58 ASME (1996) 333-340.

[Jun 2005] M.B. Jun, Modeling and Analysis of Micro-End Milling Dynamics, Ph.D Dissertation, University of Illinois Urbana-Champaign (2005).

[Kalpakjian 2002] S. Kalpakjian, S.R. Schmid, Manufacturing Processes for Engineering Materials, Prentice Hall (2002).

[Kern Co.] KERN Micro- und Feinwerktechnik, website; www.kern-microtechnic.com

[Kim 1992] C. J. Kim, A. P. Pisano, R. S. Muller, Silicon processed overhanging micro gripper, Journal of Microelectromechanical Systems 1(1) (1992) 31-36.

[Kim 1995] Jeong-Du Kim, Dong Sik Kim, Theoretical analysis of micro-cutting characteristics in ultra-precision machining, Journal of materials Processing Technology, 49 (1995) 387-398.

[Kim 1996] T. Y. Kim, J. Kim, Adaptive Cutting Force Control for a Machining Center by Using Indirect Cutting Force Measurements, International Journal of Machine Tools and Manufacturing 36 (1996) 925-937.

[Kim 2001] Kim SM, Ha JH, Jeong SH, Lee SK, Effect of joint conditions on the dynamic behavior of a grinding wheel spindle, Machine Tools & Manufacture 41 (2001) pp. 1749-1761

[Kim 2004,A] B. Kim, M. C. Schmittdiel, F. L. Degertekin, T. R. Kurfess, Scanning grating micro interferometer for MEMS metrology, Journal of Manufacturing Science and Engineering 126 (2004) 807-812.

[Kim 2004,B] C. J. Kim, J. Rhett Mayor, J. Ni, A static model of chip formation in micro scale milling, ASME 126 (2004) 710-718.

[Koren 1983] Y. Koren, Computer control of manufacturing systems, McGraw Hill, New York, 1983.

[Kountanya 2004] R. K. Kountanya, W. J. Endres, Flank Wear of Edge-Radiused Cutting Tools Under Ideal Straight-Edged Orthogonal Conditions, Journal of Manufacturing Science and Engineering, 126 (2004) 496-505.

[Kugler Co.] Kugler of America, website; www.kuglerofamerica.com/micro_m.htm

[Kussul 1996] E. Kussul, T Baidyk, L Ruiz-Huerta, A Caballero-Ruiz, G Velasco, L Kasatkina, Micromechanical engineering: a basis of the low-cost manufacturing of mechanical micro devices using micro equipment, Journal of Micromechanics and Microengineering 6 (1996) 410-425.

[Kussul 2002] E. Kussul, T Baidyk, L Ruiz-Huerta, A Caballero-Ruiz, G Velasco, L Kasatkina, Development of micromachine tool prototypes for microfactories, Journal of Micromechanics and Microengineering 12 (2002) 795-812.

[Lang 1999] W. Lang, Reflexions on the future of Microsystems, Sensor and Actuators 72 (1999) 1-15.

[Lee 1999] W. B. Lee, C. F. Cheung, S. To, Materials induced vibration in ultra-precision machining, Journal of Materials Processing Technology 89-90 (1999) 318-325.

[Lee 2001] W. B. Lee, C. F. Cheung, A dynamic surface topography model for the precision of nano-surface generation in ultra-precision machining, International Journal of Mechanical Sciences 43 (2001) 961-991.

[Lee 2002] W. B. Lee, C. F. Cheung, S. To, A Micro plasticity Analysis of Micro-Cutting Force Variation in ultra-Precision Diamond Turning, Journal of Manufacturing Science and Engineering 124 (2002) 170-177.

[Li 2000] X. Li, R. Lin, K.W. Leow, Performance-enhanced micro-machined resonant systems with two-degrees-of-freedom resonators, Journal of Manufacturing Science and Engineering 10 (2000) 534-539.

[Lister 1993] P. M. Lister, On-line measurement of tool wear, Ph.D. Thesis, UMIST, Manchester, UK, 1993.

[Liu 1996] C. R. Liu, S. Mittal, Single-step super finish hard machining: feasibility and feasible cutting conditions, Robotics Comput.-Integr. Manufact 12 (1996) 15–27.

[Liu 2000] Liu, W., Ewins, D J., Substructure synthesis via elastic media part 1: joint identification, Imperial College, (2000).

[Liu 2003] K. Liu, X. P. Li, M. Rahman, Characteristics of high speed micro-cutting of

tungsten carbide, Journal of Materials Processing Technology 140 (2003) 352-357.

[Liu 2004,A] X. Liu, R.E. DeVor, S.G. Kapoor, K.F. Ehman, The Mechanics of Machining at the Micro scale: Assessment of the Current State of the Science, Journal of Manufacturing Science and Engineering 126 (2004) 666-678.

[Liu 2004,B] X. Liu, M.B. Jun, R.E. DeVor, S.G. Kappor, Cutting Mechanisms and their influence on dynamic forces, vibrations and stability in micro-end milling, Proc. ASME International Mechanical Engineering Congress and Exposition. Anaheim California, 13-20 Nov, 2004.

[Lucca 1991] D. A. Lucca, R. L. Rhorer and R. Komanduri, Energy dissipation in the ultra precision machining of copper, Annals of CIRP, 40(1) (1991) 559-562.

[Madou 1997] M. J. Madou, Fundamentals of Microfabrication, CRC Press, (1997).

[Maia 1997] Maia, N.M.M., Silva, J.M.M., Ribeiro, A.M.R., Some application of coupling/uncoupling techniques in structural sysnamics, International Modal Analysis Conference 97 (1997)

[Makino] Makino, website; http://www.makino.com/default.asp

[Mascardelli 2006] B. Mascardelli, J. Chae, S. S. Park, T. Freiheit, Y. Qi, Micro Mechanical Milling Operations, CSME, May 21-24, 2006.

[Mascardelli 2006, A] B. Mascardelli, S. S. Park, T. Freiheit, Substructure coupling of micro-end mills, IMECE 2006-13129, 2006

[Masuzawa 2000] T. Masuzawa, State of the art of micromachining, Annals of CIRP, 49(2) (2000), 473-488.

[Matsubara 2000] A. Matsubara, Y. Kakino, T. Ogawa, H. Nakagawa, T. Sato, Monitoring of Cutting Forces in End-milling for Intelligent Machine Tools, Proc. of the 5th Int'l Conf. on Progress of Machining Technology (ICPMT), 615 (2000).

[Matsushima 1982] K. Matsushima, P. Bertok, T. Sata, In process detection of tool breakage by monitoring the spindle current of a machine tool, ASME J. of Meas. and Control (1982) 145-154.

[Merchant 1945] M. E. Merchant, Mechanics of the metal cutting Process, ii. Plasticity Conditions in Orthogonal Cutting, Journal of applied physics 16 (1945) 318-324.

[Mikrotool Co.] Mikrotool Pte LTD, website; http://www.mikrotools.com/product-DT110.htm

[Mitsubishi Co.] Mitsubishi. Co., Machining Performance using the Mitsubishi micro MZS drills with 2 coolant holes through, website; http;//www.mitsubishicarbide.com/mmus/ca/product/article/mzs.pdf

[MMS online] MMS Online, Machining under the microscope, website; http://www.mmsonline.com/articles/010504.html

[Mori Seiki Co.] Mori Seiki, website; www.moriseiki.com/english/index.html

[Moriwaki 1980] T. Moriwaki, Detection for Tool fracture by AE measurement, Annals of CIRP 29 (1980) 35-40.

[Moriwaki 1991] T. Moriwaki, E. Shamoto, Ultra precision diamond turning of stainless steel by applying ultrasonic vibration, Annals of CIRP, 40(1) (1991) 559-562

[Moriwaki 1993] T. Moriwaki, N. Sugimura, S. Luan, Combined stress material flow and heat analysis of orthogonal micromachining of copper, Annals of CIRP 42 (1993) 75-78.

[Moriwaki 1995] T. Moriwaki, E. Shamoto, Ultrasonic elliptical vibration cutting, Annals of CIRP 44(1) (1995) 31-34.

[Mottershead 1996] Mottershead, J.E., Friswell, M.I., Ng, G.H., and Brandon, J.A., Geometric parameters for finite element model updating of joints and constraints, Mechanical systems and signal processing 10(2) (1996) pp. 171-182,

[Nanowave Co.] Nanowave, website; www.nanowave.co.jp

[Okazaki 2004] Y. Okazaki, N. Mishima, K. Ashida, Microfactory-concept, history, and developments, Journal of Manufacturing Science and Engineering 126 (2004) 837-844.

[Onikura 2000] H. Onikura, O. Ohnishi, Y, Take, Fabrication of micro carbide tools by ultrasonic vibration grinding, Annals of CIRP 49, 2000.

[Ozdoganlar 2004] O. B. Ozdoganlar, D. S. Epp, P. L. Reu, H. Sumali, Development of a testing facility for experimental investigation of MEMs dynamics, Proc. ASME International Mechanical Engineering Congress and Exposition. Anaheim California, 13-20 Nov, 2004.

[Park 2002] S. S. Park, Y. Altintas, Dynamic Compensation of Cutting Forces Measured From the Spindle Integrated Force Sensor System, ASME IMECE2002 DSC Conference, New Orleans, Nov, 2002.

[Park 2003] S. S. Park, Y. Altintas, M. Movahhedy, Receptance coupling for end mills, International Journal of Machine Tools & Manufacture 43 (2003) 889-896.

[Peirs 1998] J. Peirs, D. reynaerts, H Van Brussel, A micro robotic arm for a self propelling colonoscope, Proc. Actuator (1998) 576-579.

[Popa 2003] D. Popa, B. Kang, J. Wen, H. Stephanou, Dynamic modeling and input shaping of thermal bimorph MEMS actuators, IEEE Conf. Robotics and Automation 1 (2003) 1470-1475.

[Prakash 2001] J. R. S. Prakash, A. Senthil Kumar, m. Rahman, S. C. Lim, A model for predicting tool life for coated micro end mill, 4th international machining & grinding Troy, Michigan, 7-10 May, 2001.

[Rahman 2001] M. Rahman, S. Kumar, J. R. S. Prakash, Micro milling of pure copper, Journal of materials Processing Technology 116 (2001) 39-43.

[Ren 1995] Ren, Y., Beards, C.F., identification of Joint Properties of Structure Using FRF Data, Journal of Sound and Vibration, 186 (1995) 567-58.

[Rivin 2000] E. I. Rivin, Tooling structure - Interface between cutting edge and machine tool, Annals of CIRP 49(2) (2000) 591.

[Rooks 2004] Brian Rooks, The shrinking sizes in micro manufacturing, Assembly Automation 24(4) (2004) 352-356.

[Robert 2005] Robert Bos, Xavier Bombois, Paul M. J., Van den Hof, Designing a kalman filter when no noise covariance information is availbe 2005 IFAC.

[Sampath 1987] A. Sampath, S. Vajpayee, Tool health monitoring using acoustic emission, Int. J. Prod. Res. 25(5) (1987) 703-719.

[Santos 2004] Santos, I.O., Zhang, W., Goncalves, V.M., Bay, N., Martins, P.A.F., Weld bonding of stainless steel, International Journal of machine tools & manufacture. 44 (2004) pp.1431-1439.

[Schaller 1999] Th. Schaller, L. Bohn, J. Mayer, K. Schubert, Microstructure grooves with a width of less than 50 μm cut with ground hard metal micro end mills, Precision Engineering 23 (1999) 229-235.

[Schmitz 2000] Schmitz, T.L., Donaldson, R., Predicting High Speed Machining Dynamics by Substructure Analysis, Annals of CIRP 49 (2000) 303-308.

[Schmitz 2002] T. L. Schmitz, M. Davies, M. D. Kennedy, Tool point frequency response

prediction for high-speed machining by RCSA, Journal of Manufacturing Science and Engineering 123 (2002) 700-707.

[Shabouk 2003] S. Shabouk, T. Nakamoto, Micro machining of single crystal diamond by utilization of tool wear during cutting process of ferrous material, Journal of Micromechatronics 2(1) (2003) 13-26.

[Shaw 1995] M.C. Shaw, Precision Finishing, Annals of CIRP 44(1) (1995) 343-348.

[Shen 2000] Shen, J., Astaneh-Asl, A., Hysteresis model of bolted-angle connections, Journal of Constructional steel Reseach Vol 54, (2000) 317-343,

[Son 2005] S. M. Son, H. S. Lim, J. H. Ahn, Effects of the friction coefficient on the minimum cutting thickness in micro cutting, International Journal of Machine Tools & Manufacture 45 (2005) 529-535.

[Song 2004] Song, T., Hartwigsen, C.J., Mcfarland, D.M., Vakakis, A.F., Bergman, L.A., Simulation of dynamics of beam structures with bolted joints using adjusted Iwan beam elements, Journal of Sound and Vibration 273 (2004) pp. 249-276.

[Sutherland 2000] J. W. Sutherland, V. N. Kulur, N. C. King, An experimental investigation of air quality in wet and dry turning, Annals of CIRP 49(1) (2000) 61-64.

[Suzumori 1991] K. Suzumori, S. likura, H. Tanaka, Flexible micro actuator for miniature robots, Proc. IEEE MEMS workshop (1991) 204-209.

[Takeuchi 2000] Y. Takeuchi, Y. Sakaida, K. Sawada, T. Sata, Development of a 5-axis control ultra precision milling machine for micromachining based on non-friction servomechanisms, Annals of CIRP (2000).

[Tanaka 2001] M. Tanaka, Development of Desktop Machining Microfactory, Riken Review 34 (2001) 46-49.

[Tansel 1998] I.N. Tansel, A. Nedbouyan, M. Trujillo, B. Tansel, Micro-end-milling-Extending tool life with a smart workpiece holder, International Journal of Machine Tools & Manufacture 38 (1998) 1437-1448.

[Tansel 2000,A] I.N. Tansel, T.T. Arkan, W.Y. Bao, N. Mahendrakar, B. Shisler, D. Smith, M. McCool, Tool wear estimation in micro-machining. Part 1, International Journal of Machine Tools & Manufacture 40 (2000) 599-608.

[Tansel 2000,B] I.N. Tansel, T.T. Arkan, W.Y. Bao, N. Mahendrakar, B. Shisler, D. Smith, M. McCool, Tool wear estimation in micro-machining. Part 2: neural-network-based

periodic inspector for non metals, International Journal of Machine Tools & Manufacture 40 (2000) 609-620.

[Tarn 1989] J. H. Tarn, M. Tomizuka, On-line monitoring of tool and cutting conditions in milling, ASME J. of Eng. For Industry 111 (1989) 206-212.

[Tarng 1994,A] Y. S. Tarng, M.C. Chen, An intelligent sensor for detection of milling chatter, J. Intelligent manufacturing 5 (1994) 193-200.

[Tarng 1994,B] Y. S. Tarng, T.C. Li, On-line monitoring and suppression of self-excited vibration in end milling, Mechanical Systems and Signal Processing 8 (1994) 597-606.

[Tarng 1994,C] Y. S. Tarng, Y.W. Hseigh, S. T. Hwang, An intelligent sensor for monitoring milling cutter breakage, Int. J Advanced Manufacturing Technology 9 (1994) 141-146.

[Tlusty 1975] J. Tlusty, P. Macneil, Dynamics of cutting forces in end milling, Annals of CIRP 24 (1) (1975) 21–25.

[Tlusty 1983] J. Tlusty, G.C. Andrews, A Critical Review of Sensors for Unmanned Machining, Annals of CIRP 32 (2) (1983) 563-572.

[Tobias 1958] S. A. Tobias, W. Fishwick, A theory of regenerative chatter, The engineer (1958) London.

[Tobias 1965] S. A. Tobias, Machine Tool Vibrations, Blackie and Sons.(1965).

[Tonshoff 1988] H.K. Tonshoff, Developments and trends in monitoring and control of machining Processes, Annals of CIRP 37 (2) (1988) 611-622.

[Tsai 1988] Tsai, J.S., Chou, Y.-F., The Identification of Dynamic Characteristics of Single Bolt Joint, Journal of Sound and Vibration 125 (1988) 487-502.

[Ulsoy 1989] A.G. Ulsoy, Y. Koren, Applications of adaptive control to machine tool process control, IEEE Control Systems Magazine 9(4) (1989), June.

[Uhlmann 2005] E. Uhlmann, K. Schaeur. Dynamic load and strain analysis for the optimization of micro end mills. Annals of CIRP 54 (2005), 75-78.

[Vallance 2004] R. R. Vallance, E. Marsh, P. Smith, Effect of spherical targets on capacitive displacement measurements, Journal of Manufacturing Science and Engineering 126 (2004) 822-829.

[Van Brussel 2000] H. Van Brussel, J. Peirs, D. Reynaerts, A. Delchambre, G. Reinhart, N. Roth, M. Weck, E. Zussman, Assembly of Microsystems, Annals of CIRP 49 (2000)

451-472.

[Vogler 2002] M. P. Vogler, X. Liu, S. G. Kapoor, R. E. Devor, K. F. Ehmann, Development of meso-scale machine tool (mMT) systems, Society of Manufacturing Engineers. MS n MS02-181 (2002) 1-9

[Vogler 2003] M. P. Vogler, R. E. Devor, S.G. Kapoor, Microstructure-level force prediction model for micro-milling of multi-phase materials, Journal of Manufacturing Science and Engineering 125 (2003) 202-209.

[Vogler 2004] M. P. Vogler, R. E. Devor, S. G. Kapoor, On the modeling and analysis of machining performance in micro endmilling, Journal of Manufacturing Science and Engineering 126(4) (2004) 685-705.

[Wang 1990,A] Wang, J., Sas, P., A method for identifying parameters of mechanical joints, Journal of Applied Mechanics 57 (1990)

[Wang 1990,B] Wang, J.H., Liou, C.M., Identification of Parameters of Structural Joints by Use of Noise-Contaminated FRFs, Journal of Sound and Vibration 142 (1990) 261-27.

[Wang 2004] Wang, J.H., Chuang, S.C., Reducing errors in the identification of structural joint parameters using error functions, Journal of Sound and Vibration, 273 (2004) 295-316.

[Weck 1997] M. Weck, S. Fischer, M. Vos, Fabrication of micro components using ultra precision machine tools, Nanotechnology 8 (1997) 145-148.

[Weck 1997] M. Weck, J. Hummler, B. Petersen, Assembly of hybrid micro systems in a large chamber electron microscope by use of mechanical grippers, Proc. of SPIE, Micromachining and Micro fabrication Process Technology III (1997) 3223:223-229.

[Weinert 2004] K. Weinert, V. Petzoldt, Machining of NiTi based shape memory alloy, Materials Science and Engineering A 378 (2004) 180-184.

[Weule 2001] H. Weule, V. Huntrup, H. Tritschler, Micro-Cutting of Steel to Meet New Requirements in Miniaturization, Annals of CIRP 50 (2001) 61-64.

[Willemin-Macodel] Willemin-Macodel SA, website; http://www.willemin-macodel.com/

[Wong 1995] Wong, C.W., Mak, W.H., KO, J.M., System and paprmetric identification of flexible connection in steel framed structures, Engineering Structure Vol 17, No. 8, (1995) pp. 581-595.

[Xiao 2003] M. Xiao, K. Sato, S. Karube, T. Soutone, The effect of tool nose radius in

ultrasonic vibration cutting of hard metal, International Journal of Machine Tools & Manufacture 43 (2003) 1375-1382.

[Yan 1995] D. Yan, T. ElWardany, M.A. Elbestawi, A multi-sensor strategy for tool failure detection in milling, International Journal of Machine Tools & Manufacture 35 (1995) 383-398.

[Yao 1990] Y. Yao, X. D. Fang, G. Amdt, Comprehensive tool wear estimation in finish-machining via multivariate time-series analysis of 3-D cutting forces, Annals of CIRP 39 (1990) 57-60.

Appendix A. Survey of Micro Mechanical Machining Research

Research Areas	Approaches	Remarks	Reference
Micro Tools	Ultrasonic vibration grinding to fabricate 11 μm pins and 17 μm flat drill	Recommendation: compress force for grinding force	[Onikura 2000]
	Focused Ion Beam to fabricate 25 μm end mills	Very expensive to fabricate	[Benavides 2001]
	Evaluate various shaped carbide tools with FEM	No helix angle tool causes poor surface finish	[Fang 2003]
Precision Machine Tools	Spindle speed- 140,000 rpm, Accuracy: 0.1 μm	Micro milling: 70 micro meter fin, 100 micrometer slot	[Microtool]
	Fly cutter machining spindle	Hydrostatic/aerostatic bearings	[Kugler]
	Spindle speed: 40,000 rpm or 170,000 rpm, Accuracy: 0.3 μm	Spindle lubricant controller: Prevent the thermal effect of the spindle	[Makino]
	Vertical machine center Spindle speed: 15,000 rpm	Pallet loading capacity: 150 kg	[Moriseiki]
Miniature Machine Tools (Micro Factories)	Surveys of micro factories	Advantages from micro factories	[Okazaki 2004]
	Micro factory concept; desk-top factory, palm-top machine tools, mobile factory, on-site production facility	Main goal: saving energy and economizing	[Tanaka 2001]
	Micro machine tool Spindle speed- 200,000 rpm	225*150*175 mm machine footprint, 0.5 μm encoder resolution	[Vogler 2002]
	Voice coil motors-5G's acceleration in each direction Spindle speed- 160,000 rpm	180*180*300 mm machine footprint, Tri-load cell mounted	[Jun 2005]
	5 axis micro milling machine	294*220*328 mm 50 nm x, y, z feed resolution	[Bang 2004]
	Development from Micro machine tool to micro assembly device	130*160*85 mm, Backslash compensation algorithm	[Kussul 2002]
Chip Formation and	Orthogonal micro machining FEM Cutting test with copper	The ratio of tool edge radius to the depth of cut: 0.2 ~1	[Moriwaki 1993]

Minimum chip thickness	Analytical model for shear stress Cutting test with copper	under 1 um depth of cut: elastic recovery of the material	[Kim 1995]
	FE simulation Grain size effect	Critical chip thickness: 0.2~ 0.35 times tool radius.	[Vogler 2004]
	Examination of the chip formation with SEM when the tool cutting edge radius is fixed	the ductile mode cutting is mainly determined by the undeformed chip thickness	[Liu 2003]
	Dynamic chip thickness Process parameters, dynamic vibration, elastic recovery	Chip load and force relationship for pearlite	[Liu 2004, B]
	Friction effect between a workpiece and tool Measuring the edge radius with SEM	friction coefficients: 0.2~0.4	[Son 2005]
Micro Cutting Forces	Relationship between cutting force and chip thickness	cutting force is nonlinear due to minimum chip thickness	[Kim 2004, B]
	Analytical model for cutting force	minimizing tool deflection error	[Ikua 2001]
	Evaluation of the cutting force the undeformed chip thickness	the mean force	[Fang 2003]
	Analytical model chip thickness Aluminum cutting test	considering negative rake angle of the tool	[Bao 2000]
Materials	Influence of the workpiece material to the cutting force Aluminum and Silicon	the workpiece is heterogeneous	[Weule 2001]
	Effect of the workpiece material to the surface roughness. Pre-requirement for micro cutting	quenching and tempering the steel to obtain the homogenized workpiece	[Grum 2003]
	Mapping the micro structure	ductile iron: three distinct metallurgical	[Vogler 2004]
	Examining vibration caused by non-homogeneous materials	the changing crystallography and orientation affects shear angle and strength	[Lee 1999]
Tool Deflection	Measuring Static deflection and bending stress	compensating the errors by redefining the depth of cut	[Dow 2004]
	Cutting force	Increasing the negative rake angle of the tool	[Son 2005]

	NC machining simulator	Simulator calculates the static deflection of the tool	[Dugas 2002]
Instability	Tool vibration and frequency spectrum	very low feed rates result in instability due to elastic deflection of the workpiece	[Liu 2004]
Burring	Burr formation in milling and drilling	Reductions in burr formation increase the tool life	[Byrne 2003]
	Cutting process in brass and stainless steel, Burr removing method	polymeric material and electro-chemical polishing techniques	[Schaller 1999]
Tool Wear	Using cutting force Neural network model	predicting tool wear	[Tansel 2000]
	Using Lamp and SEM	Monitoring tool wear	[Dow 2004]
	Using SEM	Monitoring tool wear	[Winert 2004]
	Shaping single crystal diamond tools	Utilization of the effect of tool wear	[Shabouk 2003]
Dynamic Testing	Isolation Dynamic test system 1 kHz ~ 100 kHz	Piezoelectric shaker and laser Vibrometer	[Ozdoganlar 2004]
	Dynamic measurement system Static measurements	Micro-grating interferometer and electro static actuator	[Kim 2004,A]
	Dynamic model for micro manipulator	Frequency domain curve fitting	[Hart 2000]
	Energy method Superposition of three different sinusoidal inputs	The identification model errors from different static/dynamic coefficients	[Popa 2003]
Metrology	LED instead of Laser based stroboscopic interferometer	small amplitude 2□m	[Hart 2000]
Handling and assembly	Piezo type gripper SMA micro gripper	holding micro structures	[Van Brussel 2000][Popa 2003]

Appendix B. Design of micro CNC machine

B.1. Exploded view of micro CNC machine at MEDAL.

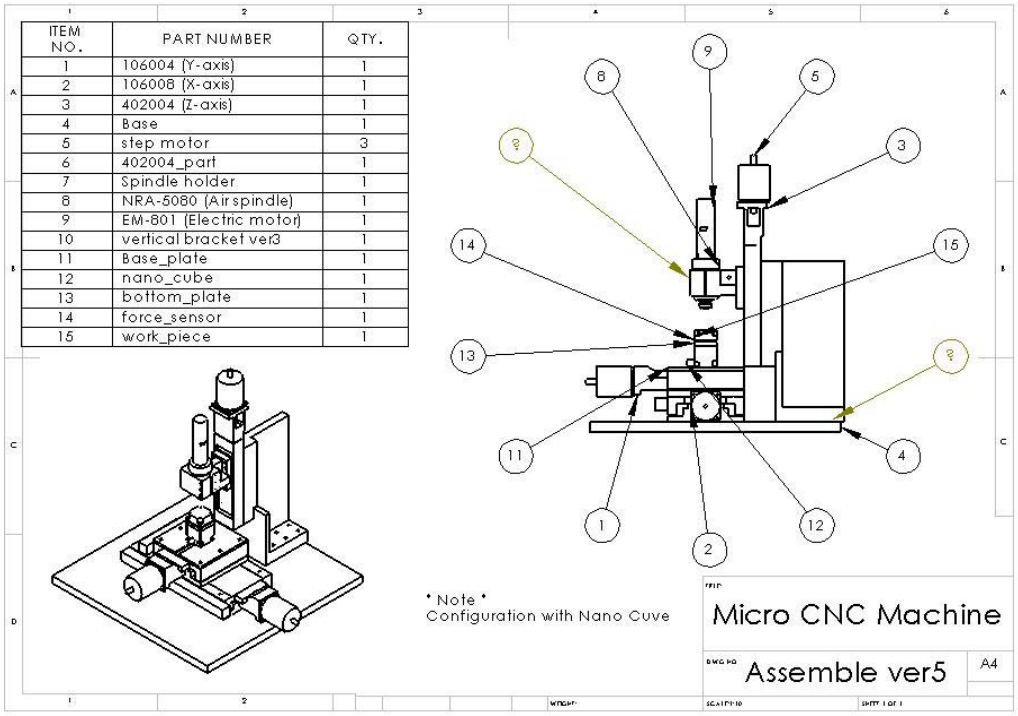

B.2. Mechanical drawing of vertical bracket.

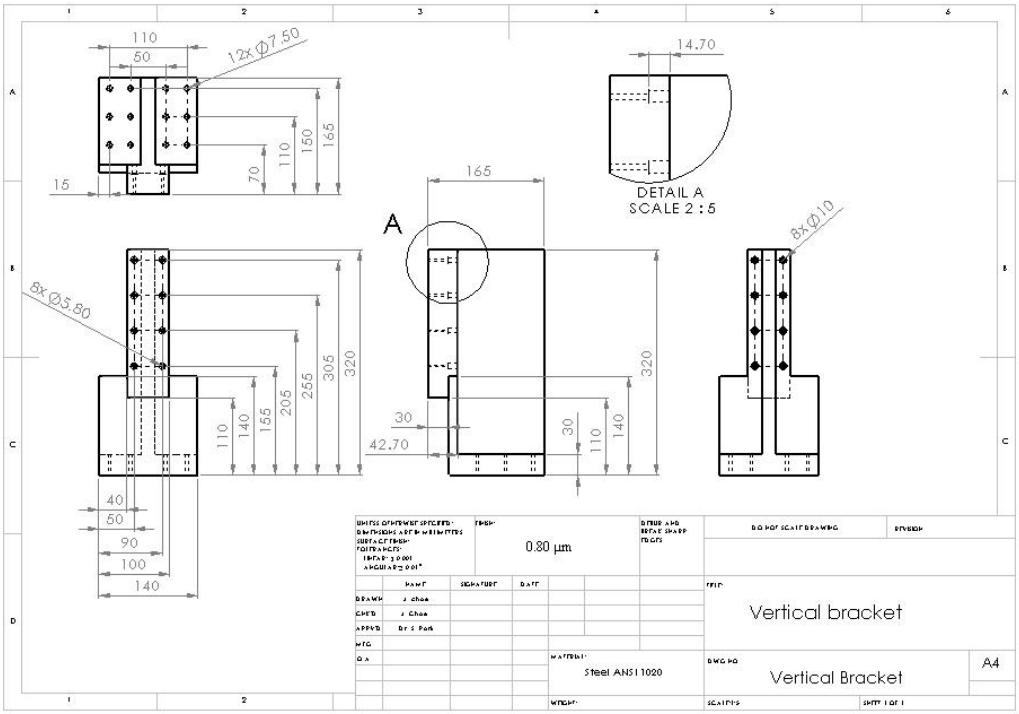

B.3. Mechanical drawing of spindle holder.

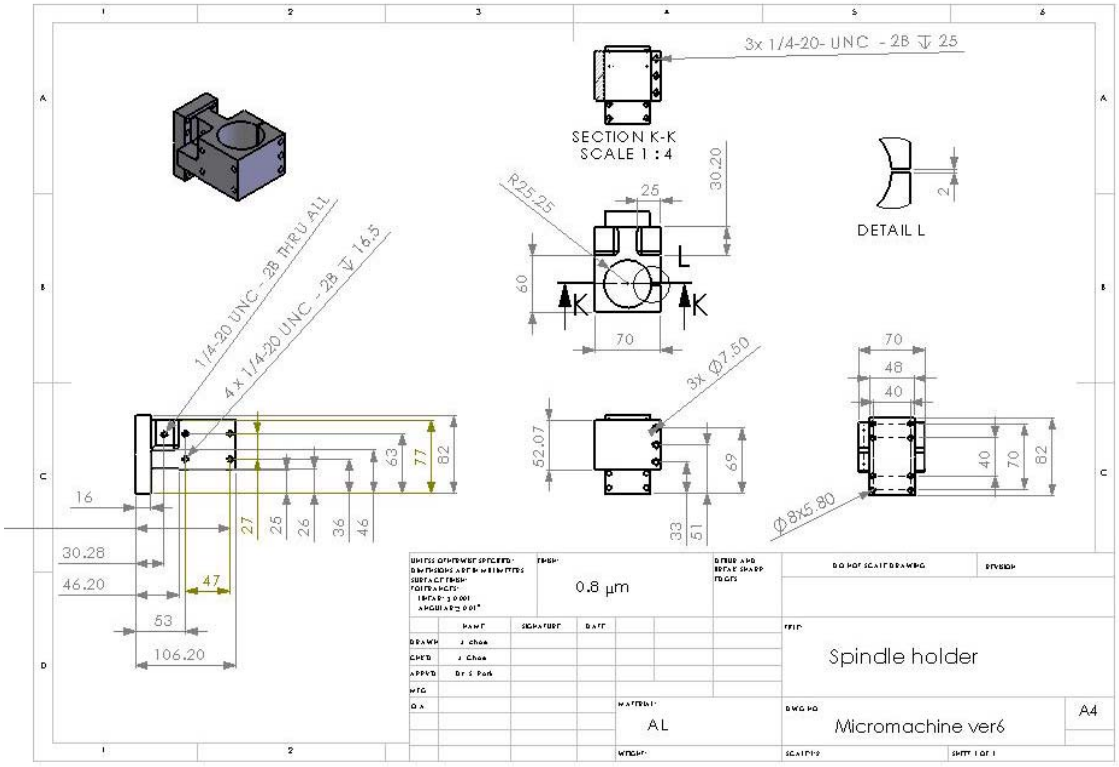

B.4. Mechanical drawing of base_connection.

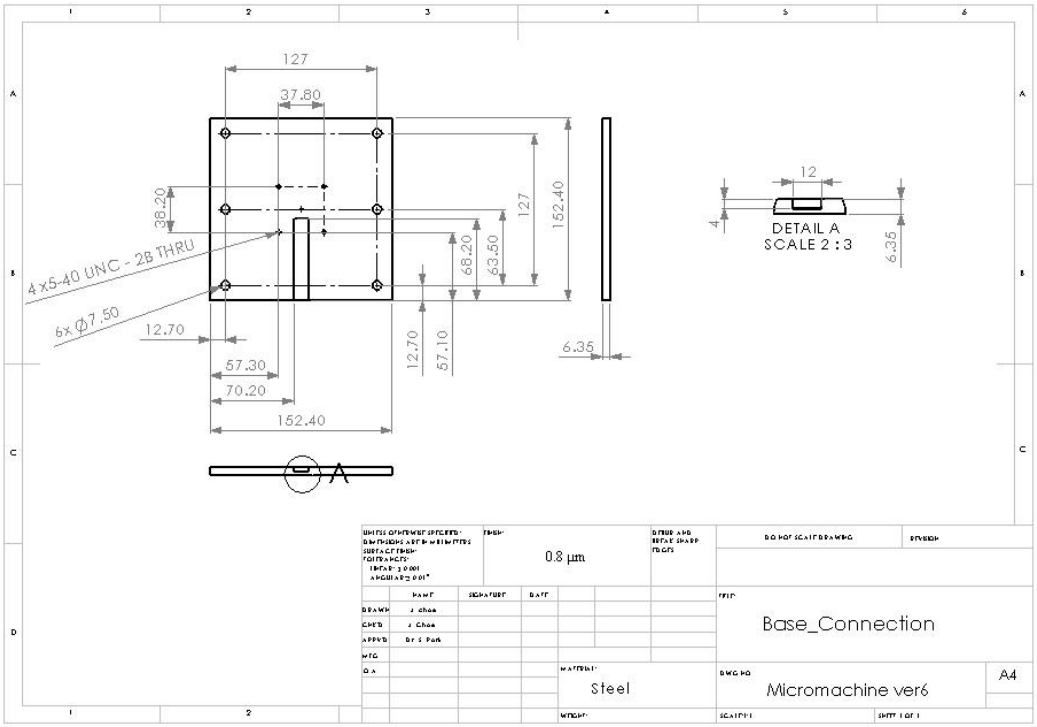

B.5. Mechanical drawing of bottom plate for force sensor.

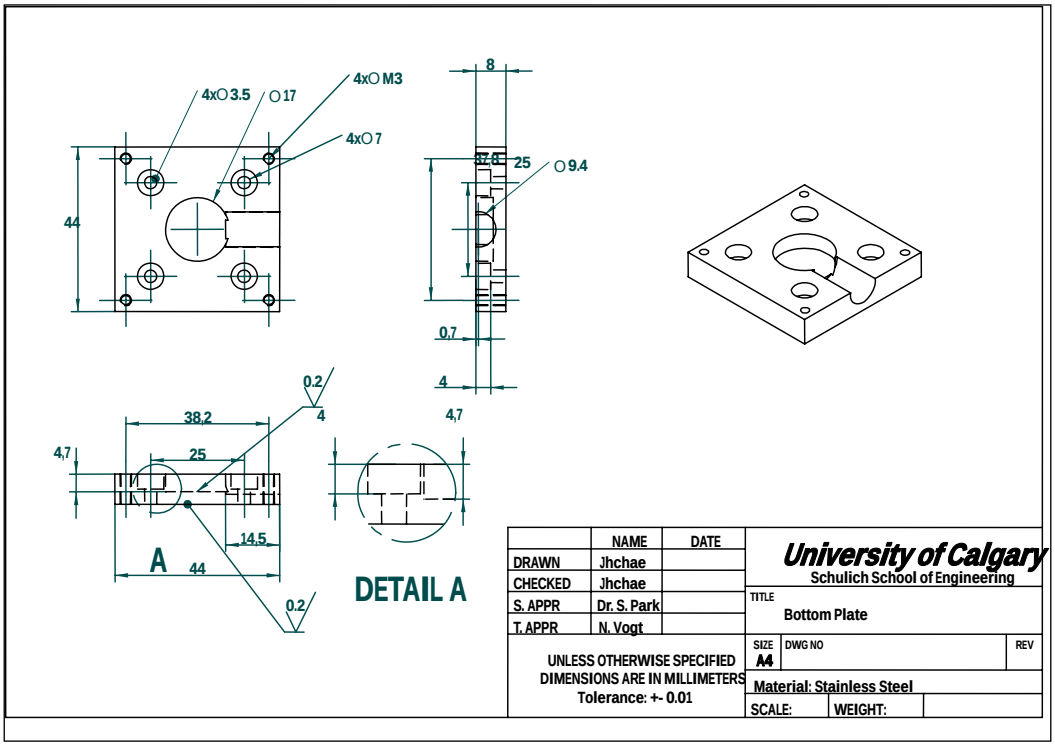

B.6. Mechanical drawing of workpiece.

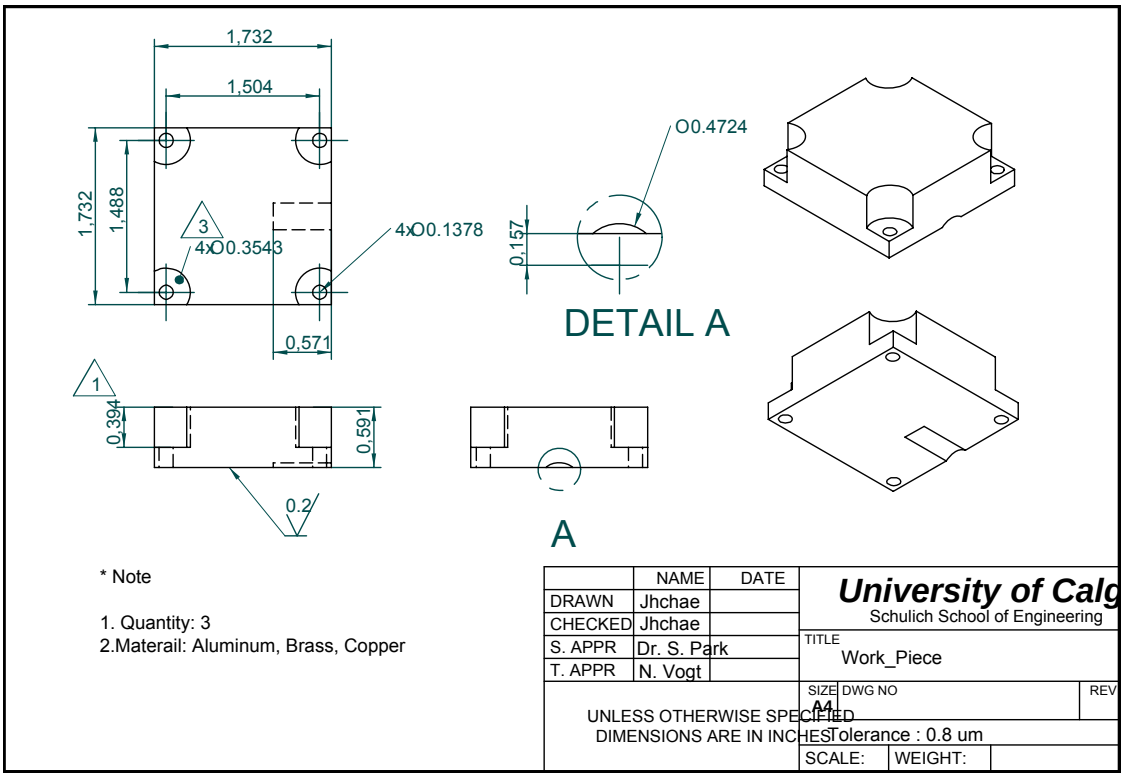

Appendix C. Control algorithm and method for the Micro CNC machine

C.1. Flow chart of control algorithm.

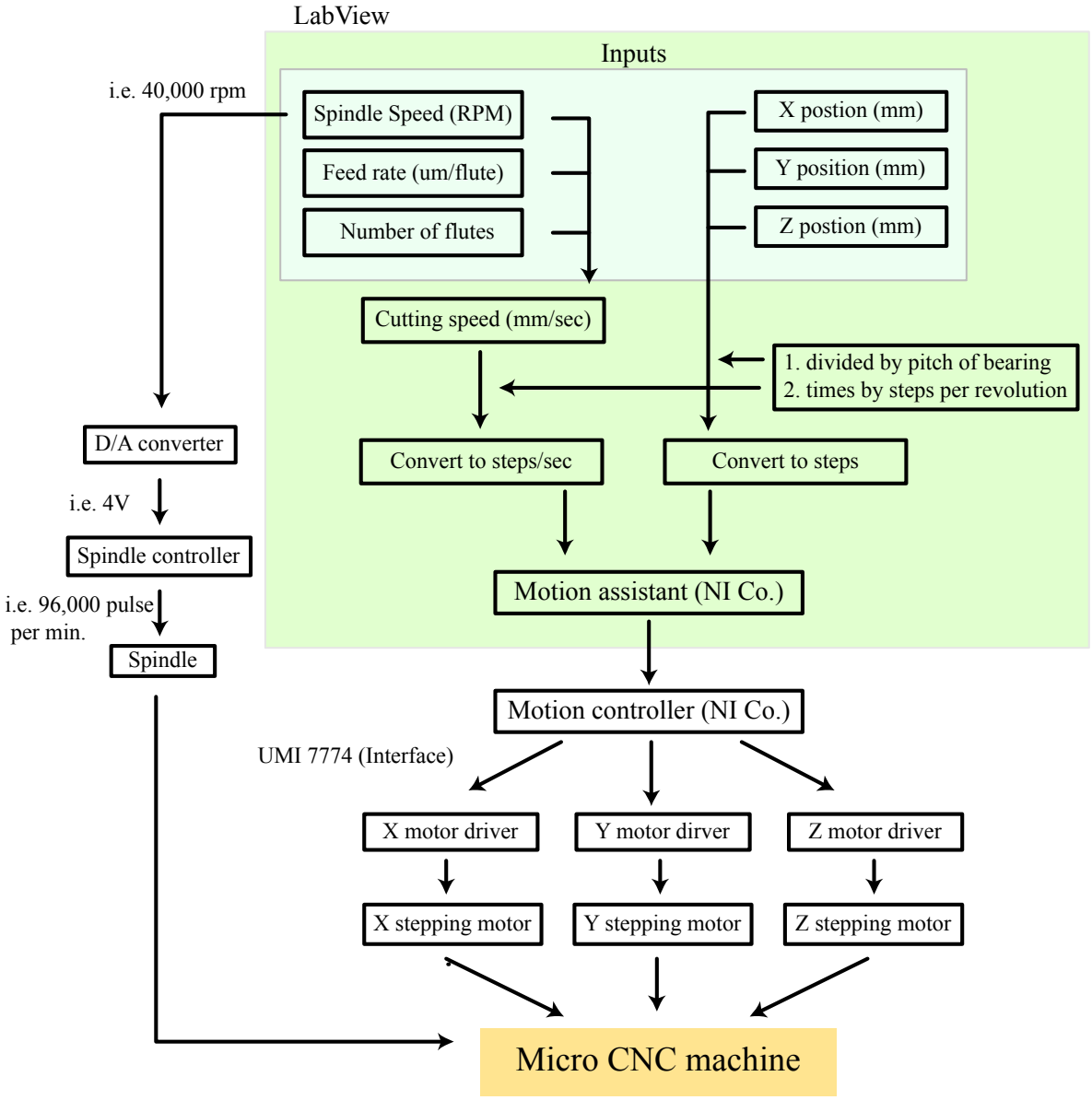

C.2. LabView program for control and measurement system.

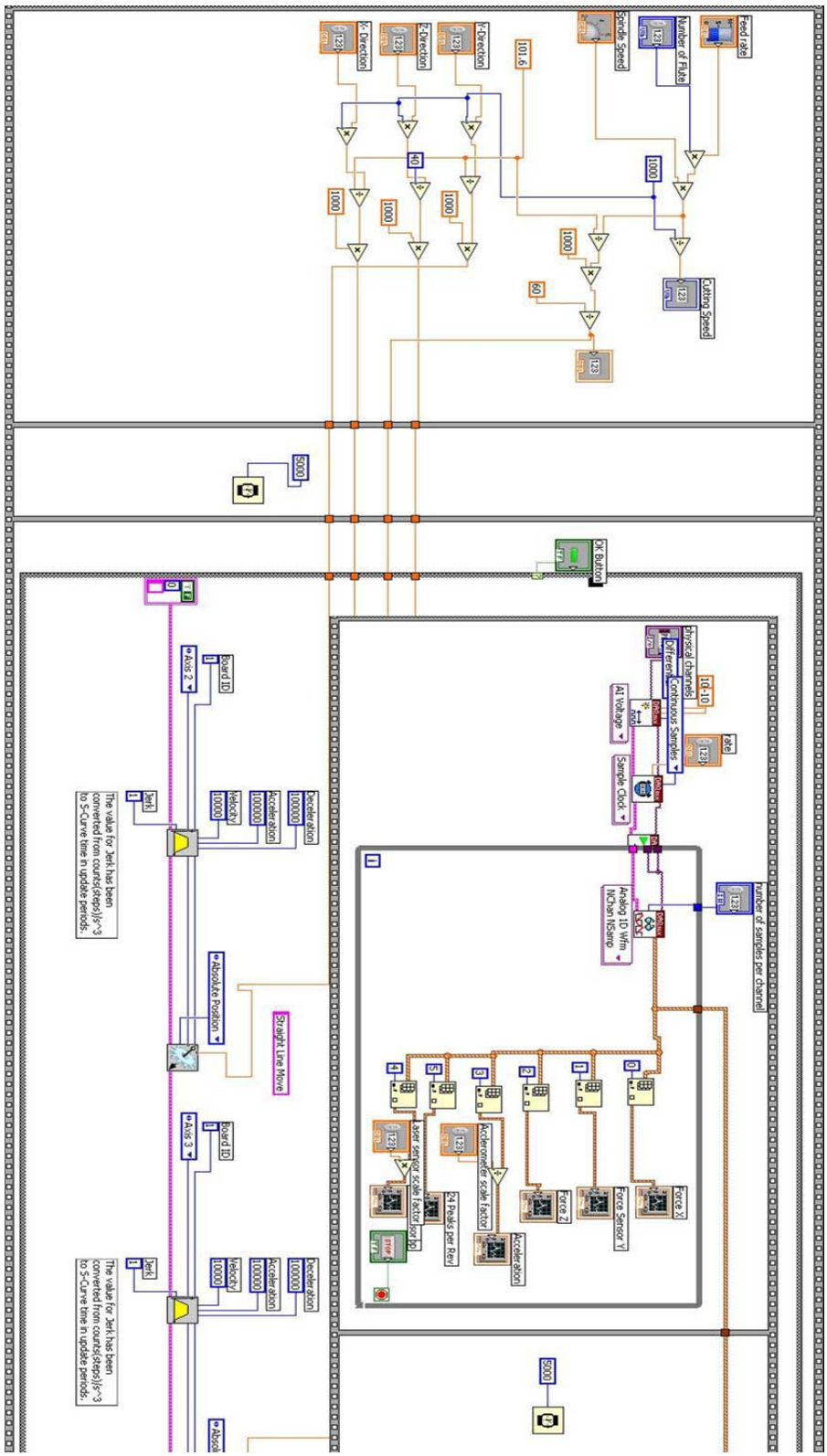

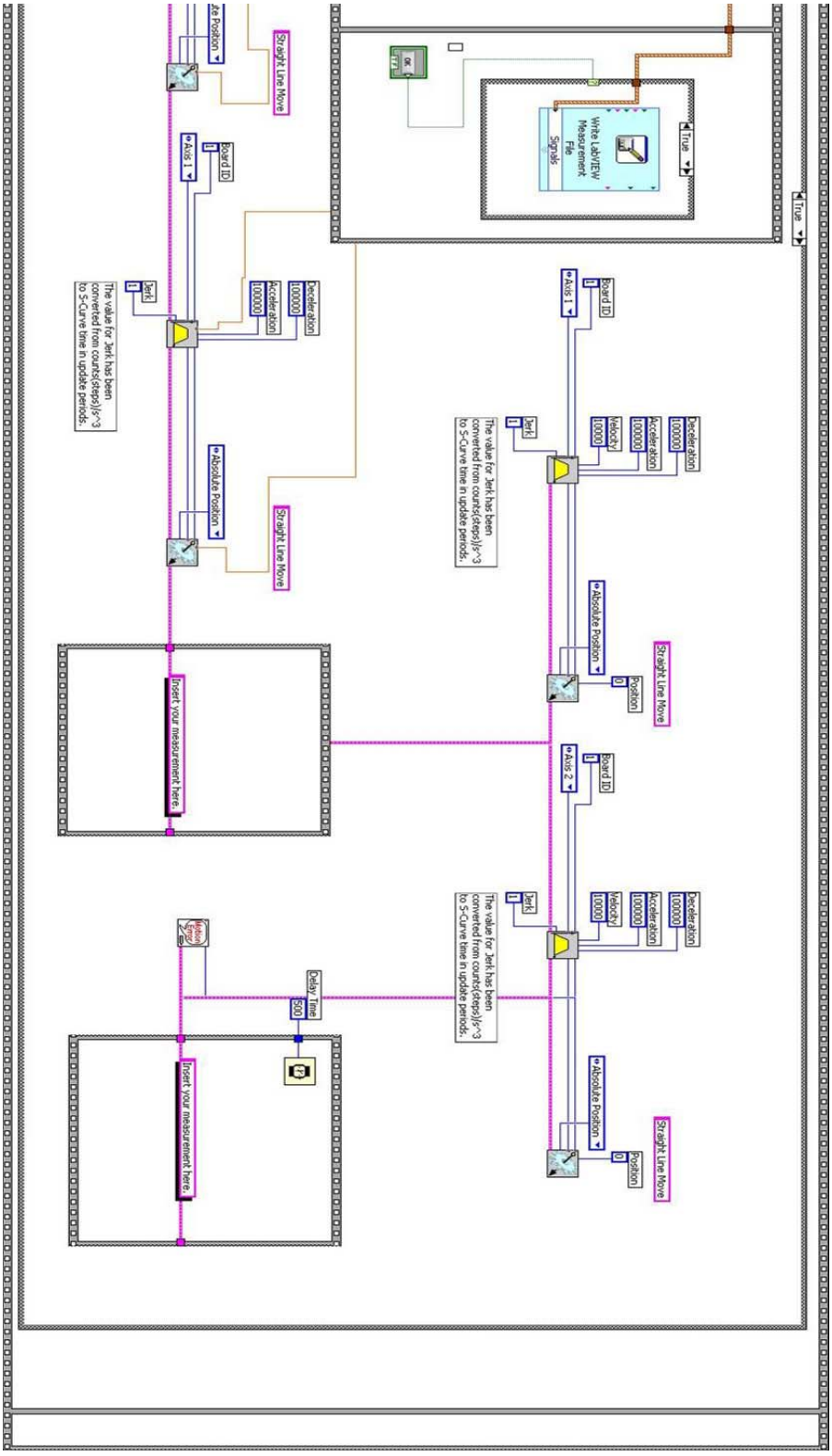
Write LabVIEW Measurement File
Signals
True
Straight Line Move
Absolute Position
Board ID
Axis 1
Axis 2
Jerk
Acceleration
Deceleration
Velocity
Position
Delay Time
500
Insert your measurement here.
The value for Jerk has been converted from counts/(steps)/(s^3 to S-Curve time in update periods.

C.3. Configurations of linear table systems.

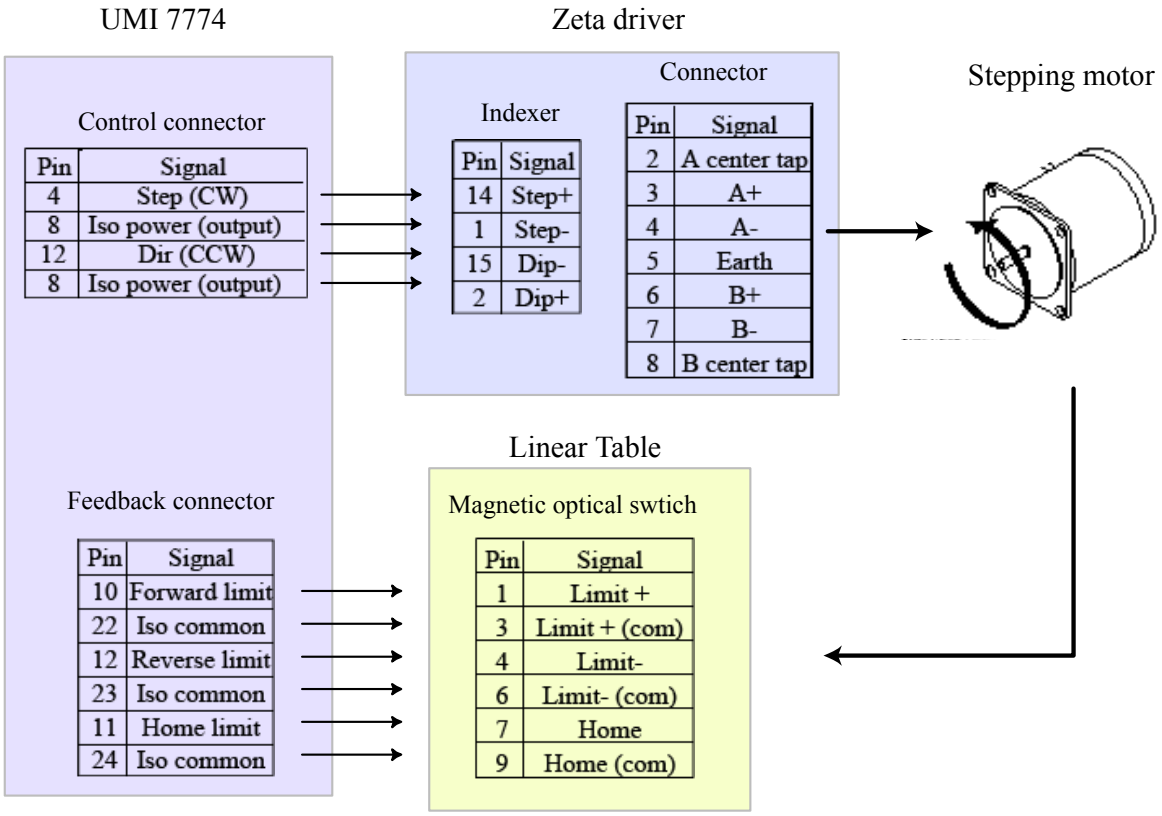

C.4. Specifications for Precision stages

Specification	Y direction precision table	X direction precision table
Positional accuracy (μm)	8	16
Positional repeatability (μm)	±1.3	±1.3
Straight line accuracy (μm)	8	16
Flatness accuracy (μm)	8	8
Drive screw (in)	0.20 in lead	0.20 in lead
Travel range (in)	4 in	8 in

Appendix D. Poor performance of Kalman filter due to small singular values

D.1. Poor performance of Kalman filter due to small singular values [Robert 2005]

The optimal KF design requires a full description of the relation between the states and measurements including noise. However, it is difficulty to model the full physical systems due to the limited amount of measurement. In other words, the models of physical system are not fully observable, which means the obsevaility matrix has some singular values (small of even zero). This ill conditioned obsevability matrix for the system can lead to poor estimated results from KF.

Let's consider linear system as this:

$$\begin{aligned} x(k+1) &= Ax(k) + Bu(k) \\ y(k) &= Cx(k) + v(k) \end{aligned} \tag{D-1}$$

Based on Equation D-1, the optimal estimator can be written as:

$$\hat{x}(k+1) = A\hat{x}(k) + Bu(k) + K(y(k) - C\hat{x}(k)) \tag{D-2}$$

Where, Kalman filter gain K

$$K(k) = \left[M - A\sum(k)C^T\right]R_e(k)^{-1} \tag{D-3}$$

Where, $R_e(k) = R_y(0) - C\sum(k)C^T$, $\sum(k+1) = A\sum(k)A^T + K(k)R_e(k)K(k)^T, \sum(0) = 0.$

, The covariance function of the measurements

$$R_y(0) = C^T \Phi C + R_e(0) \tag{D-4}$$

, and the cross-covariance between the state and the output

$$M = E[x_s(k+1)y_s(k)^T] \tag{D-5}$$

M can be estimated easily by the following relation

$$\mathrm{O}M = [R_y^T(1)\cdots R_y^T(N-1)]^T, \ \ with \ \ \mathrm{O} = \left[C^T \ (CA)^T \ \ldots \ (CA^{N-2)T}\right]^T \tag{D-6}$$

The covariance function $R_y(i)$ would be easy to estimate if the signal $y_s(k)$ would be available. If A is stable, the signal $y_s(k)$ can be approximately

$$y_s(k) \approx \bar{y}_s(k) = y(k) - \sum_{i=0}^{k-1} CA^{k-1-i}Bu(i) \tag{D-7}$$

The signal $\bar{y}_s(k)$ can be use dot estimate the covariance function $R_y(i)$

$$\hat{M} = \mathrm{O}^{+}[\hat{R}_y(1) \cdots \hat{R}_y^T(N-1)]^T, \quad with\ \mathrm{O}^{+} = (\mathrm{O}^T\mathrm{O})^{-1}\mathrm{O}^T \qquad \text{(D-8)}$$

Therefore, the accuracy of the estimates of the obtained KF can be very poor if the matrix O has one or several small singular values.

D.2. Similarity Transformation

Let's assume that the system is observable. The observability of original pair can be checked with observable canonical form:

$$\mathrm{O} = \begin{bmatrix} C \\ CA \\ \vdots \\ CA^{n-1} \end{bmatrix} \qquad \text{D-9}$$

Due to the similarity transform $\overline{A} = Q^{-1}AQ,\ \ \overline{C} = CQ$, the observable canonical form also needs to be transformed:

$$\overline{\mathrm{O}} = \begin{bmatrix} \overline{C} \\ \overline{CA} \\ \vdots \\ \overline{CA}^{n-1} \end{bmatrix} \qquad \text{D-10}$$

Then

$$\overline{\mathrm{O}} = \begin{bmatrix} \overline{C} \\ \overline{CA} \\ \vdots \\ \overline{CA}^{n-1} \end{bmatrix} = \begin{bmatrix} CQ \\ CAQ \\ \vdots \\ CA^{n-1}Q \end{bmatrix} = \mathrm{O}Q \qquad \text{D-11}$$

Therefore, observable similarity transforms Q can be founded as

$$Q = \mathrm{O}^{-1}\overline{\mathrm{O}} \qquad \text{D-12}$$

In this thesis, the diagonal similarity transformation matrix is found using Matlab function 'SSBAL'.

Appendix E. Matlab code for High frequency bandwidth measurement

```
format long e;

%Error covariance
Rn=[0.05 0;0 0.4];
% System Disturbance Variance
Qn=1e8;

% Modal parameters for load cell and Accel.
me_ff=[3021 0.00896 -2.4874
       3312 0.0190 -6.008
3571 0.02369 -2.749];

me_af=[3021 0.00896 9.5672e7
       3312 0.0190 2.1959e8
3571 0.02369 1.0436e8];

H_ff=tfH(me_ff,3);    H_af=tfh(me_af,3);

% Steady State formulation

[Haff Hbff Hcff
Hdff]=tf2ss(H_ff.num{1},H_ff.den{1});
[Haaf Hbaf Hcaf
Hdaf]=tf2ss(H_af.num{1},H_af.den{1});

Haf=Haff;    Hbf=Hbaf;    Hcf=[Hcff;    Hcaf];
Hdf=Hdff;

HF2=ss(Haf,Hbf,Hcf,Hdf);
GGG=1
%Kalman filter
[KF,T,L,Gmdss,P] = kfdirect2(H,GGG,Qn,Rn)
[Gmdss T]=ssbal(HF2);
Amd=Gmdss.A;                    Bmd=Gmdss.B;
Cmd=Gmdss.C; Dmd=Gmdss.D;
% Extending the system
n=length(Amd);
nu=length(Bmd(1,:));
A=[Amd Bmd;zeros((nu),n+nu)];
B=[];
C=[Cmd Dmd];
D=[];%Cacc Dacc]; D=[];
% Checking Observability
bmb = obsv(A,C);                % checking
observability
ccc=rank(bmb,1e-4);       % checking the rank
unob = length(A)-ccc;
if ccc < n
       disp('Not Observable');
else
       disp('Full rank, Observable');
end
G2=[zeros(n,nu); GGG];          % input vector
HH=0;
Nn=0;     no cross-correlation between cutting force
change and force measurement noise
[Kest L P]=kalman(ss(A,[B G2],C,[D HH]),Qn,Rn,Nn);
% Contiuous time KF formualation
% KF State space
KF=ss(A-L*C,L,[zeros(2*nu,n)      ones(2*nu,1)],zeros
(2,2));

[num1,              den1]=ss2tf(A-L*C,L,[zeros(2*nu,n)
ones(2*nu,1)],zeros (2,2),1)
KFF=tf(num1(1,:),den1)
[num2,              den2]=ss2tf(A-L*C,L,[zeros(2*nu,n)
ones(2*nu,1)],zeros (2,2),2)
KAF=tf(num2(1,:),den2)

Gffest=KFF*H_ff
Gafest=KAF*H_af
% Analysis
 f=1:5000;

%          force sensor
[magHff        phaHff]              =bode(H_ff,2*pi*f);
magHff=squeeze(magHff); phaHff=squeeze(phaHff);
[magGffest     phaGffest]           =bode(Gffest,2*pi*f);
magGffest=squeeze(magGffest);
phaGffest=squeeze(phaGffest);
[magKFff       phaKFff]             =bode(KFF,2*pi*f);
magKFff=squeeze(magKFff);
phaKFff=squeeze(phaKFff);

%   Acclerrometer
[magHxx        phaHxx]              =bode(H_af,2*pi*f);
magHxx=squeeze(magHxx);
phaHxx=squeeze(phaHxx);
[magGxxest     phaGxxest]           =bode(Gafest,2*pi*f);
magGxxest=squeeze(magGxxest);
phaGxxest=squeeze(phaGxxest);
[magKFxx       phaKFxx]             =bode(KAF,2*pi*f);
magKFxx=squeeze(magKFxx);
phaKFxx=squeeze(phaKFxx);

% % Plotting
figure(1); clf;zoom on;
subplot(2,1,1); hold on;
plot(f,magHxx,'r--',f,magKFxx,'b-.',f,magGxxest,'k-');
grid on;
title('Impact Hammer Accel Model and K.F. Transfer
Functions');
ylabel('Mag [m/N]');
legend('Model FRF','KF FRF','Combined FRF');
subplot(2,1,2); hold on;
plot(f,phaHxx,'r--',f,phaKFxx,'b-.',f,phaGxxest,'k-');
grid on;
ylabel('Phase [Deg.]');
```

```
legend('Model FRF','KF FRF','Combined FRF');
xlabel('Frequency [Hz]');

figure(2); clf;zoom on;
subplot(2,1,1); hold on;
plot(f,magHff,'r--',f,magKFff,'b-
.',f,magGffest,'k-');
grid on;
title('Impact Hammer Force Model and K.F.
Transfer Functions');
ylabel('Mag [N/N]');
legend('Model FRF','KF FRF','Combined FRF');

subplot(2,1,2); hold on;
plot(f,phaHff-180,'r--',f,phaKFff-180,'b-
.',f,phaGffest,'k-');
grid on;
ylabel('Phase [Deg.]');
legend('Model FRF','KF FRF','Combined
FRF');%grid on;
xlabel('Frequency [Hz]');
figure(3)
 subplot(311)
 plot(f,magKFxx)
 subplot(312)
 plot(f,magGxxest)
 subplot(313)
 plot(f,magHxx)
figure(4)
 subplot(311)
 plot(f,magKFff)
 subplot(312)
 plot(f,magGffest)
 subplot(313)
 plot(f,magHff)
%          time

filename1='PCFX.dat'; % open file

A=load(filename1);  %B=load(filename2);C=load(filen
ame3);%D=load(filename4);E=load(filename5);

T1=A(:,1);          AX=A(:,2);          AY=A(:,3)/0.012%
BX=B(:,2);CX=C(:,2);%DX=D(:,2)*-1;EX=E(:,2)*-1;

 yF=lsim(KFF,AX,T1);
 yA=lsim(KAF,AY/(2*pi*2666),T1);

 Y1=yF+yA;
 rpm=80000;
 speed=rpm/60;

 figure(11)
 plot(T1*speed,-Y,T1*speed,-Y1,'g--',T1*speed,AX,'--
');legend('compensate                force','compenate
sensor_fusion','actual')
 axis([5 15 -1 1])

  figure(12)
 plot(T1*speed,AY);legend('Acceleration')
 axis([5 15 -1 1])

 Com_Cut1=[T1 Y1 Y];
       savename=['Com_Cut1','.dat'];
      save(savename,'Com_Cut1','-double','-ascii');
```

Appendix F. Matlab code for the Joint identification method.

```
format long e
% freq range
min_fre=1; max_fre=10000;
drange=min_fre:1:max_fre;
div=5;
freqrange=max_fre;
steps=max_fre

% TOOL INPUT and FEM analysis

disp('Screwed')
L2=50e-3;                          % Length 2 [m]
L1=0;              % Length 1 [m] - Fluted section
E=205e9;             % Young's Modulus [N/m^2]]
density=7800;       % Density [kg/m^3]
dia2=13e-3;          % Diameter [m]
dia1=dia2;
zeta=0.01;           % damping coefficient

[H11, H12, H21, H22, L11, L12, L21, L22, N11,
N12, N21, N22, P11, P12, P21, P22] = ...
femcutter4(dia1,dia2,L1,L2,E,density,zeta,div,fr
eqrange,steps);

%%%%%%%%%%%%%%%%
% % Loading Data

filename='H33_ff_120.frf';
filename3='50_G11.frf';
filename4='50_G12.frf';

A=load(filename);
Areal=A(drange,2);%*10^-3;
Aimag=A(drange,3);%*10^-3;
H33=complex(Areal,Aimag);
%H33=filter(b,a,H33);

D=load(filename3);
Dreal=D(drange,2);%*10^-3;
Dimag=D(drange,3);%*10^-3;
G11=complex(Dreal,Dimag);

E=load(filename4);
Ereal=E(drange,2);%*10^-3;
Eimag=E(drange,3);%*10^-3;
G12=complex(Ereal,Eimag);

% RDOF FRF (G11 AND G12)

load ('rdof33_MoT.frf');
L33=complex
(rdof33_MoT(:,2),rdof33_MoT(:,3));
P33=complex(rdof33_MoT(:,4),rdof33_MoT(:,5
));

% Finding the Joint Dynamics
for i=min_fre:length(drange)
h11=H11(i);  h12=H12(i);  h22=H22(i);  h33=H33(i);
h21=H21(i);  l11=L11(i);  l12=L12(i);  l22=L22(i);
l33=L33(i); p33=P33(i);
l21=L21(i);  n11=N11(i);  n12=N12(i);  n22=N22(i);
n21=N21(i);  p11=P11(i);  p12=P12(i);  p22=P22(i);
p21=P21(i); gg11=G11(i); gg12=G12(i);

kx(i)=((h12*h33-gg12*h22-
gg12*h33)*n21+h21*n22*gg12-
h22*gg11*l33+h22*h11*l33+h21*l33*gg12-
h21*h12*l33-h11*n22*h33+gg11*n22*h33)/((-
h12+gg12)*n21-gg11*n22+h11*n22);
      kt(i)=-p22-(gg11*l33*n22-h11*l22*n22-
h11*l33*n22+h21*l12*n22+gg11*l22*n22-
l33*n21*gg12-
n21*l22*gg12+h21*p33*gg12+n21*h12*l33+n21*h12
*l22-n21*l12*h22+h11*h22*p33-gg11*h22*p33-
h21*h12*p33)/(-gg11*h22+h11*h22+h21*gg12-
h21*h12);
      end
jointd=[drange' real(kx)' imag(kx)' real(kt)' imag(kt)'];
savename=['Modular_joint','.frf'];
save(savename,'jointd','-double','-ascii');

% Receptance Coupling

for j=min_fre:length(drange)
    IJ=[H22(j) L22(j) ; N22(j) P22(j)];
    IK=[H33(j) L33(j);L33(j) P33(j)];
    joint=[kx(j) 0;0 kt(j)];
    I=IJ+IK+joint;

     II=pinv(I);
    C1=[H11(j) L11(j); N11(j) P11(j)];
    C2=[H12(j) L12(j); N12(j) P12(j)];
    C3=[H21(j) L21(j); N21(j) P21(j)];
    C4=C2*II*C3;
    C=C1-C4;
    GG11(j)=C(1,1);

    % FOR G12
    C5=[H22(j) L22(j); N22(j) P22(j)];
    C6=C2*II*C5;
    C12=C2-C6;

    GG12(j)=C12(1,1);
    GG21(j)=C(2,1);
    GG22(j)=C(2,2);

end
% Plotting
```

```
freq=drange;


plotthick

figure(1);clf;
subplot(211)
plot(freq, real(G11), 'b', freq, real(GG11), 'k--')
title('G11 Receptance Result')
legend('Measured','Predicted');
ylabel('Real (m/N)')
subplot(212)
plot(freq, imag(G11), 'b', freq, imag(GG11), 'k--
')
legend('Measured','Predicted');
ylabel('Imaginary (m/N)')
xlabel('Frequency (Hz)')

figure(2);clf;
subplot(211)
plot(freq, abs(G11), 'b', freq, abs(GG11), 'k--')
title('G11 Receptance Result')
legend('Measured','Predicted');
ylabel('Magnitude (m/N)')
subplot(212)
plot(freq, 180/pi*angle(G11), 'b', freq,
180/pi*angle(GG11), 'k--')
legend('Measured','Predicted');
ylabel('Angle (deg)')
xlabel('Frequency (Hz)')


% Plotting Joints
figure(3);clf;
subplot(211)
plot(freq, real(kx), 'b')
title('Kx Joint Dynamics')
ylabel('Real (m/N)')
subplot(212)
plot(freq, imag(kx), 'b')
ylabel('Imaginary (m/N)')
xlabel('Frequency (Hz)')

figure(4);clf;
subplot(211)
plot(freq, abs(kx), 'b')
ylabel('Magnitude (m/N)')
subplot(212)
plot(freq, 180/pi*angle(kx), 'b')
ylabel('Angle (deg)')
xlabel('Frequency (Hz)')


figure(5);clf;
subplot(211)
plot(freq, real(kt), 'b')
title('Kt Joint Dynamics')
ylabel('Real (rad/Nm)')
subplot(212)
plot(freq, imag(kt), 'b')
ylabel('Imaginary (rad/Nm)')
xlabel('Frequency (Hz)')


figure(6);clf;
subplot(211)
plot(freq, abs(kt), 'b')
title('Kt Joint Dynamics')
ylabel('Magnitude (rad/Nm)')
subplot(212)
plot(freq, 180/pi*angle(kt), 'b')
ylabel('Angle (deg)')
xlabel('Frequency (Hz)')

figure(7);clf;
subplot(211)
plot(freq, abs(L33), 'b',freq, abs(P33), 'k--')
title('RDOF')
  legend('L33','P33');
ylabel('Magnitude (rad/Nm)')
subplot(212)
plot(freq, 180/pi*angle(L33), 'b', freq,
180/pi*angle(P33), 'k--')
legend('L33','P33');
ylabel('Angle (deg)')
xlabel('Frequency (Hz)')

figure(8);clf;

plot(df,abs(h))
```

Appendix G. Equipment Lists

- Dytran 68008L, Impact hammer
- Kistler 8778A500, Accelerometer, mass 0.29g
- LK-G32, Laser Displacement
- Kistler type 9017B, Miniature 3-component force sensor.
- PXI-6259, M series DAQ (32 Analog inputs, 48 Digital I/O, 4 Analog outputs)
- PXI-7344, 4axis Servo/Step Motion Controller
- UMI-7774 Universal Motion Interface with D-Sub Connection
- Navitar Zoom600 & TenX Zoom, High resolution Zoom lens
- Astro-E 800Z System, Air spindle (NRA-5080), Electric motor (EM-805)
- CV2600, Vision system
- Zeta4 Driver, Motor current 0-4 Amps
- P.611.3S.611.3O, NanoStage, travel range 0-100 micrometers, resolution 25nm.
- Omega DFG51-2, Force gauge
- Kron-Hite 3364, Anti-aliasing filter
- 106008CTEP-D3L2C4M1E1, Precision table